(12)

ARO-16726.2-A-GS

CHEMICAL SYSTEMS LABORATORY

CONTRACTOR REPORT ARCSL-CR-82003

CLEARING OF MILITARY SMOKE CLOUD WITH SCAVENGING TECHNIQUE

FINAL REPORT

by

Joseph Podzimek, Ph.D.

December 1982

Supersedes
AD. A108084

U.S. ARMY RESEARCH OFFICE
Contract No. DAAG29 79 C 0073

UNIVERSITY OF MISSOURI-ROLLA
Graduate Center For Cloud Physics Research
ROLLA, MO 65401

US ARMY ARMAMENT RESEARCH AND DEVELOPMENT COMMAND
Chemical Systems Laboratory
Aberdeen Proving Ground, Maryland 21010

Disclaimer

The views, opinions and/or findings contained in this report are those of the authors and should not be construed as an official Department of the Army position, policy, or decision unless so designated by other documentation.

Disposition

Destroy this report when it is no longer needed. Do not return it to the originator.

UNCLASSIFIED

SECURITY CLASSIFICATION OF THIS PAGE (When Data Entered) SUMMARY

REPORT DOCUMENTATION PAGE

READ INSTRUCTIONS BEFORE COMPLETING FORM

1. REPORT NUMBER: ARCSL-CR-82003	2. GOVT ACCESSION NO.: AD-A124265
3. RECIPIENT'S CATALOG NUMBER:	
4. TITLE (and Subtitle): CLEARING OF MILITARY SMOKE CLOUD WITH SCAVENGING TECHNIQUE	5. TYPE OF REPORT & PERIOD COVERED: Final Report 1 Mar 79 - 31 Mar 81
	6. PERFORMING ORG. REPORT NUMBER: AG-12
7. AUTHOR(s): Josef Podzimek, Ph.D.	8. CONTRACT OR GRANT NUMBER(s): DAAG 29-79-C-0073
9. PERFORMING ORGANIZATION NAME AND ADDRESS: University of Missouri-Rolla, Graduate Center for Cloud Physics Research, Rolla, MO 65401	10. PROGRAM ELEMENT, PROJECT, TASK AREA & WORK UNIT NUMBERS: 1L161102A71A-D
11. CONTROLLING OFFICE NAME AND ADDRESS: Commander, Chemical Systems Laboratory, Attn: DRDAR-CLJ-R, Aberdeen Proving Ground, Maryland 21010	12. REPORT DATE: Dec 82 ~~June 1 1981~~
	13. NUMBER OF PAGES: 138
14. MONITORING AGENCY NAME & ADDRESS (if different from Controlling Office): Commander, Chemical Systems Laboratory, Attn: DRDAR-CLB-PS, Aberdeen Proving Ground, Maryland 21010	15. SECURITY CLASS. (of this report): UNCLASSIFIED
	15a. DECLASSIFICATION/DOWNGRADING SCHEDULE:

16. DISTRIBUTION STATEMENT (of this Report)

Approved for public release; distribution unlimited.

17. DISTRIBUTION STATEMENT (of the abstract entered in Block 20, if different from Report)

18. SUPPLEMENTARY NOTES

This research was sponsored by the Army Smoke Research Program, Chemical Systems Laboratory, Aberdeen Proving Ground, Maryland 21010. Contract Project Officer: Dr. Edward Stuebing (DRDAR-CLB-PS), 671-3089

19. KEY WORDS (Continue on reverse side if necessary and identify by block number)

Settling of nonspherical particles ($450 < Re < 4700$)
Scavenging of military smoke particles
Smoke particle scavenging effect on visibility

20. ABSTRACT (Continue on reverse side if necessary and identify by block number)

A survey of parameters describing the settling of non-spherical scavengers such as disks, hexagons, triangles, ellipses, squares, rectangles, and mesh type models for settling in quiescent air and at a side wind has been obtained.

The experiments with disks exposed to smoke particle flow in a wind tunnel showed that particle deposition on the rear side of a collector represents a significant part of the total scavenging effect and that the deposition on the front (continued)

DD FORM 1 JAN 73 1473 EDITION OF 1 NOV 65 IS OBSOLETE

UNCLASSIFIED

SECURITY CLASSIFICATION OF THIS PAGE (When Data Entered)

20. ABSTRACT cont'd

side of a stationary disk can be reasonably well described by some of the existing models. The estimated scavenging efficiency of the disks in this arrangement is between 0.8% and 3.0%.

Under the experimental conditions used, dropping of a large quantity of paper punch scavengers into a smoke cloud might lead to the improvement of a visual range up to 29% after the first dropping and up to 9% after each of the subsequent droppings.

SUMMARY

The objective of the final report on the 2-year investigation of the possibility to clear a military smoke cloud with scavengers dropped into it was to perform an experimental and theoretical study of the scavenging efficiency of nonspherical collectors in a smoke consisting of particulates with diameters between 0.1 μm and 10 μm. The type of swinging motion of differently shaped collectors with sizes ranging from several mm to several cm received prime attention.

A pilot study has also been performed with models falling through a slight horizontal wind and with mesh type models falling in a quiescent medium. During several experiments the number of smoke particles deposited on models was evaluated. Finally, the effect of many collectors, settling in a smoke cloud, on the visibility through the remaining smoke has been assessed.

The experimental study of smoke particle scavenging in a quiescent medium with the light extinction measurement was made in a large cylindrical chamber and for comparison, several models were placed in a small horizontal wind tunnel. A large environmental chamber with a horizontal flow of about 1 m s^{-1} was used for the observation of the scavenger motion at side wind conditions.

All results of the pilot experiments and theoretical studies on scavenger orientations and smoke particle scavenging can be summarized as follows:

A survey of parameters describing the settling of nonspherical scavengers such as disks, hexagons, triangles, ellipses, squares, rectangles and mesh type models for settling in quiescent air and at a side wind has been obtained.

The experiments with disks exposed to smoke particle flow in a wind tunnel showed that particle deposition on the rear side of a collector represents a significant part of the total scavenging effect and that the deposition on the front side of a stationary disk can be reasonably well described by some of the existing models. The estimated scavenging efficiency of the disks in this arrangement is between 0.8% and 3.0%.

Under the experimental conditions used, dropping of a large quantity of paper punch scavengers into a smoke cloud might lead to the improvement of a visual range up to 29% after the first dropping and up to 9% after each of the subsequent droppings.

PREFACE

The work described in this report was authorized under Project No. 1L161102A71A-D, Aerosol/Obscuration Science. The period covered by this report is from March 1979 through March 1981.

Our 2-year investigation of scavenging techniques for clearing military smoke clouds included the modification and expansion of several techniques suggested in the original proposal of 1979. New and more effective instruments were designed, which required more time than was scheduled in the Grant Proposal Budget for 1979-1980.

The use of trade names in this report does not constitute an official endorsement or approval of the use of such commercial hardware or software. This report may not be cited for purposes of advertisement.

Acknowledgments

The author is grateful to his closest fellow worker, Dr. P. C. Yue, who left the laboratory in the middle of the second vear, and to graduate student G. Frick for their support and experimental skill. Several student research assistants should be especially commended: Messrs M. Schenewerk for the calculation of the flow field around an obstacle, D. Reed for the design of electronic equipment and smoke scavenging

experiments, and D. Fortner for effective and enthusiastic work in the environmental chamber where the model settling experiments were performed. In the final stage of the work, the author was effectively supported in the theoretical analysis of settling plate motion by Dipl. Ing. M. Straka. Mrs. Vickie Maples and Mrs. C. Turek ably prepared the report for printing.

The author appreciates the support of this grant by the U.S. Army Armament R&D Command and the effective monitoring of the program by Dr. E. Stuebing and Mr. G. Rubel.

CONTENTS

LIST OF FIGURES AND TABLES

Figure

Figure

8 Curves $C_D = f(Re)$ for different models of hexagons and rectangles falling in quiescent air and at a side wind.

9 Stroboscopic picture of an oscillating paper disk 1.9 cm in diameter.

10 Stroboscopic picture of a quietly settling paper square (1.4x 1.4 cm^2).

11 Gliding regime of a falling paper hexagon of 1.98 cm in diameter.

12 Smoke particle distribution on the frontal side of a disk (d = 0.5 cm).

13 Smoke particle distribution on the disk's rear side (d = 0.5 cm).

14 Smoke particle distribution on the frontal side of a disk (d = 1.0 cm).

15 Smoke particle distribution on the rear side of a disk (d = 1.0 cm).

16 Transmission light detector voltage measurement in a dense $TiCl_4$ smoke in which a large quantity of computer card punches (1x3 mm) was dropped in five batches per 4 ounces. Aitken nuclei (AN) counts are marked in thousands per cm^{-3}.

Figure

D-1 Plate type ice crystal with protrusions and deposited small droplets. The mean diameter of circumscribed circle is 1200 µm.

D-2 Star type ice crystal with deposited frozen drops and aerosol particles. Mean size is 1000 µm.

D-3 Cumulative size spectrum of sodium chloride aerosol generated by fluid atomization aerosol generator. Particles, evaluated from SEM electronmicrographs, are plotted as a total number of particles smaller than a specific size.

D-4 The X-ray energy spectrum analysis of the $TiCl_4$ aerosol deposited on the electron microscopical grid.

D Size distribution of $TiCl_4$ particles evaluated from SEM pictures. Particle frequency is plotted as a total number of particles larger than a specific size.

D-6 a,b $TiCl_4$ smoke particles deposited on a metallic substrate in an electrostatic precipitator. SEM picture at a 5000 x magnification.

D-7 Red phosphorus smoke particles deposited on an electron microscopical grid. SEM magnification 2500 x.

D-8 Red phosphorus and titanium chloride particle size distribution evaluated from electronmicrographs. Plotted are cummulative particle size spectra (concentration of particles larger than a certain size--expressed in percent of the total number).

D-9 Main parts and wiring diagram of the licht extinction measurement.

Figure

D-10 Air velocity vertical profiles in the Large Environmental Chamber. Using different screens and flow straighteners three velocity profiles were finally reached. Arrangement 3 was used for most experiments. Later several experiments were also performed with arrangement 1.

D-11 Vertical camera record of a settling disk at a Re_z = 6120 (Podzimek, 1970).

D-12 Side view on a settling and oscillating disk at a Re_z = 6120 (Podzimek, 1970).

D-13 Variation of the components of velocity and acceleration of a paper disk (d = 1.9 cm) falling in the air.

D-14 Variation of the components of angular velocity and its time derivation of a paper disk (d = 1.9 cm) falling in the air.

D-15 Variation of the components of velocity and acceleration of an aluminum disk (d - 5.0 cm) falling in the water.

D-16 Variation of the components of angular velocity and its time derivation of an aluminum disk (d - 5.0 cm) falling in the water.

D-17 Calculated velocity distribution around a hexagonal model (d - 1.0 cm) placed in the air flow of 0.5 m s^{-1} (Sasyo, 1971).

D-18 Calculated velocity distribution around a hexagonal model (d = 1.0 cm) placed at 45° angle to the airflow of 0.5 m s^{-1} (Sasyo, 1971).

D-19 Calculated streamlines of a viscous fluid around a two-dimensional obstacle at Re = 1000 (Schenewerk, 1979).

Figure

D-20 Deposited $TiCl_4$ particles on two scavengers of 1 x 3 mm in size placed in a crossed position 1.2 mm one behind the other. In the lower part of the figure is the front plate (both plates were photographed in parallel position unlike during the exposure).

D-21 Aitken nuclei counts (n) and smoke particle concentration calculated according to Lindauer-Castleman (1971) model plotted together with measured light extinction as a function of time in a clearing smoke cloud.

D-22 Light extinction measurement in a $TiCl_4$ smoke cloud in which 60 plastic disks (d = .66 cm) were dropped.

D-23 Light extinction measurements in $TiCl_4$ smoke clouds in which 64 fine fiber mesh models (1.5 x 1.5 cm^2) were dropped at once or in several batches.

LIST OF TABLES

1. INTRODUCTION

The idea to clear a military smoke cloud with scavenging technique stems from the observation of very small droplets and aerosol particles on the surface of falling ice crystals (figures D-1 and D-2 in appendix D).[1,2] These findings do not agree with the low collection efficiency of spherical scavengers (water droplets) found by several authors,* or with only 1% to 4% scavenging efficiency of ice crystals collecting particles of 1.0 to 3.4 um in diameter reported by Sood and Jackson.[3] On the other hand, the studies by Starr and Mason,[4] Sasyo,[5] and Yue and Podzimek[6] and some theoretical calculations (e.g. Pitter et al.[7]) indicate a potential use of the technique of nonspherical collectors for an effective particle scavenging.

Without analyzing all mechanism potentially contributing to an effective scavenging by a nonspherical collector (e.g. electrostatic, diffusiophoretic forces), one can ask first some very simple questions: Do we know all about the motion of nonspherical collectors and, consequently, does not the additional motion superimposed to the main trajectory of falling models influence the collector's scavenging efficiency? Is the deposition of particulates on the rear side of collectors in a specific domain of collector and particle sizes significant? What is the effect of many collectors released simultaneously, and is there a "falling scavenger zone" effect helping to deposit the smoke particles on the ground?

In order to answer these and similar questions, a 2-year research

*Podzimek, J., and Yue, P.C. Clearing of Military Smoke Cloud with Scavenger Technique. pp 35-37. Proposal to U.S. Army Armament R&D Command. January 1979.

program has been undertaken which encompasses a theoretical study, a literature survey, and a broad experimental effort with the main goal that of finding a promising basis for a detailed study. Reported here are the results of that exploratory study. The motion of falling scavengers, the deposition of smoke particles on a scavenger, the effect of a large population of scavengers, and the scavenger "falling zone" effect on light extinction are discussed.

2. MATERIALS AND EXPERIMENTAL APPROACHES

Models for scavenging included different shapes, disc, strip, hexagon, triangle, L-type models, etc., with sizes ranging from several millimeters to several centimeters. (see table D-1 in Appendix D). Emphasis was put on the use of the most common inexpensive materials (paper, styrofoam) which were available in large quantities (e.g., punch card pieces). For measurement in an aerodynamic wind tunnel, models of other materials such as plexiglas and stainless steel were used. In order to reach a high scavenging efficiency, certain collectors, each a rigid fine mesh of synthetic fibers, were used mainly for experiments in a quiescent smoke cloud.

Three different types of smoke aerosol were used: sodium chloride, titanium chloride, and red phosphorus.

2.1 Smoke Aerosols.

2.1.1 Sodium Chloride.

The sodium chloride (NaCl) aerosol was generated from 0.91%, by weight, salt solution in water with a fluid atomization generator (Environmental Research Corp. Model 7300 with a collision flow of 4 lpm and a dilution flow of 2.7 lpm). Filtered air or nitrogen was

used for the dispersion of the aerosol, the concentrations of which reached nearly 300,000 cm^{-3} at the source. The size distribution of NaCl aerosol is presented in figure D-3, which shows that the aerosol contains more than 31% by number in the 0.02- to 0.06- μm (diameter) size range and more than 72% in the 0.02- to 0.08- μm size range. Sodium chloride aerosol was used only for some preliminary studies of deposited aerosol particles on models covered by a gelatin layer sensitized by 5% silver nitrate solution. A detailed description of this technique is given elsewhere.[8]

2.1.2 Titanium Chloride.

Titanium chloride ($TiCl_4$) smoke was generated by passing humidified nitrogen through a vessel containing liquid $TiCl_4$. At a nitrogen flow rate of 10 lpm, we usually obtained a fog with initial particle density as high as 100,000 cm^{-3}. This concentration was measured by a Gardner counter. The X-ray spectrum analysis of particles deposited on an electron microscope grid revealed that apparently most of the particles were composed of $TiCl_4$ (fig. D-4). The size distribution of $TiCl_4$ in figure D-5 was plotted from scanning electronmicrographs. It shows that particle diameters between 0.4 to 0.8 μm have the highest frequency. The majority of these particles have spherical shape (fig. D-6).

2.1.3 Red Phosphorus.

Red phosphorus particles were generated by burning the powder in a Spinning Disk Aerosol Generator and venting it into the aerodynamic wind tunnel. The aerosol has mixed shapes as shown in figure D-7. The majority of aerosol deposited on an electron

microscope grid had spherical shapes, which at a relative humidity around 30% reveal their highly hygroscopic nature. However, there are many aggregates showing a fiber-like structure with very fine deposited particles - probably room air aerosol. The particle size distribution curve in figure D-8 features a broad size spectrum, with the majority of particle diameters between 0.95 and 1.50 μm. For comparison, a size distribution curve for titanium chloride aerosol is plotted in the same diagram.

2.2 Experimental Facilities.

The main experimental facilities used for scavenger motion and particle deposition were a large cylindrical settling chamber for experiments in quiescent smoke cloud, a large environmental chamber with circulating air flow for observance of scavenger settling at side wind conditions, and a small aerodynamic wind tunnel for the study of particle deposition on quiescent and slightly oscillating models. Many experiments with settling scavengers were also performed in a simple cylinder of plexiglas with an internal diameter of 23 cm.

2.2.1 Large Cylindrical Settling Chamber.

This chamber, 0.78 m in diameter and 1.6 m in height, is composed of a glass frontal half-cylinder and an aluminum half-cylinder (black-coated inside). The two half-cylinders are jointed by grooved slats. At the top and bottom are aluminum lids; the one at the top has an opening in the center into which models are dropped. In the side wall are several openings enabling the introduction of smoke, and the withdrawal of samples for measuring particle size distribution. Above the bottom plate is a large

opening through which the sampling device for settling scavengers is inserted or pulled out. This chamber, adapted from the facility originally used for washout study, is equipped with a light extinction measuring system (developed by Dr. J. L. Schmitt for the Cloud Simulation Chamber) and a recording and evaluating system (designed by our research assistant, Mr. D. E. Reed). The light source is a "modified" moderately intense red light emitting diode (Fairchild FLV-104 red LEDO). The detector is a silicon photodiode (Bell and Howell, Model 520). The output of the photodiode is measured with a digital voltmeter and may be recorded by two devices: a digital recorder (Hewlett-Packard, Model 5055A), which prints the data at 1- or 10-second intervals, and a Wang Calculator (Model 380K/380-2K). The latter, with interface and associated electronics, calculates the extinction and prints the data via an IBM typewriter at intervals selectable from 5 to 999 sec. Rough calculation indicates that the light extinction meter is accurate to 0.02% over short periods of time and drifts less than 0.2% in 2 hours of measurement. The setup of scavenging experiments in this chamber is presented in figure 1. The main parts and the wiring diagram of the light extinction measurement are apparent in figure D-9.

2.2.2 Large Environmental Chamber.

A chamber originally used for an Army program was adapted through substantial changes as a large environmental chamber. The main experimental space of this chamber (4.10 m long, 1.70 m wide, and 2.00 m high) was divided into two parts, one of which (adjacent to the frontal wall with windows) was converted into

a "two-dimensional" aerodynamic wind tunnel with an effective cross section of the experimental space of 1.80 x 0.65 m (fig. 2). The air is drawn out by ventilators (outside of the chamber) and circulates back to the entrance of the experimental space. The air can be bypassed through the charcoal layer and absolute filter system. The maximum air velocity which can be reached in the measuring cross section is several meters per second. The models are dropped through an opening in the ceiling. Their path, illuminated by a stroboscope (1531-AB Strobotac Electronic Stroboscope, General Radio), is recorded by a photographic camera located in the front of a Plexiglas tunnel wall inside the chamber. The vertical profile of the horizontal component of the air velocity (fig. D-10) reveals that, after several attempts to make the velocity vector distribution more uniform, we succeeded and obtained a reasonable uniform profile for horizontal velocities around 0.7 meters per second. The pictures from only one camera do not allow an accurate evaluation of the position of a drifted scavenger. However, from the model size in the camera image plane and from the photographed scales in the wind tunnel, the possible error in locating the model was estimated to be less than ±10% of the camera distance from the model (approximately 50 cm).

2.2.3 Small Aerodynamic Wind Tunnel.

A small aerodynamic wind tunnel (Scott-Engineering Sciences, Pompano Beach, FL) with a test section 13.0 cm in diameter was used for most of the laboratory studies of aerosol deposition on scavengers. The entrance of the wind tunnel was connected with

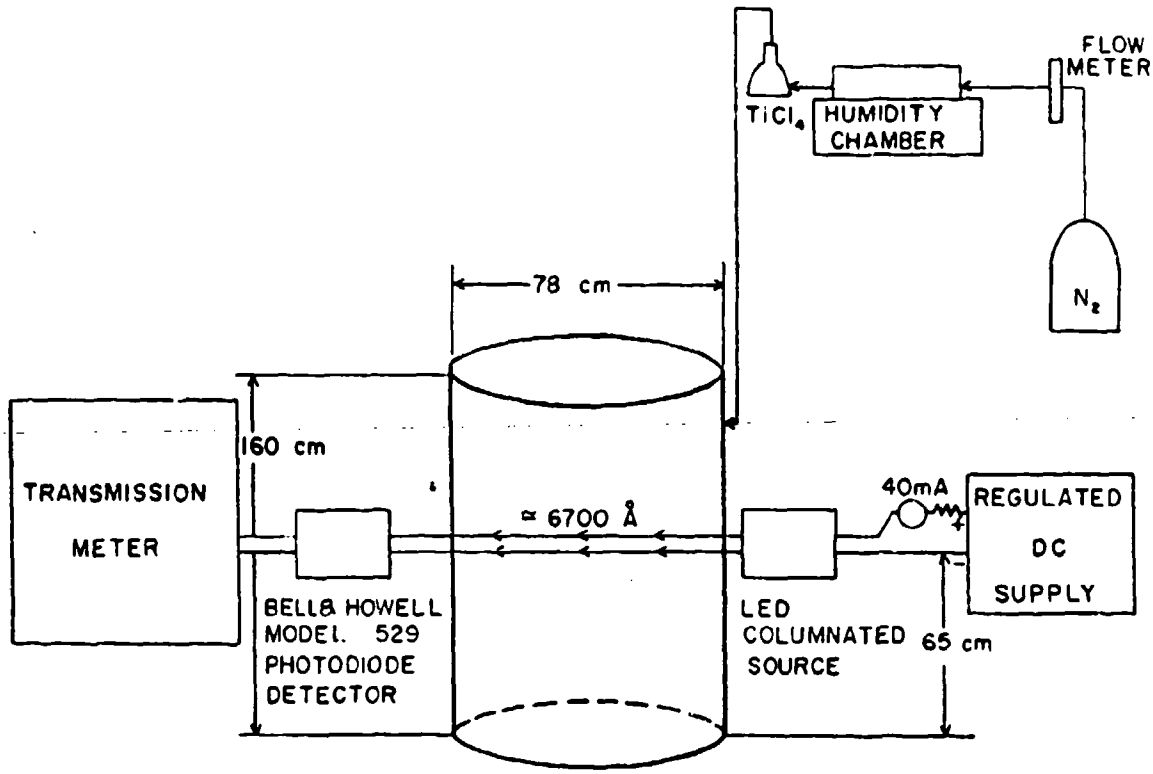

Figure 1. Large Cylindrical Settling Chamber for Scavenging Experiments and Light Extinction Measurement

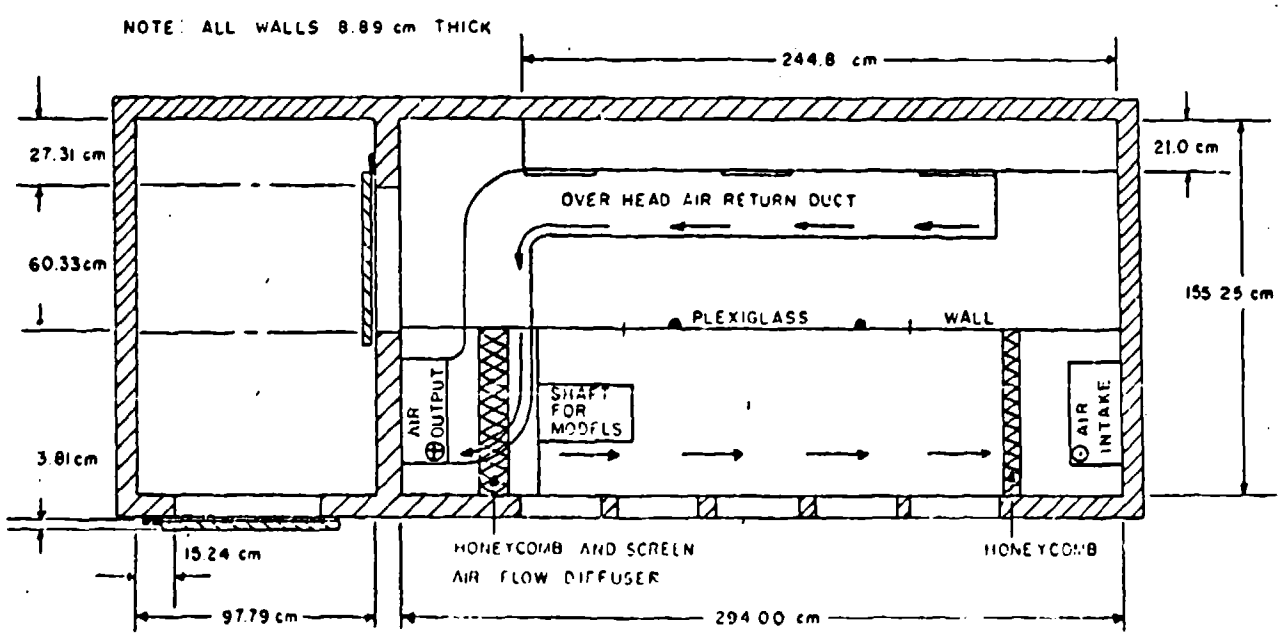

Figure 2. Large Environmental Chamber for Scavenger Settling Experiments at side wind of 0.7 or 0.5 m s^{-1}

(The stroboscope and photographic camera were located in the frontal part (close to the air inlet) of the Plexiglas window approximately 50 cm above the bottom.)

an aerosol generator (e.g., Spinning Disk Generator) and the outlet was extended into a fume hood (fig. 3). The calibration of the velocity in the test section was made with a hot-wire anemometer. For comparability of wind tunnel measurements with settling models, a velocity of around 1 meter per second was preferred. The models were attached to the tip of a needle. A special device was made for future experiments with particle deposition on slightly swinging models.

2.2.4 Other Instrumentation.

Other instrumentation was used mainly for particle measurements, particle sampling and evaluation in a transmission and scanning electron microscope, and in the laboratory for optical microscopy. The instruments listed below were used in accordance with instructions supplied by the manufacturer:

Gardner Counter Cat. 70.004G-2 Serial 1250; Gardner Assoc., Schenectady: Used for Aitken nuclei (particles with $r < 0.1$ µm) counting in the concentration range 100 to 100,000 AN cm^{-3}. Manual operation - discontinuous measurements.

Laser Cavity Active Scattering Aerosol Spectrometer (Knollenberg); Model ASAS-300A; Particle Measuring Systems Inc., Boulder, CO: Used for the measurement of particle size distribution and concentration in five particle size ranges: 0.157 - 0.336 µm, 0.284 - 0.748 µm, 0.355 - 1.160 µm, and 0.639 - 3.000 µm. Continuous recording of 15 size groups in each range.

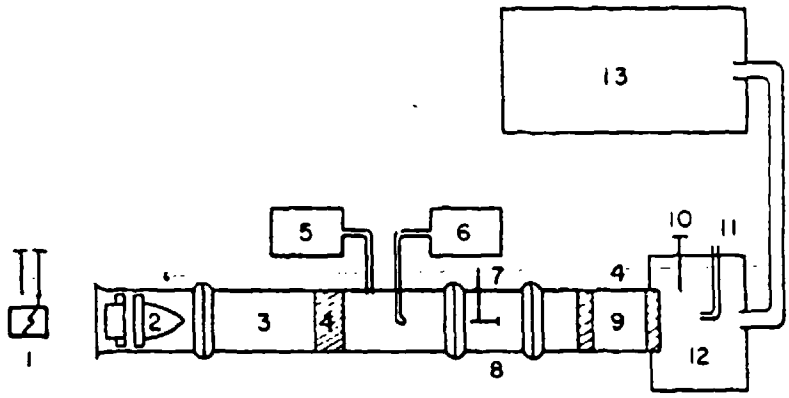

1 WET- AND DRY-BULB THERMOMETERS
2 ROTOR FAN
3 WIND CHANNEL
4 HONEYCOMB FLOW STRAIGHTENER
5 DEW POINT HYGROMETER
6 CLIMET PARTICLE COUNTER
7 MODEL SUPPORT
8 TEST SECTION
9 CHANNEL EXTENSION
10 THERMOMETER
11 AEROSOL INLET
12 HUMIDIFIER
13 AEROSOL/FILTERED AIR STORAGE TANK

Figure 3. Arrangement for the Deposition of NaCl Aerosol on Models in the Horizontal Aerodynamic Wind Tunnel

(In the case of using $TiCl_4$ or red phosphorus aerosol, the humidifier (12) and the aerosol storage tank were replaced by a Spinning Disk Generator, and the outlet was extended into a fume hood.)

Electrostatic Aerosol Sampler - Model 300; TSI Inc., St. Paul, MN: Used for sampling of particles for transmission and optical electron microscopy; particle size range between 0.02 and 10.00 μm at a flow rate 5 to 10 lpm.

Particle Size Semiautomatic Evaluator TGZ3 - Carl Zeiss, Germany: Used for the analysis of particle photographs from an optical microscope, transmission or scanning electron microscope. Data are recorded as a function of linear or logarithmic scales of particle size.

Transmission and scanning electron microscope (with the X-ray spectrum energy analyzer) were frequently used in the university's central laboratory.

2.3 Experimental Approaches.

The methodological approach to the study of the scavenger motion and particle deposition can be summarized in the following way:

A theoretical analysis of the forces and environmental parameters affecting the scavenger motion in the domain of Reynolds number (Re) beyond the validity of the Stokes resistance law will enable one to establish the decisive factors which should be measured for obtaining the simplified trajectory of a scavenger. In the first approximation, models symmetrical in one plane will be tried first, and their trajectory deduced from stroboscopic pictures will be compared with a simple model. This semianalytical approach is supposed to be the most promising with regard to the mathematical difficulties encountered while solving a system of

nonlinear equations. A simple scavenger trajectory will be used for estimating the volume of air with smoke particles swept by the falling scavenger and, assuming a known collection efficiency, for calculating the number of deposited smoke particles.

Experimental approach will be based on scavenger trajectory deduced from stroboscopic pictures and on direct particle counting on the surface of a specific model in the optical or scanning electron microscope. The cardinal question which has to be answered is how far an experiment done in a wind tunnel is comparable with the evaluation of the same particles deposited on a freely falling scavenger of the same type.

Finally, one cannot completely exclude an empirical approach in investigating the effect of a large population of scavengers on clearing a smoke cloud. This approach, although less elegant, is based on the application of a large number of scavengers of a specific type and size falling through a homogeneously dispersed smoke cloud in an experimental chamber and measuring the light extinction. Also the "recovery time" of light extinction after the scavenger zone fell through the smoke seems to be an important factor for judging the efficiency of a specific scavenging process. In all of these approaches, the smoke particle concentration and size distribution should be measured before, during, and after the scavenging experiment.

There are basic difficulties, however, in sampling the scavengers (with deposited smoke particles) for microscopical analysis. The scavengers reaching the bottom of the chamber are immediately contaminated on their front sides by the smoke particles which

settled before on the substrate where the scavengers are collected. On the other hand, the rear sides of the scavengers are covered settling smoke particles while the scavengers are resting on the substrate. For this reason, a simple probe with a lid was designed which allows sampling of scavengers for a relatively short time when the scavengers have just reached the probe. The distortion of size spectra of deposited particles on scavengers cannot be avoided, mainly in the domain of large particulates.

3. METHODS

3.1 Motion of Falling Scavengers.

The knowledge of scavenger motion during fall is of primary importance for calculating the scavenging efficiency of a nonspherical collector in a smoke cloud. Such knowledge enables calculation of the mean settling velocity, the area covered by an oscillating scavenger, and its detailed position (angle of attack) along the trajectory. The important parameters of similarity which must be observed in order to perform meaningful laboratory experiments can also be determined.

Our previous experiments[9,10] made with plate and columnar type models falling in a large tank filled with glycerol-water mixtures, and our current task to study scavenger motion in the air*,[8,11] led to the division of the mode of a falling nonspherical scavenger into five main groups characterized by: arbitrary motion, steady motion, regular oscillation, sliding, and tumbling. Several of these modes have been described by Stringham et al.,[12]

*Podzimek, J. and Yue, P.C., op. cit.

and others. These modes are usually related to the value of Reynolds number (Re), although in several modes other parameters of similarity might play an important role. Therefore, in case, e.g., of a falling disk, its arbitrary position is found at $Re < 1$, steady fall for $1 < Re < 100$, regular oscillation for $100 < Re < 1{,}000$, gliding (slipping) for $1{,}000 < Re < 5{,}000$, and tumbling for $Re < 5{,}000$. The transition from oscillation to gliding and tumbling is not well defined, especially for paper models with slight irregularities falling in the air. In figure 4 we compared our measurements of disks falling in liquids (marked with crosses) and from the air (marked with triangles) with the measurements by Stringham et al.[12] and by Shemenauer (1969).[13] From all the measurements and studies performed by many authors, it is clear that only the case of steady fall can be treated analytically or seminalytically for $Re < 1.0$ and numerically for $Re < 100.0$,[14] and one can hope to obtain at least a qualitative picture in describing regular oscillation and gliding. The analytical treatment of particle deposition on an oblate or prolate spheroid[15] reveals that one can probably expect a scavenging efficiency for a very thin oblate spheroid in a population of particulates with diameters of around 1.4 μm of around 5.5×10^{-2} for 1.0—mm disk type scavenger. In addition, the inclusion of electrostatic and thermo-or diffusio—phoretic forces can increase this value by one order of magnitude under favorable conditions.[16,17] It was concluded that Brownian diffusion dominates the deposition of particulates with $r < 0.1$ μm, phoretic forces in the range $0.01 \leq r \leq 0.1$ μm; electrical forces act in the range $0.01 \leq r \leq 5.0$ μm,

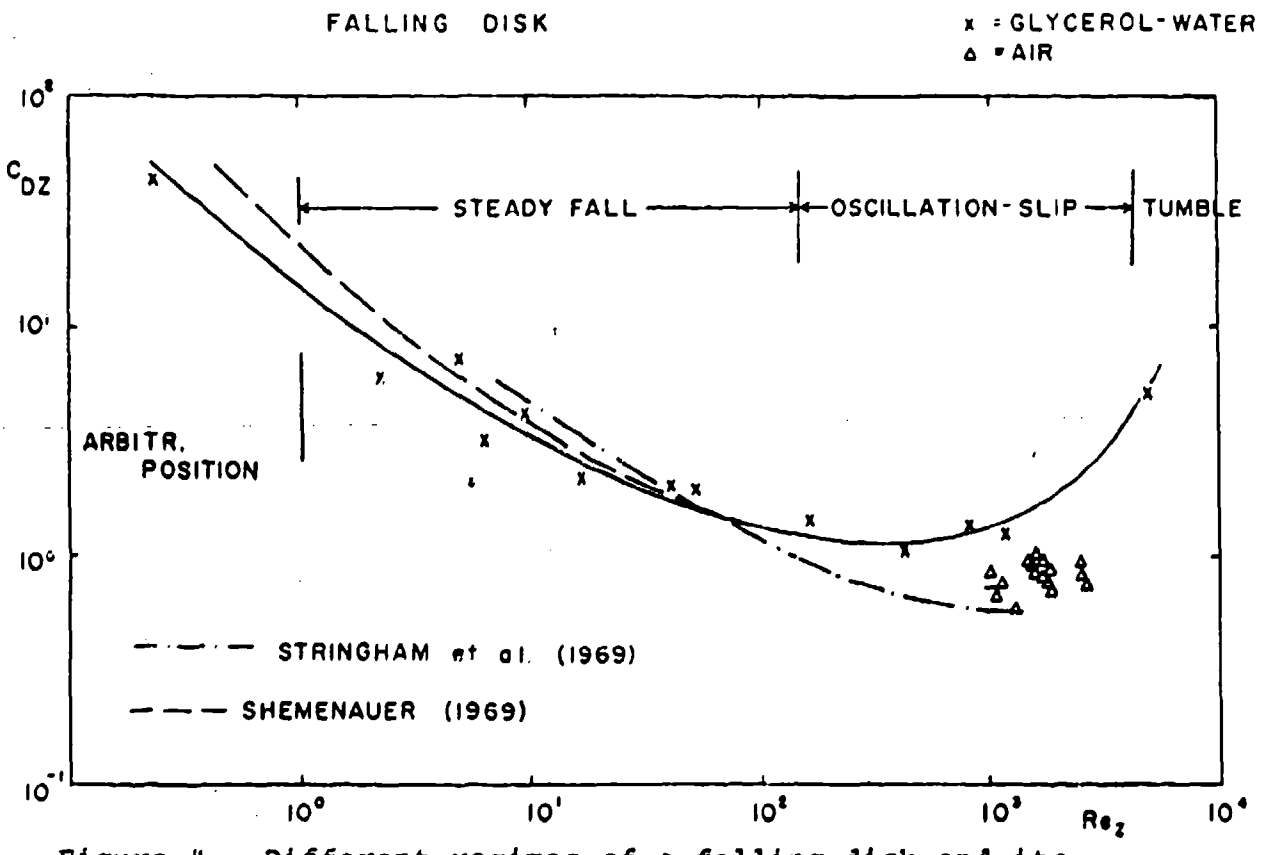

Figure 4. Different regimes of a falling disk and its $C_{DZ} = f(Re_z)$ curve

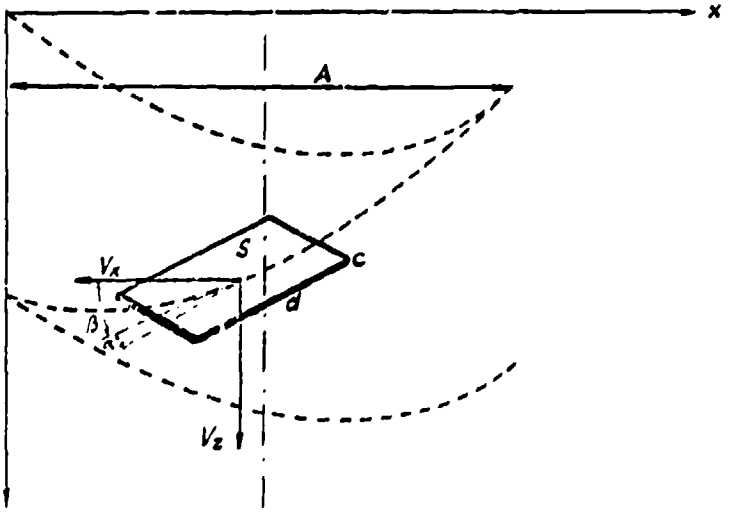

Figure 5. Some of the parameters Featuring the Two-Dimensional Motion of a Settling Scavenger: Velocity Components V_x, V_z; Model Axes d, c; Amplitude of the Motion A

(In addition, the angular velocities around the axes x and y (ω_x, ω_z), the angle of attack α, mass of the scavenger m, cross section S, and scavenger mean density ρ_s are also considered.)

and inertial forces prevail for r > 0.1 μm. Our conclusion is that, apparently, the regime of a steady fall of a scavenging disk does not produce the sought high efficiency of plate-type crystals found by several authors in nature. The logical conclusion was to investigate the oscillatory, gliding and tumbling regime which can under specific conditions (unsymmetrical crystal riming, shear wind, and turbulence) develop in nature. This study should be extended later into the domain of electrostatic and phoretic forces.

The oscillation and sliding was first observed on disks (and on other nonspherical models too) in quiescent air. Time-lapsed camera pictures and stroboscopic record combined with the knowledge of the geometrical parameters of the model and with the known parameters of the medium enable one to identify the following elements of each experiment (fig. 5): scavenger velocity $\vec{V}(V_x, V_y, V_z)$, angular velocity ω_x, ω_y, ω_z, and angle of attack α along the trajectory; total mass of scavenger - m, surface area - S; major and minor (thickness) axes - d,c; and scavenger mean density - ρ_s. Analyzing the scavenger velocity and angular motion, one obtains information about the driving force F. From the scavenger trajectory one can deduce the mean frequency of oscillatory motion - n and the corresponding amplitude A. In addition, we know the medium density ρ_f and the dynamic viscosity μ. The properties of scavenger surface and electric charges are neglected in the first approximation.

Because some of the measured parameters can be neglected or expressed by others, we found, finally, the following dimensionless

parameters important for the description of scavenger motion (in one plane):

$$\frac{V_z \rho_f d}{\mu} = Re_z \; ; \quad \frac{V_x \rho_f d}{\mu} = Re_x \; ; \quad \frac{\rho_s}{\rho_f} \; ; \quad \frac{c}{d} \; ; \quad \frac{F}{\vec{V}^2 \rho_f d^2} = C_D \; ;$$

$$\frac{d \cdot n}{\vec{V}} = f; \quad \frac{S}{d^2} \; ; \quad \frac{A}{d} \; ; \quad \frac{V_x}{V_z} \; .$$

Combination of $(\rho_s \cdot c)/(\rho_f \cdot d)$ leads to Wilmarth's stability number I (for disks $I = (\pi \rho_s c)/(64 \rho_f d)$. The Best number can be obtained from C_D and Re ($Be = C_D \, Re^2$). The ratios V_x/V_z can be expressed by other parameters, so that the A/d, shape factor (S/d^2), and the frequency (Strouhal) number $f = (d\,n)/V$ are with the Reynolds and Best number and Wilmarth's parameter the most important factors featuring the free-falling collectors. The simplified picture of two-dimensional motion of a scavenger does not necessarily reflect the real motion of a falling scavenger, which oscillates in a plane which regularly rotates. In our earlier experiments with models falling in liquids, the period of a rotating oscillatory plane was of the order of several seconds.

The domain of scavenger Reynolds numbers during our measurements in quiescent air covers, in the case of disks, a steady fall regime with very slightly perturbed trajectory (at Re equal to several hundred), regular oscillation with a large amplitude (around Re = 1000), and gliding)at Re > 1000). Exceptionally, a regular tumbling was observed. Models other than thin disks performed differently. For instance, an L-shaped paper model,

several times, showed an intense rotation around a z-axis. For reasons of systematic investigation, a two-dimensional model is described of a falling disk or square based on several simplifying assumptions, such as the independence or predetermined dependence of the disk drag and lift coefficients on time (or position) along the trajectory of its motion. According to the figure 5, the forces acting on a thin-plate type model can be expressed in the form

$$m \frac{du}{dt} = - D \sin \beta + L \cos \beta \qquad (1)$$

$$m \frac{dw}{dt} = - D \cos \beta - L \sin \beta + mg \ . \qquad (2)$$

In addition, the moment of aerodynamic forces (couples) which tends to kipp the plate is approximately

$$I \frac{d^2\alpha}{dt^2} = \frac{\rho a}{2} (u^2 + w^2) \ \ell S \ (C_D \sin^2 \alpha + C_L \cos^2 \alpha) \ . \qquad (3)$$

Equations (1), (2), and (3) can be deduced from the more general system of equations describing the plate motion in three dimensions (Note a of appendix A). The lift L and drag D are expressed in terms of model geometry, velocity, and medium density

$$D = C_D \frac{\rho a}{2} (u^2 + w^2) \ S \ ; \ L = C_L \frac{\rho a}{2} (u^2 + w^2) \ S \ . \qquad (4)$$

Equations (1), (2), and (3) indicate that measuring u, v, α and β, and the time derivatives of u, v, and α, one can obtain a picture of plate (scavenger) motion. A considerable simplification of this description can be obtained if one assumes the equilibrium of forces according to Eqs. (1) and (2) where $\cos\beta = \frac{u}{\vec{v}}$

and $\sin\beta = \frac{w}{\bar{V}}$. Then

$$m \frac{du}{dt} = C_L \frac{\rho a}{2} S \frac{\sin\beta}{\cos^2\beta} u^2 - C_D \frac{\rho a}{2} S \frac{1}{\cos\beta} u^2 \quad (5)$$

$$m \frac{dw}{dt} = -C_L \frac{\rho a}{2} S \frac{\cos\beta}{\sin^2\beta} w^2 + C_D \frac{\rho a}{2} S \frac{1}{\sin\beta} w^2 + mg \quad (6)$$

which for very small β ($\sin\beta \doteq \beta$ and $\cos\beta = 1$) and $w = \bar{w}$ ($\frac{dw}{dt} = 0$) transforms in

$$m \frac{du}{dt} = (C_L\beta - C_D) \frac{\rho a}{2} S u^2 \quad (7)$$

$$mg = (\frac{C_L}{\beta} - C_D) \frac{\rho a}{2} S \bar{w}^2 . \quad (8)$$

The attempt to solve this equation with that for medium resistance, under specific conditions, was made by Dipl. Inq. M. Straka and is presented in Note b of appendix A. The final results can be summarized as follows:

There are only approximate solutions of Eqs. (7) and (8) which can give an idea about the amplitude of the oscillatory motion (Note b of appendix A). In the case of the validity of Stokes resistance law, e.g., the amplitude is expressed by Eq. A-17

$$\bar{A} = \frac{A}{m\omega\sqrt{\gamma^2+\omega^2}} . \quad (9)$$

where A is the amplitude of a lift force (can be obtained with the frequency or angular velocity ω from the experiment), m is the mass of a scavenger, and $\gamma = \frac{C_L}{m}$ (C_L = lift coefficient). Relationship (9) indicates also the fact that, for the same scavenger model, the amplitude of oscillation $\bar{A}$ is inversely proportional to the factor $\sqrt{1+km^2}$, where $k = \frac{\omega^2}{C_L^2}$. In other words, increasing the scavenger's mass m, we will decrease the amplitude of its osscillation. In the case of the resistance proportional to the square of the particle velocity, more complicated dependence of the amplitude

on the scavenger's parameters was obtained (Note b of appendix A).

Assuming the described scavenger plate (of radius R) settling (with the mean velocity along its trajectory $\overline{v_R}$) through the smoke layer of the depth h, one can estimate the effect of the concentration of N_R scavengers on the successive smoke particle removal (Note c of appendix A). After a time νt_1 (t_1 is the time necessary for scavenger settling through the fog), the depleted number is

$$N_{dep}(r,\nu t_1) = \sum_{i=1}^{\nu} n(r,it_1) \exp(-\sigma t_1) ,$$

in which the parameter $\sigma = \pi R^2 N_R \bar{v}_R E(R,r)$ is most important for a large scavenging effect. Its value increases with the coefficient of collection efficiency $E(R,r)$, $\bar{v}_R$, N_R, and R.

The other approach to describe the scavenger motion is entirely empirical, although hampered by considerable errors in determining position, velocity, angles, angular velocity, and acceleration of a swinging plate. For different points along the trajectory of the scavenger, the directional angles of its surface and their time change are plotted together with the velocity and its time derivation. As an example, we plotted velocity fluctuation and acceleration as a function of time (figs. D-13 and D-14). This enables not only estimation of the scavenger's trajectory and the volume swept by a falling scavenger, but also the very important magnitude of acceleration of a collecting surface. The latter parameter, combined with the estimated smoke particle acceleration in the air flow around the scavenger, determines finally the efficiency of scavenging in a non-steady state motion. Several numbers can illustrate clearly how different the deposition might be in accelerated and steady flow (table - Motion characteristics). For comparison, data on falling disks from our old measurements in glycerol-water mixtures are

added (figs. D-15 and D-16).

The table shows clearly that it is impossible to use the measurements made in liquids for describing scavenger motion in the air, as several authors have done in the past. Consequently, these measurements cannot be used for calculating scavenging efficiency for a specific model or for smoke particles. The additional scavenger acceleration in air and non-steady flow field around the model can considerably alter the picture of particle deposition on a plate-type scavenger obtained for a specific angle of attack and steady state flow.[5] The other important conclusion is that, looking at the sequence of data for decreasing sizes of the disks, the larger size and/or weight of a scavenger model slows down the angular velocities. We will attempt to deduce a well-defined relationship between these parameters from our measurements after analyzing all trials.

An attempt was made to characterize the motion of different models falling in still air or in a slight horizontal airflow. The models were made of ordinary light materials enabling to disperses them in large quantities, e.g. from a helicopter. The parameters featuring their motion were deduced from the stroboscopic pictures when the model resumed its reproducible motion important for modeling the scavenging effect if, in the first approach, the hydrodynamic interaction of several scavengers was neglected.

In total, 71 experiments with falling models have been made in quiescent air. The survey of the models used and their main characteristics are presented in table D-1. The main characteristics are: type of the scavenger or of its main cross section, model

Table. Motion Characteristics For Falling Disks

Disk Model	Model Material	Diameter cm	Model Mass g	Medium	Mean Fall Veloc. $cm\ s^{-1}$	AMPLITUDES											
						Velocity $\pm[cm\ s^{-1}]$			Acceleration $[\pm cm\ s^{-2}]$			Angular Velocity $\pm[grad\ s^{-1}]$			Angular Acceleration $\pm[grad\ s^{-2}]$		
						u	v	w	$\frac{du}{dt}$	$\frac{dv}{dt}$	$\frac{dw}{dt}$	ω_x	ω_y	ω_z	$\frac{d\omega_x}{dt}$	$\frac{d\omega_y}{dt}$	$\frac{d\omega_z}{dt}$
PD-2	Aluminum	5.0	6.690	Water	12.25	35.2	27.6	13.7	143.0	157.6	106.9	95	137	63	542	745	259
PD 1.9	Paper	1.9	0.0286	Air	136.5	37.0	62.4	16.8	789	5554	978	419	1608	315	58671	88007	31819

dimensions (e.g. size, diameter, cross section, thickness), mass, vertical fall velocity and corresponding drag and Reynolds number, horizontal velocity components, angle of attack, and mode of fall. Triangles, hexagonal plates, squares, disks, ellipses, and strips with dimensions ranging from 0.7 to 3.0 cm were used; the majority were made of paper 0.018-cm thick. Several models were made of light foam (mainly styrofoam) with material thicknesses of 0.15 cm to 0.62 cm. Besides these models, several experiments have been done with disks made of thin aluminum foil, 0.7 cm in diameter, and with squares or strips made of mesh-type synthetic fiber material. The fibers had mean diameters between 46 and 92 μm. In a square of 1 cm^2 was approximately 18.1 cm total length of 92 μm fiber and 96.08 cm of 46 μm fiber length.

The most important parameters for scavenging calculations are the vertical (settling) velocity of a scavenger of a specific type, the drag coefficient, and the Reynolds number (Re) referred to the largest cross section of the model and its mean fall velocity. The two latter parameters, however, give very little information about the real scavenger motion if the model starts to oscillate and tumble. This is clearly demonstrated in the table in the case of disks 0.66 cm in diameter which were made of paper, plastic, and foam material. Different materials (weights) caused different oscillation, sliding, and tumbling which is reflected in the Re_z numbers and C_D coefficient, ranging from 517 (foam - $C_D \cong 0.067$) to $Re_z \cong 1256$ (plexiglas - $C_D \cong 0.152$). The paper disks (0.018-cm thick) were featured at the same geometry by the $Re_z = 689$ and $C_D \cong 0.447$. For the same reason, the curves in figure 4 for $C_D = f(Re_z)$ differ strongly for disks falling in liquids and in the air

at Re_z > 200 where the oscillatory motion starts to be effective. The same dispersion of points can be observed at Re_z > 500 for different types of scavengers settling, oscillating, and sliding in the air (figs. 6, 7, and 8). There seems to be an influence of Willmarth's parameter I^{18} on the location of the points in the $C_D = F(Re_z)$ diagram for disks; however, the relationship cannot be described by a steadily increasing or decreasing function. On the other hand, all points belonging to the same Willmarth's parameter lie on the line with the same slope very close to -2 (figs 6-8).

The estimates of important factors for inertial particle deposition, such as acceleration (see the analysis in 3.2), were evaluated from stroboscopic pictures. Usually, a stroboscope frequency of 70 flashes per second was used, and the photographic record was plotted into diagrams similar to figures 9, 10, and 11. The amplitude is smaller and the oscillations faster when compared to the model fall in liquids (figs. D-11 and D-12). To this, correspond the components of the flow velocity and acceleration and the components of the angular velocities and their time derivatives. A detailed example analysis was made for a paper disk model, 1.9 cm in diameter, falling in the air with the mean settling velocity of 136.5 cm s^{-1} (the mean Re_z = 1640.5 and C_D = 0.84). The paper disk mass was 0.0286 gm. Due to the use of only one photographic camera, the most reliable components will be u, $\frac{d\omega_x}{dt}$, ω_y, and $\frac{d\omega_y}{dt}$. The components of angular velocity and acceleration around the z-axis are hampered by large errors, as mentioned earlier.

Comparison of velocities and accelerations of models falling in a liquid (fig. D-15) with those in air (fig. D-13) shows that particle settling rate in air is approximately one order of

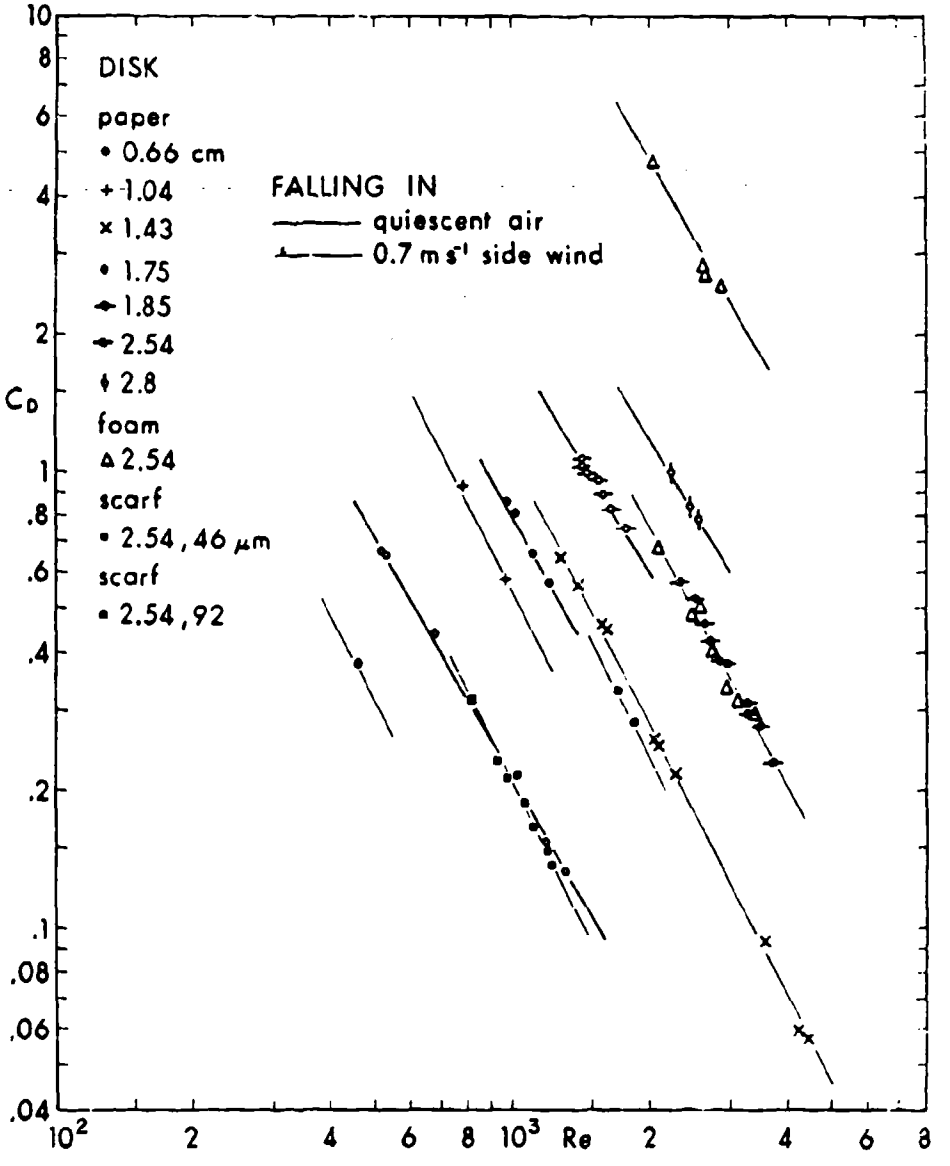

Figure 6. Curves $C_D = f(Re)$ for Different Models of Disks Falling in Quiescent Air and at a Side Wind

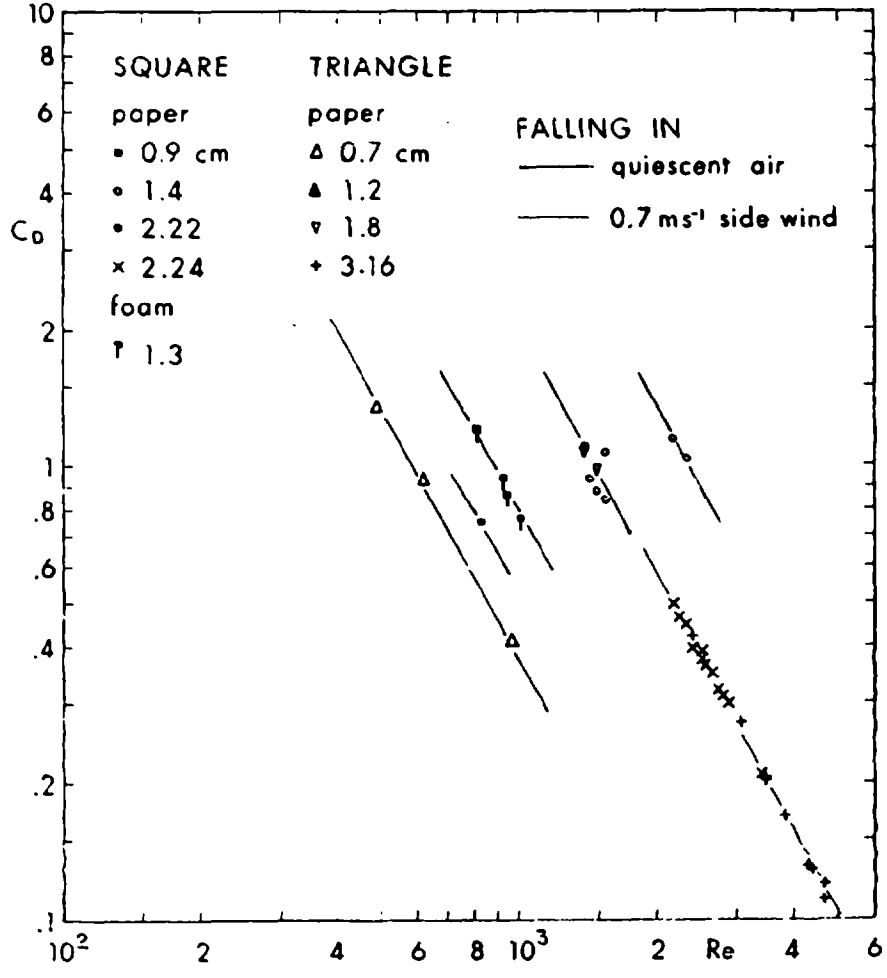

Figure 7. Curves $C_D = f(Re)$ for Different Models of Squares and Triangles Falling in Quiescent Air and at a Side Wind

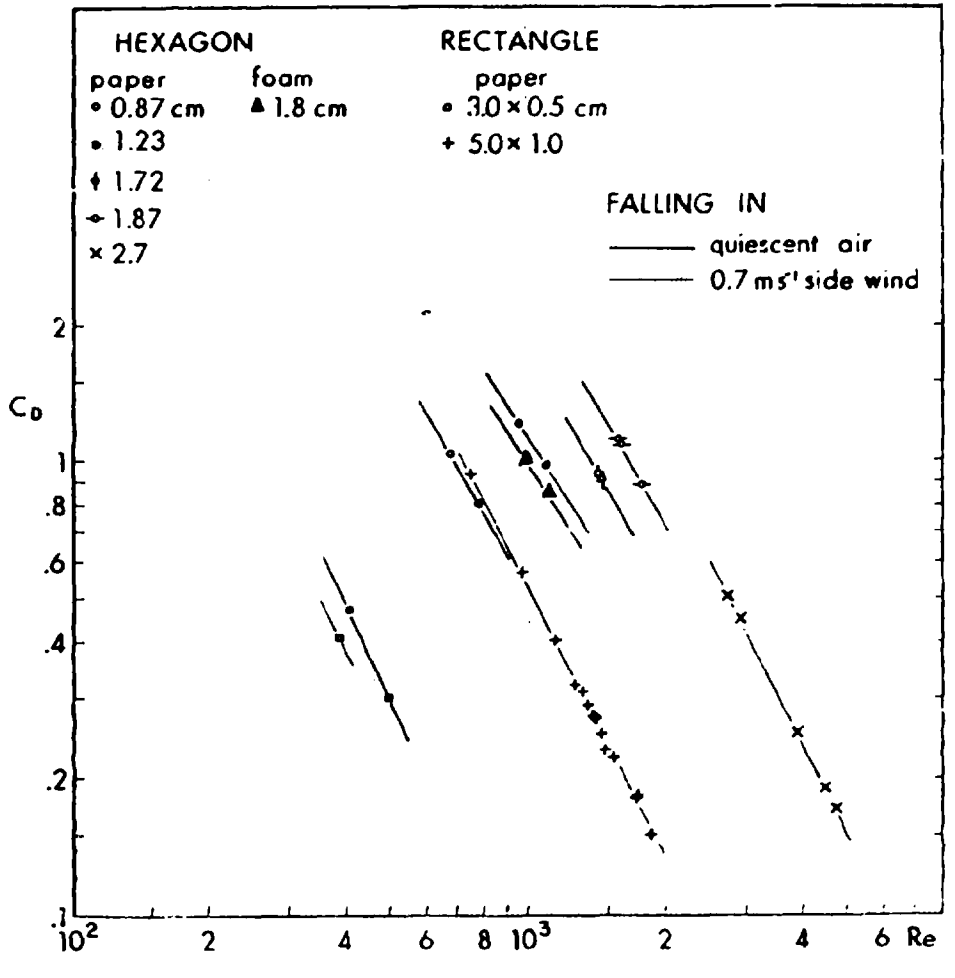

Figure 8. Curves $C_D = f(Re)$ for Different Models of Hexagons and Rectangles Falling in Quiescent Air and at a Side Wind

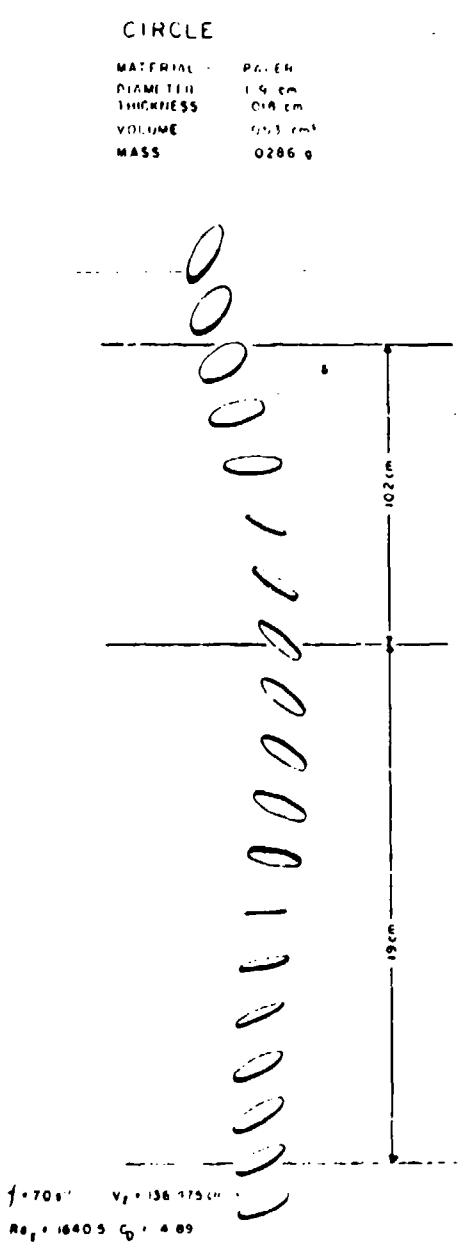

Figure 9. Stroboscopic Picture of an Oscillating Paper Disk (1.9 cm in diameter).

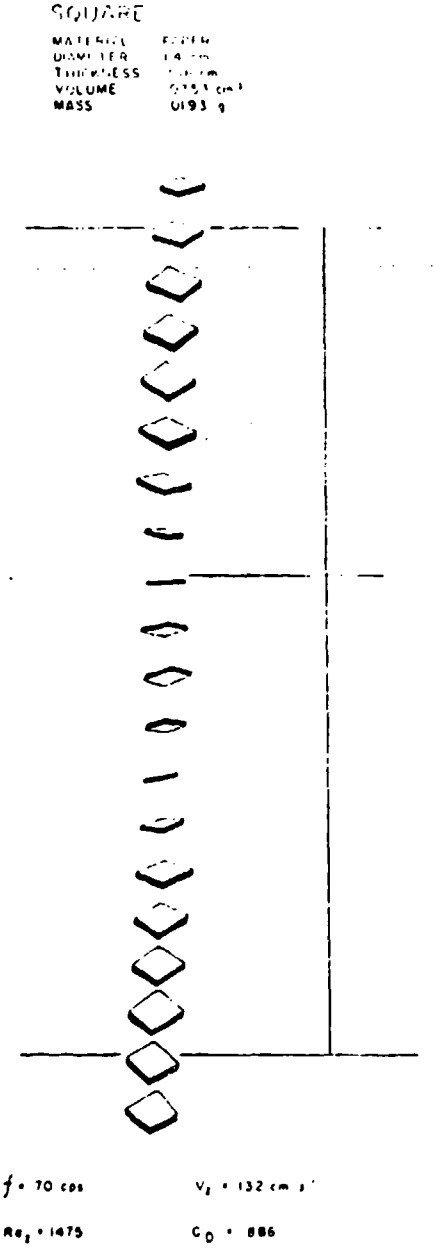

Figure 10. Stroboscopic Picture of a Quietly Settling Paper Square (1.4 x 1.4 cm^2).

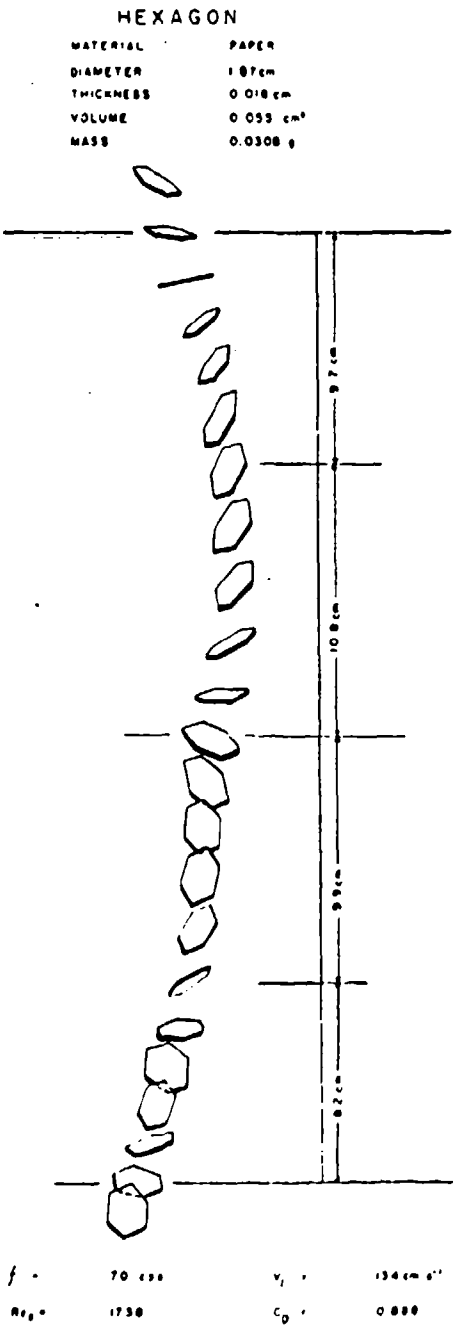

Figure 11. Gliding Regime of a Falling Paper Hexagon 1.87 cm in Diameter

magnitude larger. The most dramatic change happened in the x- and y- components where temporary fluctuations of acceleration in the air surpassed the value of 1000 cm s^{-2}. How far the particulate deposition on a scavenger is affected by these accelerations is discussed in 3.2. The fluctuating accelerations of scavengers falling in the air are paralleled by large amplitudes of the time variation of the angular velocity components (fig. D-14). The maximum values of time derivations ($\frac{d\omega_x}{dt}$, $\frac{d\omega_y}{dt}$, and $\frac{d\omega_z}{dt}$) important for the description of kipp moments and force couples acting on a scavenger are two orders of magnitude larger than those in fluids or slowly moving models in the air.

A glance at table D-1 gives an idea which models should be investigated in more detail in the future. These will be scavengers performing very fast oscillatory, sliding, or tumbling motion, especially those which maintain a large angle of attack for an effective particle scavenging. Among the most promising models are triangles, foam disks, ellipses, and strips (including L-shaped models). In addition, one has to bear in mind that many of these models will behave differently at slight horizontal wind, which usually features the conditions in the atmospheric ground layer.

The influence of the horizontal wind component on the mode of a scavenger fall was investigated in a large environmental chamber especially adapted for this study. As described earlier, horizontal air-flow velocities were maintained between 60 to 70 cm s^{-1} and were constant through the 100-cm vertical path of the settling scavenger. All stroboscopic pictures of falling models were taken in this region (fig. 2). The survey of all measurements at horizontal wind component are presented in table D-2. In total, 108

stroboscopic records at side wind conditions were made with the following models: disks (38), squares (12), strips-rectangles (15), L-shape models (13), hexagons (4), triangles (4), stars (3), and crosses (4). Fourteen experiments were made with different types of veil (mesh) models. Approximately 10% of the most promising cases were analyzed in detail, and the remaining experiments were characterized by the prevailing mode of particle settling that enables a comparison with the settling of the same model in quiescent air.

It should be stressed that the drag coefficients C_D and Reynolds numbers Re in table D-2 have an orientational character. Their meaning as a mean value is very difficult to interpret in simple physical relationships due to the nonlinear effects involved. They can, however, reveal how far the simple steady fall will fit a description of a specific falling scavenger, which is important to the validation of any numerical model. This is clearly demonstrated in figures 6, 7, and 8 where individual data points from the motion of falling scavengers are plotted in the C_D - Re diagram. Simultaneously a comparison of $C_D = f(Re)$ curves is made for models falling in quiescent air and at side wind conditions.

If one assumes that a falling scavenger will reach, after a certain time, a quasi-steady mode of motion, then its drag coefficient C_D can be expressed in the form

$$C_D = \frac{2g(m - \rho_a Q)}{\rho_a \bar{V}^2 S}, \qquad (11)$$

where g is the acceleration due to gravity, m is the scavenger's mass, ρ_a is the air density, Q is scavenger's volume, $\bar{V}$ is the

mean (terminal) scavenger's velocity, and S is the maximal cross-sectional area of the scavenger to the air flow, which is usually expressed by a characteristic length of the scavenger (e.g. diameter). Because the buoyancy force in the air is negligible, and $\bar{V}$ can be expressed by Re, we can write for a disk

$$C_D = \frac{2gh\ \rho_a\ \rho_s\ D^2}{Re^2\ \mu^2}, \qquad (12)$$

where h is the scavenger's thickness, ρ_s is the scavenger's density, and μ is the air dynamic viscosity. Eq. (12) shows that for the same model and the same environment, the curve $C_D = f(Re)$ should have the ideal slope - 2. This is shown in figure 6 for disks, where only slight deviation of this rule is observed, due probably to the excessive sliding or to the imperfect model fabrication. An important finding seems to be the fact that both curves for disk models settling in quiescent air and at side wind conditions can be described by a simple relationship (12), except for thick models made of styrofoam. Even the motion of mesh (scarf fiber) models can be described by Eq. (12); however, the curves are considerably shifted in the C_D - Re diagram. A shifting towards higher values of the C_D at the same Re was also observed when curves for a similar model falling in quiescent air and at the side wind were compared. This shifting, probably strongly expressed for scavengers of the smallest size (d = 0.66 cm), can be referred to the Best number if one realizes that

$$Be = \frac{2gm\ \rho_a\ D^2}{S\mu^2} \equiv C_D\ Re^2\ .$$

A picture similar to that for disks can be deduced from figures 7 and 8 for squares, triangles, hexagons, and rectangles. Because several models of different types were made intentionally with the same maximal cross section (e.g., 5.0 cm^2), an interesting comparison has been made of how far the scavenger shape changes its aerodynamic characteristics (C_D, Re) at side wind conditions. In figure 7, data are plotted for squares (with a side of 2.24 cm) and triangles (right angle with two sides of 3.16 cm) falling at a side wind of 0.7 m s^{-1}. Both curves for two different models with the same area S fit very well and indicate that unless an intensive sliding or tumbling occurs (rectangles in fig. 8, or ellipses), the cross-sectional area (at the same thickness h and material density ρ_s) determines sufficiently the mean settling parameters of a scavenger.

3.2 Deposition of Smoke Particles on a Scavenger.

The deposition of smoke particles on a scavenger can be investigated in several different ways. Theoretical study is based on the known steady air-flow field around the falling scavenger, the known smoke particle properties and their size distribution, and the force field acting on a particle moving close to the scavenger. This complex process might include inertial, gravitational, electrostatic, and phoretic forces. It is almost impossible to assess the significance of individual processes under specific conditions encountered in a smoke cloud.

The computation of the viscous flow field around an ice crystal (scavenger) has been done for a two-dimensional case and different angles of attack by Sasyo[5] (figs. D-17 and D-18) and later by Pitter et. al.,[7] for low and intermediate Reynolds numbers. Schenewerk[19],

working in the author's group, checked the feasibility of numerical techniques described by others and worked out a method to model the flow field around a two-dimensional obstacle for Re = 1000 (fig. D-19). Finally, no original approach similar to the efforts by Rimon[20] or Pitter and Pruppacher[21] was attempted in this study. The main reasons were the ample research program developed in other institutions (e.g., Parker[22], and Martin et. al.[15,16]) and the notion of a limited applicability of similar studies for the transitional region of Re when the scavenger starts to oscillate and slide.

Therefore, the main attention was paid to the evolution of experimental techniques enabling collection and identification of smoke particles deposited under well controlled conditions on scavengers. The final goal was to determine experimentally the collection efficiency of a specific scavenger. We attempted to use independently the deposition on scavengers freely settling in the cylindrical smoke chamber and on models fixed in a small horizontal wind tunnel. Special attention has been paid to the potential combination of inertial deposition with diffusional deposition on mesh type models, and to the hydrodynamic interaction of two scavengers that are close together.

The determination of the scavenging efficiency Λ of a specific model is based on a traditional scenario of estimating the removal of aerosol particles after a scavenger fell during the time t through the smoke cloud:

$$n(t) = n(o) \exp (- \Lambda t) . \qquad (13)$$

In this equation n(o) is particle concentration at a time t=0. If one assumes that the collector is much larger than the smoke

particles (the smoke aerosol does not disturb the flow around the scavenger) and that the smoke particle concentration is so low that the individual particles do not interfere with each other, Starr and Mason[4], Sood and Jackson[23], Sasyo[5], and others have defined a mean scavenging (collection) coefficient in a form similar to

$$\bar{\Lambda} = \sum_i P_i \int_{r_2}^{r_1} \pi (R_i + r)^2 E_i(R_i, r, \vec{U}, \vec{u}) [\vec{U}(R_i) - \vec{u}(r)] N(r)\, dr. \quad (14)$$

In this equation R_i and r are the "radii" of the scavenger (e.g., a disk) and of the "spherical" smoke particles, and $\vec{U}(R)$ and $\vec{u}(r)$ are their corresponding velocities. $N(r)$ is the smoke particle size distribution function and $E_i(R_i; \vec{U}, \vec{u})$ is the kernel of the collection efficiency for i-th scavenger, with a mean probability of occurrence P_i. The simplest form of the Eq. (14) assumes a monodisperse smoke aerosol, the same size and shape of scavengers, and a kernel of the collection efficiency similar to that defined by Langmuir as $E_L = \frac{\pi y^2}{\pi (R+r)^2}$ (y is the initial offset of the aerosol particle center of the line going through the scavenger's center). This form will be used often in this study.

The experience gained from the former study of supercooled droplets scavenged by ice crystals[6] was used in the pilot experiments with falling scavenger models in the cylindrical chamber; the results, however, were inconclusive. The NaCl aerosol was very unsuitable because of the uncertainty about the particle composition at humidities between 75% and 85% RH (fig. D-3) and because of sample contamination at the bottom of the chamber. It was impossible to increase the NaCl aerosol concentration in the chamber to a value necessary for obtaining statistically significant results (more than 5000 p cm^{-3}), in spite of its high

concentration at the source. The maximum number of NaCl particles deposited on the plastic disk scavenger, 0.66 cm in diameter, strongly varied between several tens and hundreds - if both sides of a scavenger coated by a sensitized gelatin layer were evaluated[24,6]. Assuming a mean particle concentration of 104 per cubic cm (measured by laser cavity spectrometer) and a scavenger path of 160 cm, we obtain a scavenging efficiency of 0.175% for 100 deposited particles on the 0.342-cm^2 surface of the plastic disk.

Much higher concentrations in the cylindrical settling chamber were attained with titanium chloride aerosol. However, a simple calculation shows that a $TiCl_4$ particle concentration of 10^4 cm^3 in the sedimentation chamber and a disk with d = 0.66 cm in diameter falling along the path of 1.6 m (in 0.6 sec) corresponds to the total number of 8.208×10^3 smoke particles deposited on the scavenger's surface, if the collection efficiency equals 0.015. This illustrates sufficiently the problems inherent to direct particle scavenging in an experimental tank where the path of falling models is not sufficient to ensure reproducible results. For this reason, scavenging was investigated in an aerodynamic horizontal wind tunnel where titanium chloride or red phosphorus particles were deposited on stationary models. The main advantage is that the experiment can be run for tens of minutes at almost constant parameters. The disadvantage of a fixed model condition will be improved in the future where the models will slightly oscillate around the mean position in an aerosol flow.

Wind tunnel experiments were performed with disks, hexagons, and rectangles fixed on a needle in a smoke cloud moving with a mean flow rate of 1.0 and 1.8 m s^{-1}. The particle size and position on a scavenger were evaluated from the photographs taken in

both optical and scanning electron microscopes. The estimate of the scavenger's collection efficiency was made under the assumption that it is evenly covered by smoke particles (which was supported by observing the pattern of deposited particles at a low magnification), and that one or two sets of pictures (each set contains more than 25 pictures) taken across the scavenger's front and rear surface are sufficient for reproducible results. A background laboratory aerosol was deposited at the same air flow on the model for comparison.

The results of the evaluation of red phosphorus particles on a plastic disk 0.5 cm in diameter are plotted separately for front and rear sides (figs. 12 and 13). The distance from the scavenger's center ($r/R = 0$) to its edge ($r/R = 1.0$) was divided into 27 intervals (photographic frames corresponding to the 640 x magnification in an optical microscope). For each frame, particle size frequency was evaluated on the basis of 20 particle size classes (0.5 μm to 10 μm). In both figures the total particle concentration (thick line) is plotted together with four or five distribution curves for particles having the highest frequency (0.5, 1.0, 1.5, 2.0, and 2.5 μm). The total number of deposited particles (6,284 for front side and 9,590 for rear side) along the disk radius (with a width of 157.5 μm) was used to calculate the total number of particles with the size distribution similar to figure D-8 scavenged by the model. For a 4-min. sampling time the front side had 313,361 cm^{-3} and the rear side, 478,220 cm^{-3}. This, compared to the smoke particle concentration in the wind tunnel (11,096 cm^{-3}), gives a scavenging at an air flow of 1 m s^{-1} of 2.02% in mean. The efficiency is different for differently sized smoke particles

(figs. 12 and 13). There is a basic difference between the pattern of deposited smoke aerosol on the front and rear sides of the scavenger. The first has the maximum of deposited particles close to the edge, where inertial forces can play an important role. The rear side of a scavenger is featured by a very high concentration of small particulates around $r/R \cong 0.5$. One can hypothesize as to the influence of the almost steady vortex behind a falling disk at the Re = 317. Other forces which might act on the circulating aerosol particles in the wake behind a disk must also be considered, especially close to its surface (electrostatic and phoretical). In conclusion, the deposition on the rear side of a plate-type scavenger in this domain of Re and St (Stokes numbers) is real and significant. This is confirmed also by figures 14 and 15, valid for a 1.0-cm diameter disk at Re = 633. In this case, the calculated scavenging efficiency was 2.69%. There is a significant change in the pattern of deposited smoke particles on the rear and front sides of the scavenger. Unlike the case of a disk falling at a Re = 317, the fall of a larger disk of 1.0 cm in diameter (Re = 633) is characterized by more intense air fluctuation in the wake. This might explain the more uniform deposition of smoke particulates on the rear side, and on the average a lower number of deposited particles on the rear side compared to the front side of the disk.

Pilot experiments with smoke particle scavenging in a cylindrical settling chamber have been done with scavengers made of artificial fibers (veil and scarf fabrics). An assumption was made that these materials with small fiber diameters (46 μm and 92 μm) might support smoke particle deposition on their surface.

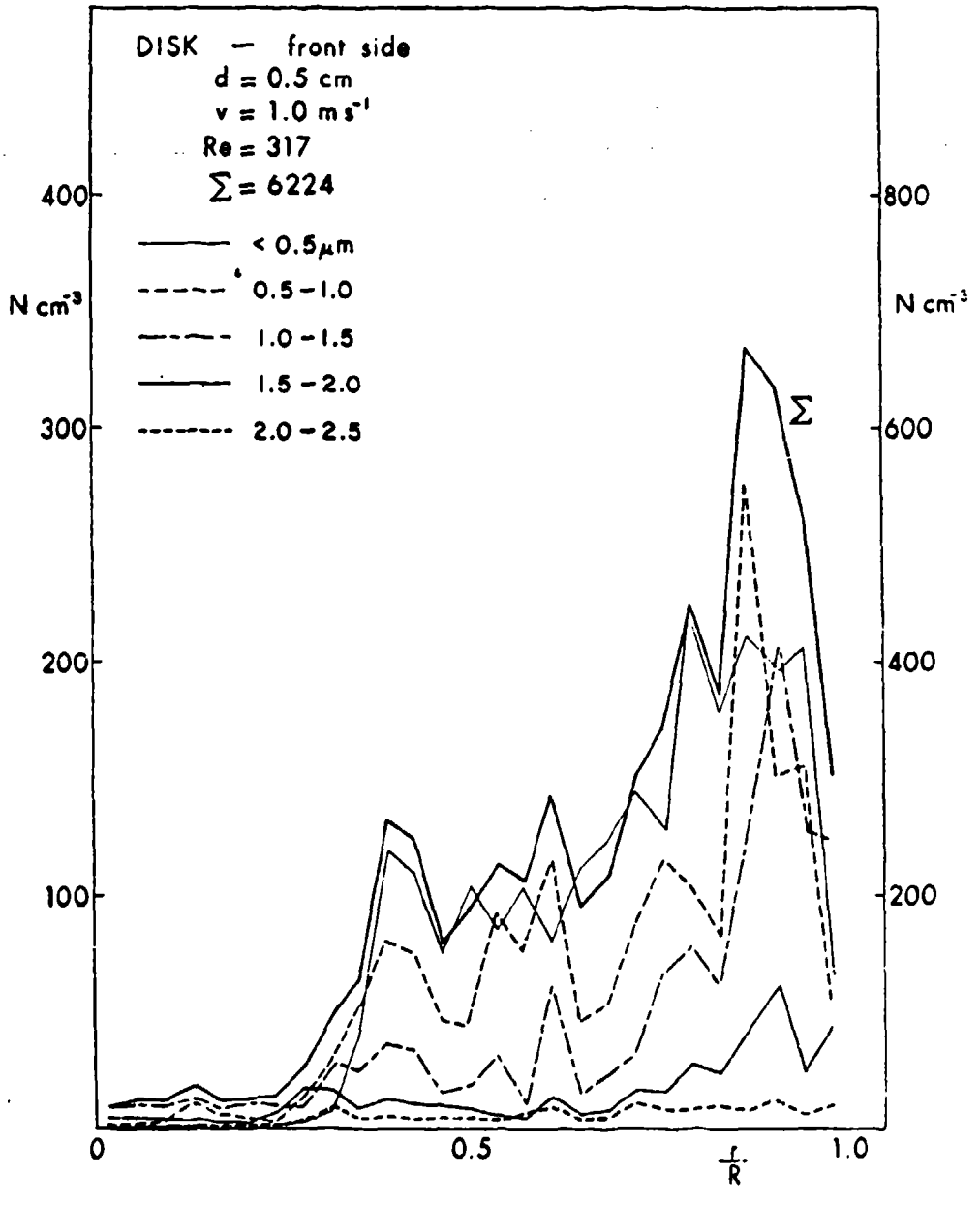

Figure 12. Smoke Particle Distribution on the Frontal Side of a Disk (d = 0.5 cm)

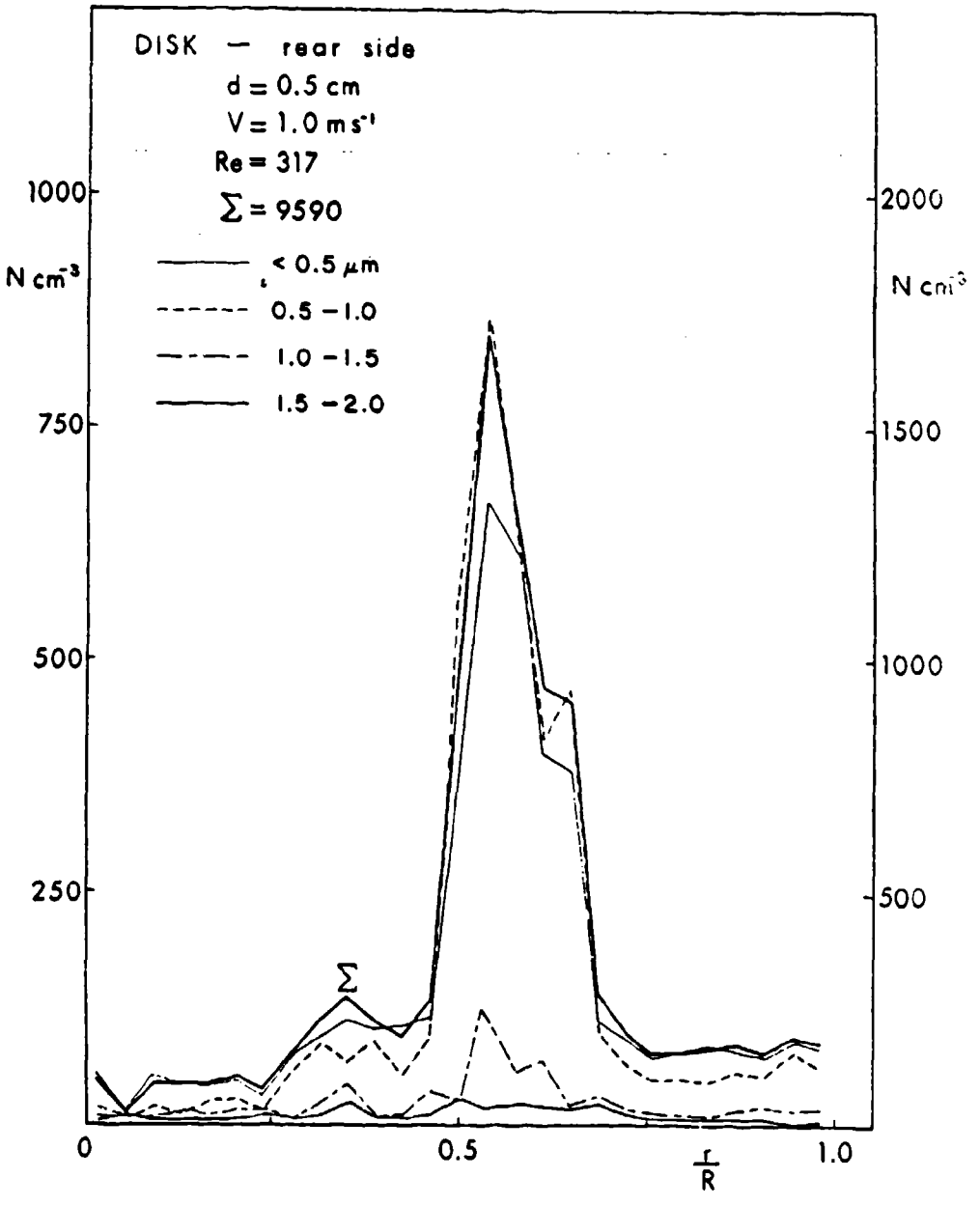

Figure 13. Smoke Particle Distribution on the Rear Side of a Disk (d = 0.5 cm)

In appendix B, the results of a simple calculation of the scavenging capability (Stokes number) of these fibers and estimates of the scavenging efficiency in % are presented. Two sets of experiments were performed: dropping scavengers of different types of veil material into a $TiCl_4$ cloud and placing an electromicroscopical grid in a red phosphorus or $TiCl_4$ smoke in a wind tunnel. Compared to the background aerosol (see 3.4), the mesh-type scavengers were effective (tables D-4 and D-6); however, no quantitative data are available yet. There seems to be good reason to continue these experiments and extend them into a systematic study in a wind tunnel. Organic or inorganic substances should be found which could crystallize in the form of fine aggregates and fibers when dispersed in the air and act as smoke particle scavengers. Scavenging by chemical substances will be the subject of a patent application by the author of this report.

3.3 Effect of a Large Population of Scavengers

There is very little information about the effect on motion and smoke particle scavenging of a large population of scavengers falling simultaneously. Khorguani[25] observed the behavior of many spheres released in a special arrangement in a liquid. He was able to observe that after a certain time an "internal circulation" among the spheres evolved, depending on the initial conditions. Podzimek[26] evaluated the acceleration and distortion trajectories of two- or three-plate or columnar type models falling simultaneously in a liquid. The most important result was the determination of a critical distance within which a plate falling in the wake of its precursor will reach it and, under favorable configuration,

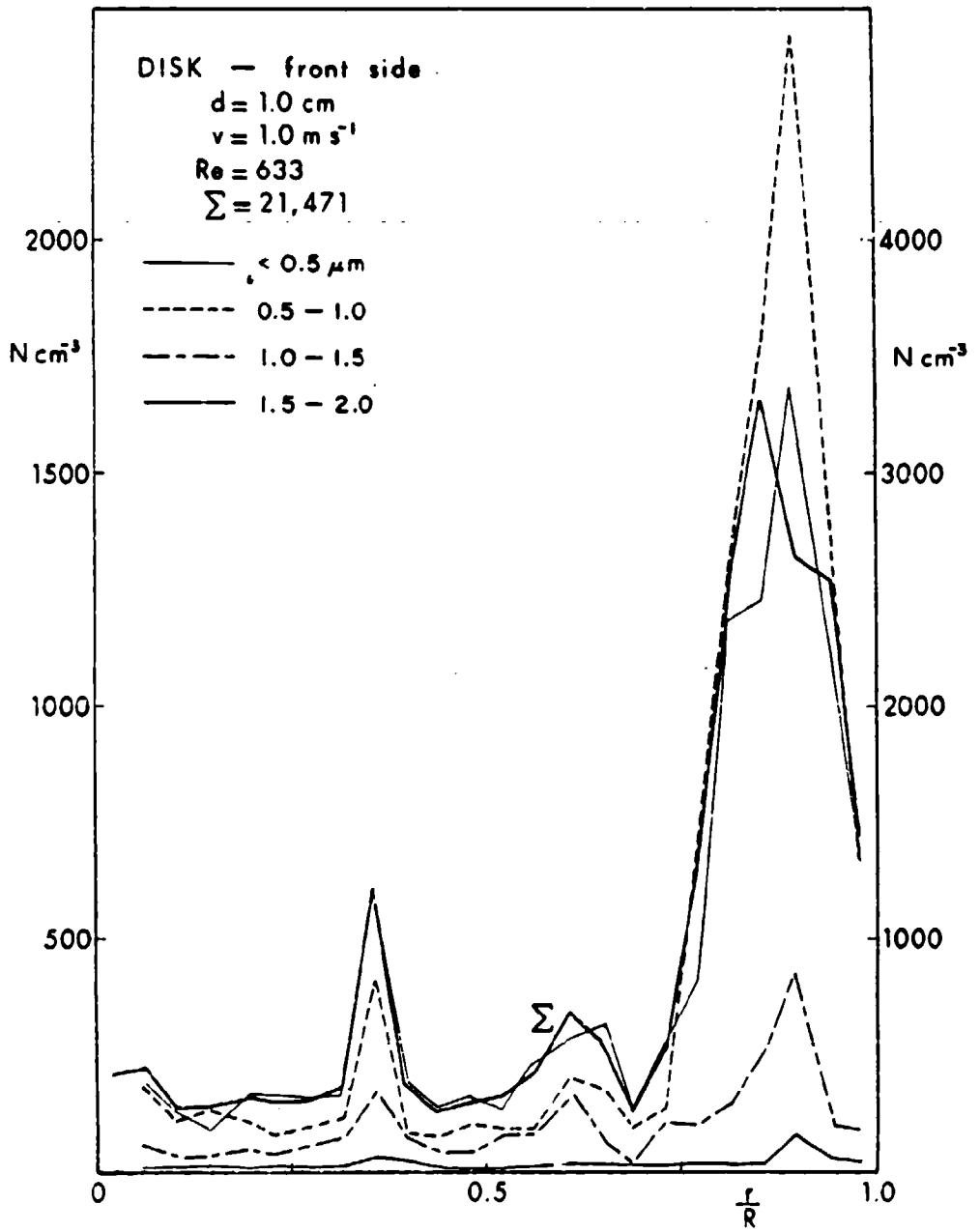

Figure 14. Smoke Particle Distribution on the Frontal Side of a Disk (d = 1.0 cm)

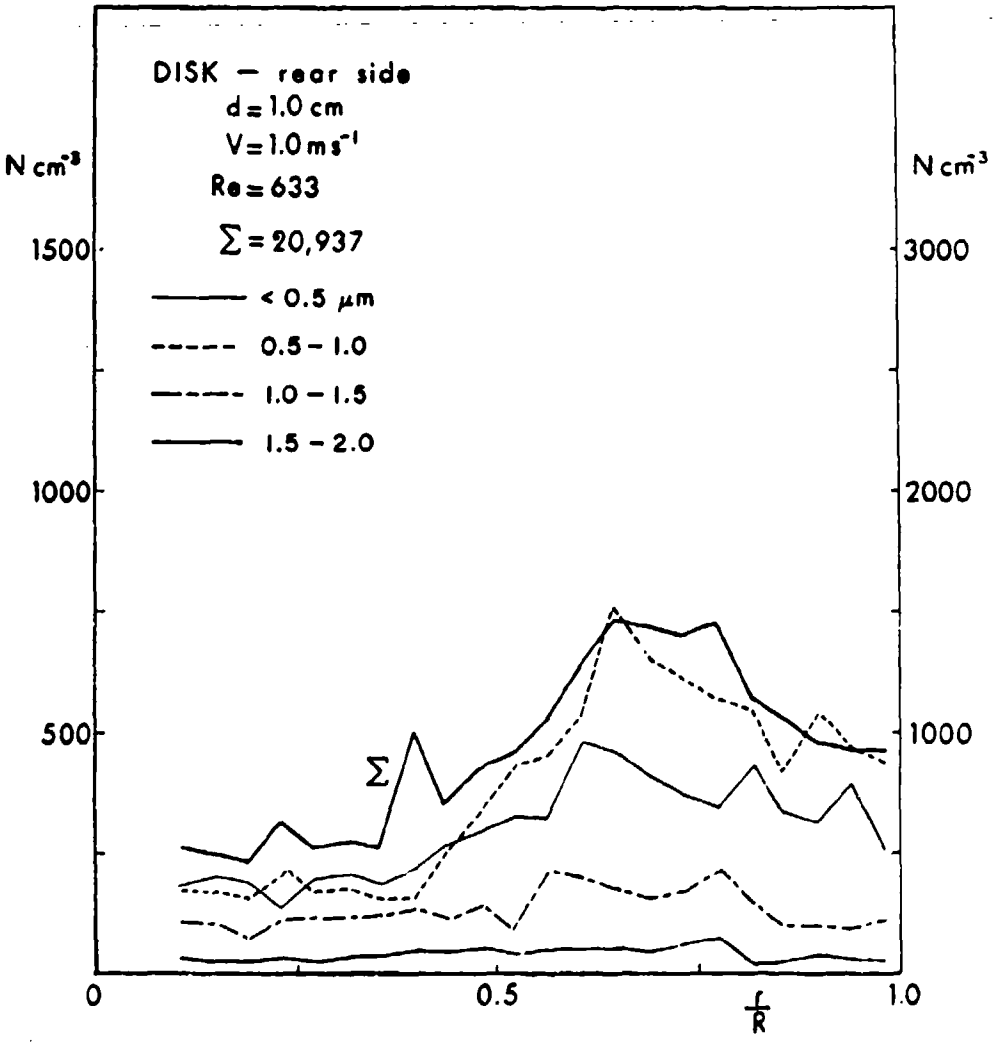

Figure 15. Smoke Particle Distribution on the Rear Side of a Disk (d = 1.0 cm)

make a stable aggregate. These hydrodynamic forces, acting over a small distance, will be influenced in case of a large population of scavengers by the air motion which is entrained in the wake behind them. A similar problem is treated in precipitation physics as a "falling particle zone effect" and discussed several times in the literature.[27, 28]

A few examples will be given here of the behavior of models (scavengers) released simultaneously and recorded on a stroboscopic picture. These observations were aimed at showing the potential problems of experimenting in the air. However, in a real atmosphere, there is a very limited possibility for controlling the homogeneous dispersion of a large quantity of scavengers.

Experiments have been conducted with several models of the same type falling simultaneously in the quiet air and at a horizontal air flow of 0.7 m s^{-1}. There is solid evidence that the models do hydrodynamically interact at a distance or several diameters (or a multiple of their main dimension). In this way, a change in velocity and additional accelerations are observed in the case of two falling disks, squares, rectangles, triangles, and L-shape models. The change in settling velocity after the aerodynamic interaction of two models amounted up to 60% in the case of small paper disks. Less distorted were the velocities and trajectories of interacting L-shaped models, which usually differed within a few percent. A detailed evaluation of the effect of aerodynamic interaction, e.g., on the change of acceleration, was not in this program. This would require the use of two photographic cameras and a very powerful stroboscope.

Unlike fluids of high viscosity,[26] no markable sticking and clustering of paper scavengers has been observed in the air. A

sufficient number of observations have not been made for analysis of foam and plastic scavengers.

In addition, the scavenger distribution in the falling zone will certainly be influenced by the concentration, size, and shape and by the method of dispersion, which might generate electrostatic charges. These factors should be investigated to find the best technology for scavenger dispersion.

As an example of the relevance of similar investigations to the practical application of scavenging technique in the field, we performed a model experiment in our laboratory wind tunnel with two metallic pieces 3 mm x 1 mm placed one behind the other (1.2 mm apart) in a crossed position. At a flow rate of 1.82 m s^{-1} (Re = 114), the $TiCl_4$ aerosol was deposited for 24 minutes on both plates, and the effect of interacting aerodynamic fields on the particle distribution observed. Figure D-20, taken in a scanning electron microscope at the magnification 33 x, shows the particle deposition on the front plate (in the lower part of the figure) and on the other plate which was placed in a crossed position behind the front one. There is a marked difference in smoke particle distribution on both plates which simulate paper punches from the punch card machine. The wake behind the first plate appears clearly. The particles are evenly distributed on the front plate and, in mean, they have smaller sizes than those close to the edge of the wake marked on the plate behind. There is an indication that increased coagulation happens in the wake behind the first plate, as suggested by table D-7 which shows a rough evaluation of particles deposited on both plates.

The concentration of particles deposited on the second plate

is greater than that on the frontal plate in spite of the fact that, in its central part, the particle concentration is much lower due to the wake from the first plate. This stationary configuration of two scavengers can simulate the real situation only to a limited extent; however, it shows how important the mean distance is between scavengers for an optimal effect. Future research should assess the effect of air entrainment and mean intensity of turbulence on particle deposition. Unfortunately, only smoke particles larger than the limit of particle detectability at this low magnification (33 x) (that means with $d > 1.5$ μm) have been evaluated.

This pilot experiment brings new momentum into the search for a scavenger form with maximum scavenging efficiency: a scavenger with "internal ventilation" (composite structure), or the use of many small scavengers, due to their aerodynamic interaction, will increase the coagulation of small particulates and, in this way, their deposition on scavengers.

3.4 Effect on Light Extinction Due to a Zone of Falling Scavengers

Extinction was measured in the cylindrical settling chamber, 65 cm above the bottom with a LED collimated light source of λ = 6700Å and a Bell and Howell photodiode detector (Model 529) connected with a transmission meter. The beam, 1.6 cm in diameter, energizes a silicon photodiode receiver, and the signal is automatically recorded and evaluated in terms of transmission or extinction.*

---

* The equipment was designed by Dr. J. L. Schmitt aided by D. Reed.

The smoke aerosol, generated via reaction of the vapors of titanium chloride with humidified nitrogen, flowed for approximately 10-15 minutes into the chamber through an orifice in the top lid. Another 10 minutes (mean) was needed to stabilize and homogenize the smoke before the extinction measurement started. The scavengers were dropped 20 minutes after the supply of aerosol stopped; extinction measurement continued afterwards for at least 15 minutes when one scavenger was dropped, and for approximately 30 minutes when several scavengers were released. Because we wanted also to evaluate the number of smoke particulates collected on different types of scavengers (paper, plastic, and aluminum foil disks, and fiber mesh models), a special catching device was placed at the bottom of the chamber to cover the deposited models with a lid to prevent model contamination by other slowly settling smoke particles.

The scenario for investigating the effect of a zone of falling scavengers on light extinction follows:

We assume that detector voltage is proportional to the incident light intensity I. If the light path (ℓ = 78 cm), the light beam width D = 1.6 cm, light wavelength λ, and the reference light intensity I_o are kept constant, the change of the light intensity I can be expressed in the form

$$\frac{dI}{dt} = \frac{1}{C_1} \frac{dV}{dt} , \tag{15}$$

where I is only a function of particle concentration n and size distribution $f(r_i)$, and the constant C_1 is defined if we know ℓ, D, λ, I_o, and the characteristics of the detector. If one assumes further a monodisperse aerosol of spherical particles ($r = r_m$)

with constant optical properties, one can relate directly the change in light intensity (detector voltage) to the change of smoke particle concentration

$$\frac{dN}{dt} = \frac{1}{C_2} \frac{dV}{dt}. \qquad (16)$$

In Eq. (16) C_2 depends now on N_o, r_m, ℓ, D, λ, I_o. In observing the clearing of a smoke in our cylindrical chamber, we further simplified the situation by assuming that at the time t = 0 the light intensity I_o is defined by the light source, the medium and detector properties, the particle concentration (n_o), and size (r_m) and that the Mie function remains constant during the extinction measurement. This implies a negligible influence of particle coagulation and sedimentation on size distribution and smoke particle composition. This is not true at a particle concentration of about 2×10^4 cm^{-3}. On the other hand, the effect of coagulation and sedimentation cannot affect sudden changes in extinction which last for 1 or 2 minutes in the particle size range and concentration considered in this case. This is supported by monitoring the concentration of condensation nuclei in the settling chamber with a Gardner or General Electric counter. In any case, the estimated effect of particle scavenging can be corrected to particle settling and coagulation if the particle size spectrum and concentration are monitored. Rarely did the $TiCl_4$ fog last more than 1 hour, which is demonstrated in fig. D-21 where Aitken nuclei counts and Lindauer-Castleman (1971) model calculations for a typical $TiCl_4$ fog dissipation (with initial size distribution according to

fig. D-5) are presented together with the extinction measured during dissipation. The meaning of the term of extinction with the explanation of how our diagrams are plotted is contained in the appendix C.

The Eq. (16) can be converted into a more convenient form if one considers that the total number of particles in the light beam is $N = \pi (D^2/4)\ \ell \cdot n$, where n is the particle concentration in 1 cm^3. This is justified, however, only when scavengers released at a wide opening in the top lid are dispersed homogeneously and cover the whole chamber's space after a settling path of approximately 0.9 m. In reality, we found that a Gauss distribution would describe better the scavenger distribution around the axis of the cylindrical chamber. Also the dispersion cone angle is different in mean for different type of collectors. For paper punches 1x3 mm is around 30°. One can observe wider dispersion for paper disks 0.7 cm in diameter and very little for fiber mesh models falling in quiescent air. This type of correction was not considered in the following pilot experiments, which were aimed at checking the practical applicability of scavenging technique without taking into account all possible effects, (e.g., the effect of a cylindrical vessel of specific dimensions) on the scavenger zone motion and mean scavenging efficienty.

Most of the scavenging experiments were performed with paper disks 0.7 cm in diameter and meshes with fine fibers of nylon and polyvinylacetate (with fiber diameters of 46 μm and 92 μm). Usually scavengers were dropped in one group containing several tens or hundreds of collectors. Dropping the scavengers in several

groups in time intervals of several minutes seemed to yield better results (figs. D-22, D-23). In general, the total concentration of scavengers was found insufficient. During the first 50 experiments and after making an estimate of the effect of efficient mesh type models (0.812% collection efficiency for 32 square mesh 1.5x1.5 cm^2 models dropped through the sensitive volume of the light intensity sensor) on smoke clearing, the results were found insignificant and inconclusive. More detailed justification of this statement is in the appendix C.

Another series of experiments investigated the effect of a large quantity of small scavengers (computer-card paper punches 1x3 mm), without attempting to establish a theoretical model of scavenger dispersion (in a relatively dense cloud), and the scavenging mechanism of the $TiCl_4$ particles. The scavenger density was estimated from weight, so that 39,367 punches corresponded to 1 ounce. Approximately 1028 scavengers fell from 1 ounce through the sensitive volume of the light sensor. One of these experiments is described in fig. 16 where the detector voltage is plotted as a function of time. Arrows indicate the time at which 4-ounce batches of punches were dropped five times into the settling chamber filled with $TiCl_4$ smoke. The mean concentration of Aitken nuclei (smoke particles) was at the beginning of the experiment, around 75,000 AN cm^{-3}, and at the end, 28,000 AN cm^{-3}. A definate and long lasting effect occurs from dropping a large quantity of small scavengers. Each dropping was followed by an improved transmission of light (visibility) and a dramatic change of the slope of the V = f(t) curve. A simple formula was used to calculate the change of the visual range L_2 from its value before

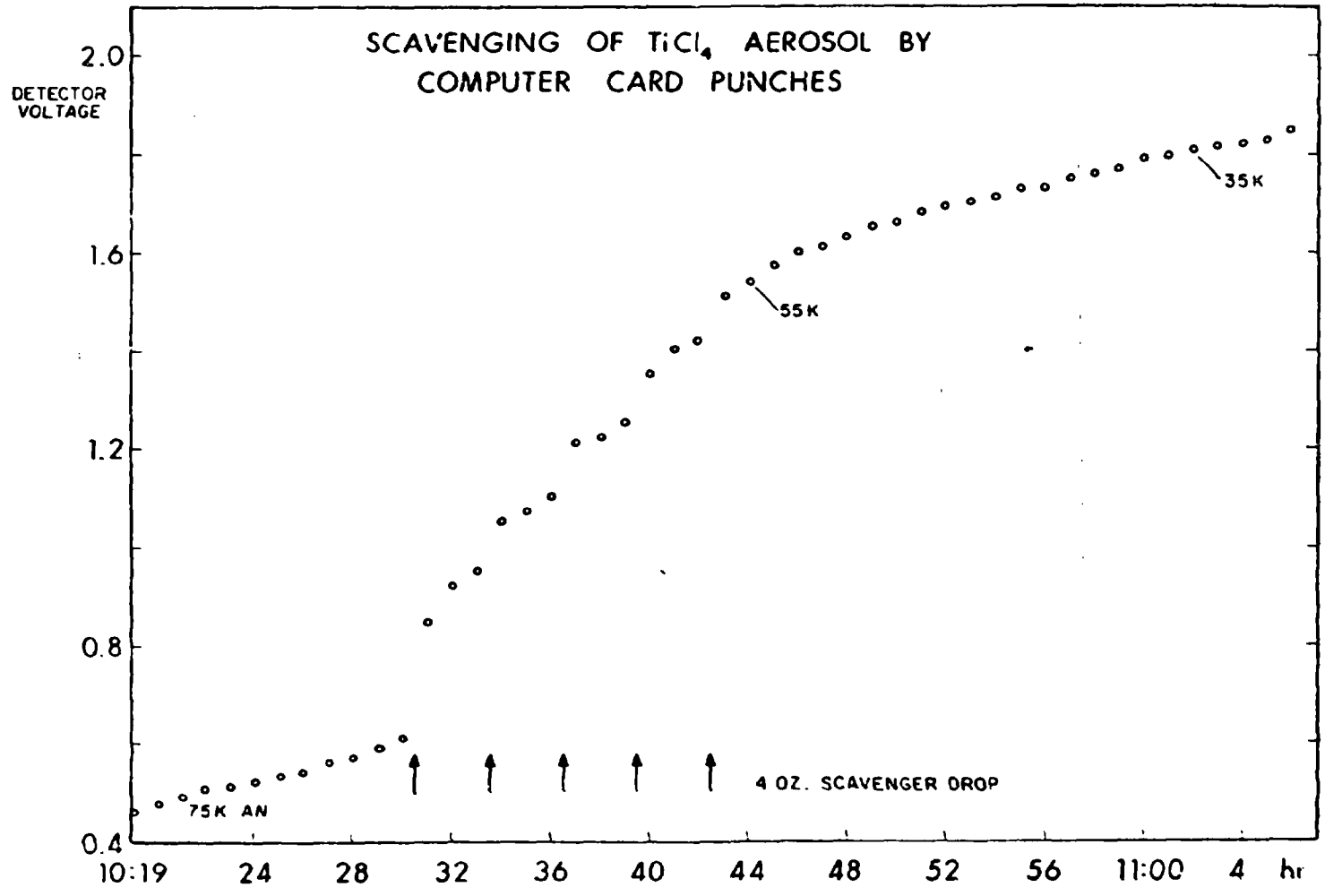

Figure 16. Measurement of Transmission Light Detector Voltage in a Dense $TiCl_4$ Smoke in Which a Large Quantity of Computer Card Punches (1x3 mm) was Dropped in Five Batches per Four Ounces. Aitken nuclei (AN) counts are marked in thousands per cm^{-3}.

model dropping L_1:

$$\frac{\ell n\,(V_1/V_2)}{\ell n\,(V_1/V_o)} = -\frac{L_2-L_1}{L_1}\,, \qquad (17)$$

where V_1, V_2 are the detector voltages measured before and after scavenging, and V_o refers to the clear space. Eq. (17) is based on the Eq. (A-29) and the simplifying assumption mentioned in appendix D. The effect of batch dropping on the improvement of the visual range was estimated this way; it was 28.55% after the first 4-ounce scavenger dropping (figure 16). After each of the four consecutive droppings, it was 8.71%, 9.50%, 8.79%, and 8.22%, respectively. From the other experiments we learned that the 4-ounce batches of punches are probably not as effective as 2-ounce quantities of the same total weight. After the first 2-ounce batch dropping, the improvement in visual range was 31.87%; the consecutive dropping of the 2-ounce batch resulted in the improvement larger than 14%. Future experiments should determine the optimum concentration of scavengers for a specific smoke cloud.

4. RESULTS AND DISCUSSION

The chief results of this study are summarized here.

4.1 The Mode of Fall of Scavengers.

Different scavenger models were used (table D-1) to investigate the stability of motion and the main character of the trajectory of falling models. The most used model was the disk at Re ranging from 517 to 2780 in quiescent air, and from 461.4 to

4423 at a side wind of 0.5 to 0.7 m/s^{-1}. In these ranges the most important parameters for modeling scavenging effects were determined: settling velocity, drag coefficient, and character of motion. For thin paper disks, where no markable oscillation is observed (Re < 900), our data correspond well to studies employing liquids and air.[12,18,29,30,31] A reasonably good transition of C_D coefficients, measured in liquids and in air, was also obtained in this region (fig. 4). The C_D values, however, started to differ strongly from the expected dependence if an intense oscillation or gliding was observed. The transition into gliding (and in some cases tumbling) happened sooner with lighter models with a large cross section or, with 0.66-cm plastic disks, if the surface was bent or the edge imperfect. The sliding or tumbling does not greatly influence the settling rate of the scavenger when compared to the regular oscillatory regime. The amplitudes of oscillation amounted usually only to a few centimeters, and were evaluated only for models with diameters larger than 1.75 cm due to the insufficient power of our stroboscope. Large disks perform a wave-like motion, in addition to oscillation, with a high frequency between several hundredths or tenths of a second. The wavelength usually surpasses 20 cm and, rarely, 30 cm.

Other types of models (squares, hexagons) behave similarly to disks if their mass is symmetrically distributed around the scavenger's center. If the major parameters, such as main size and mass, are kept constant, models of different shapes can be substituted by an "equivalent" disk,[32] with the exception of a thick foam disk. In Table D-1 is compared a paper hexagon with a

foam hexagon having the same size cross section, 2.22 cm^2, however with a different mass. Models with no central symmetry in the cross-sectional plane, such as narrow rectangles (e.g., 3.0 x 0.5 cm), are much different, $C_D \cong 0.4$ at a Re $\cong$ 425, mainly because of the definition of their Re (referred to the width 0.5 cm) and their gliding motion. The same holds for ellipses with a large axis ratio (2.85:1.64 cm). There are very few experiments in the available literature which could be compared to our study. Mostly the investigators looked at the falling of disks and three-dimensional bodies in fluids at intermediate Re,[12] or at low Re.[31] The latter measured $C_D = 1.5$ for a disk at a Re $\cong$ 200, which is very close to our extrapolated data for paper disks, squares, and hexagons. We found exceptionally low C_D's for disks (d = 0.66 cm) made of paper ($C_D = 0.447$), foam ($C_D = 0.670$), and thin Plexiglas ($C_D = 0.140$). These disks usually tumbled in a very fast way, probably due to their uneven surface. Thick foam disks (h = 0.62 cm and d = 2.54 cm) showed a very high C_D, $\cong$ 2.690, at a Re $\cong$ 2650 due to their special gliding.

The behavior of different models at side wind conditions, to our knowledge not studied to the same extent in other laboratories, shows several very interesting features. These conditions yielded higher mean settling rates (higher Re) for all models comparable to the experiments in quiescent air. This leads to lower values of C_D. In only one case out of 122 experiments, we found $C_D \cong 1.27$ (for an L-shape model). A vast majority of the trials yielded C_D values below 0.6 for disks, below 0.5 for squares, hexagons, and stars, below 0.5 for rectangles and

L-shape models, and below 0.4 for triangles and crosses. This finding is a little unexpected. Probably, a side wind permanently changes the angle of attack of the models, which contributes to faster settling of scavengers. An exception to this rule was found in the settling of fine fiber mesh models, which fell quietly and maintained a horizontal position along their path at side winds varying from 0.5 to 0.7 m s^{-1}. At side wind conditions, many more models did tumble, namely unsymmetrical models, than in quiescent air.

Syntheses of the measurements in quiescent air and at a side wind are shown in figures 6, 7, and 8, with a typical C_D - f(Re) curves having the slope of -2. This corresponds to the relationship

$$C_D = \frac{2gh\ \rho_a\ \rho_s\ D^2}{Re^2\ \mu^2} \quad ,$$

where D and h are the characteristic length and thickness of the model. For the higher Re, the value of C_D decreases for the same type of model and environment. If several types of models having the same size cross section are used, their C_D = f(Re) curves are very close, even if the models fell at a side wind. Exceptions to this rule are thick models of foam (different h) and models exerting a very intense gliding or tumbling.

There is a considerable difference between the mode of scavenger fall in the fluid and in the air, mainly in the role the Willmarth parameter[18] plays in the transition of a disk motion from an oscillatory regime into sliding. Our data seem to deviate considerably from the picture presented by Stringham, et.al.[12]

Several interesting results were obtained from a detailed analysis of the time-lapsed camera pictures and stroboscopic photographs. The velocities, accelerations, angular velocities, and their time derivations were found much higher than those measured on falling models in fluids (Podzimek[26] and Stringham, et. al.[12] measured only fluctuation in velocity). Our data from the stroboscopic record of the fall of disks show amplitudes of velocity fluctuation of u and v around ± 50 cm s^{-1} and overriding acceleration during a very short time (several thousands of cm s^{-2}). The corresponding angular velocity fluctuations surpassed ± 500 grad s^{-1} for ω_x and ± 1500 grad s^{-1} for ω_y. The fluctuation of ω_z was very regular and had an approximate value of ± 250 grad s^{-1}. The fluctuations of the $\frac{d\omega}{dt}$ components often surpassed the value of 50,000 grad sec^{-2}. These findings might be important for the potential explanation of the unusually high concentrations of aerosol particles found on the surface of sampled ice crystals. Only Sasyo[5] evaluated for paper fragments (2×2 cm^2 the change of direction cosines, angular velocity, and the components of force couples around the principal axes of the moment of inertia. The mass of a fragment falling in the still air was 0.0352 gm. For comparison, our data (figs. D-13 and D-14) refer to a paper disk 1.9 cm in diameter, having a mass of 0.0286 gm. Our angular velocity fluctuations ω_x and ω_y amount approximately to ± 1000 grad s^{-1}, which corresponds very well to Sasyo's mean value of ± 20 rad $s^{-1} = \pm 1146$ grad s^{-1}. Our ω_z component fluctuated approximately in the limits of ± 250 grad s^{-1} (± 4.36 rad s^{-1}), and Sasyo obtained approximately ± 4.50 rad s^{-1}.

Finally, the theoretical analysis of the scavenger motion, partly described in appendix A, did not go far beyond an exploratory stage. The investigation showed that the simplification of the particle trajectory into a problem of the motion in x-y plane with a steady moving of this plane down along the z axis, and mainly the application of the Stokes resistance law,[5] is not suitable for our scavenger model. The nonlinear Riccati equation, including the more realistic scavenger resistance, was formulated, and a semianalytical approach suggested. This would require, however, a more detailed analysis of many stroboscopic pictures, possibly taken by two cameras.

4.2 Deposition of Smoke Particles on Scavengers.

In spite of great effort, no conclusive results were obtained from the first series of experiments in the settling cylindrical chamber. This was due to the low scavenging efficiency of the models applied usually at low concentration, the short settling path for an observable effect on light extinction measurement, and a high probability of polluting the scavengers after they settled into the sampler at the bottom.

The second series separated the light extinction measurements in the settling chamber from the experiments in the wind tunnel, where a prolonged exposure of the models to the smoke flow could be realized.

Wind tunnel experiments were made with plastic and metallic disks, hexagons, and rectangles exposed to $TiCl_4$ and red phosphorus particles. The exposure time ranged frc.. several minutes to half an hour in an air flow of 1.0 m s^{-1}. The evaluation

of the number of particles deposited on a plastic disk 0.5 cm in diameter (figs. 12 and 13) and on a 1.0-cm disk (figs. 14 and 15) showed clearly that the theoretical models[21], explain qualitatively well the distribution of impacting aerosol particles on the frontal side of a model. The particle numbers found along a strip 157 μm wide and 0.25 cm long from the disk's center outwards show very low deposition rates of all particles around the center of the model. High deposition was observed at distances larger than r/R = 0.3 with a strongly expressed maximum around r/R = 0.9. This distribution, valid for Re = 317, differs considerably from that by Pedori et al.,[33] and corresponds only partly to the picture Yue and Podzimek[6] reported for a Re = 88, using, however, considerably larger droplets of NaCl for deposition. It is closer to the picture of deposited aerosol on the plate-type ice crystal presented by Prodi.[34] The most important finding seems to be the very high particle deposition on the rear side of the 0.5-cm disk with a sharp maximum around r/R = 0.5 (fig. 13). The total concentration overrides that on the frontal side. The total scavenging efficiency of this model was calculated to be 2.02% in mean. This number is a little higher than that reported by Starr and Mason,[4] Starr,[35] however, comparable to that calculated by Sood and Jackson,[3,23] who investigated experimentally the deposition of atmospheric particulates on ice crystals. Sood and Jackson's data on scavenging efficiencies (0.61% to 2%) for scavenging of 0.6- to 3.4-μm particulates are considered by several workers to be too high. On the other hand, they could well explain the high deposition rate of particulates on ice

crystals reported from Japan by Magono et al.[36-38] With regard to the size of our model, one feels that the obtained efficiency might not be far from the data published by others.

The results from the investigation of the deposition of smoke particulates on a disk 1.0 cm in diameter at an aerosol flow of 1.0 m s^{-1} show a picture (figs. 14 and 15) similar to that just described. The high counts were close to the disk's edge on the frontal side for particles with $d < 2.0$ μm and a secondary maximum, caused mainly by particles with $1.0 < d < 1.5$ around $r/R = 0.3$ (fig. 14). On the disk's rear side, the high aerosol deposition rates extended from $r/R = 0.3$ to 1.0. The maximum deposition actually covers the whole region (fig. 15), and the dominant peak observed in figure 13, around $r/R = 0.5$, is absent. This change in pattern of deposited particulates on the rear side of a disk model is probably related to the basic change of the wake structure behind a disk fixed in a wind tunnel if the Re changes from 317 to 633. An important conclusion is that particulate deposition on the rear side of our large scavenger models is real and, in the case of the smaller model ($d = 0.5$ cm), it overrides that on the frontal side. The collection efficiency of the 1.0-cm disk was in total about 2.7% (deposition on both sides).

4.3 Effect of Scavenging on Light Extinction.

The first series of scavenging experiments with simultaneous light extinction measurement revealed that reproducible measurements would require a large quantity of collectors and dropping of models in several batches. This would increase the number of

deposited smoke particles, due to the aerodynamic interference of models falling close together. To support this idea, experiments were conducted to obtain smoke particle deposition on two models simulating paper punches (with dimensions 1 x 3 mm), which were installed one behind the other, 1.2 mm apart. The second model (behind the first one in a crossed position) always showed higher smoke particle counts.

Batches of punches, dropped in 2- or 4-oz quantities (each ounce containing approximately 39,367 punches) in a dense $TiCl_4$ smoke, were followed by improved visibility which corresponded to approximately 29% in visual range with the initial dropping at a quantity of 4-oz and roughly to 9% after each subsequent dropping of the same quantity of scavengers. Repeated experiments with a smaller concentration of punch scavengers (2-oz) showed an improvement in visibility when compared to 4-oz batches. This raises new questions: What is the optimum quantity for a batch, and what time interval should be used between droppings to reach maximal effect on visibility improvement?

Another means to improve visibility in a smoke cloud is the use of fine fiber mesh-type scavengers to effectively remove the smoke particles. A rough calculation shows that 32 fine fiber mesh scavengers of 1.5 x 1.5 cm^2 (total length of the 46-μm fiber diameter is 96 cm in each scavenger) falling through the sensitive beam of the light extinction meter can improve visibility 0.812%.

5. CONCLUSIONS

This study was an exploratory investigation. Not that the

problem is unknown, but that for more than two decades after the introductory studies of rain scavenging of the radioactive and other particulate matter by Greenfield,[39] Engelmann,[40] and others, who had great hopes in obtaining significant results, came a sober reality. Precipitation Scavenging,edited by Engelmann and Slinn,[41] represents a unique document of these efforts and hopes. Precipitation by nonspherical particulates, mainly by ice crystals, is represented by one specific article (Sood and Jackson[23]) and by several comments. New achievements in particle scavenging by hydrometeors are described in the monograph by Pruppacher and Klett.[14]

The author of this proposal, who worked for a decade in the field of ice crystal motion and growth by coagulation, felt that the standard approach to ice crystal scavenging, that of using the technique found successful for rain scavenging, was inappropriate. New areas, such as deposition of particulates on the rear side of a scavenger of arbitrary shape, exploration of detailed motion of a plate-type scavenger with its fast oscillation and high acceleration rates, and the scavenging efficiency of different models, were only insufficiently explored. Would this kind of research be useful? Should it be continued?

This report touches upon many problems which might help to formulate the answers to these questions. It was shown that proper selection of size, shape, and concentration of scavengers with regard to the properties of the smoke particles obtains more effective scavenging, with the efficiency surpassing 1.0%. Very useful data on different types of scavengers, such as settling

rate, drag coefficient, Reynolds number, and mode of motion were obtained. Both the settling of scavengers in quiescent air and at side wind conditions were investigated. A side wind of 0.7 m s^{-1} seemed to change considerably the scavenger's settling rate and Re, and potentially increased the gliding and tumbling of the models.

The experiments with disk type models exposed to smoke flow in an aerodynamic wind tunnel showed that a considerable part of a smoke aerosol (with the majority of particle sizes in the submicron region) is deposited on the rear side of scavengers with diameters of 0.5 and 1.0 cm at a flow rate of 1.0 m s^{-1}. The total scavenging efficiency of these models was calculated to be close to 2.0% and 2.7%, respectively, in a steady flow.

Several pilot experiments employed the dropping of a large quantity of small punches into a smoke cloud in a settling chamber. It was concluded that this kind of scavenging is effective and can lead to improvement in visual range up to 29% after the first droping of 4-oz of paper punches (1 x 3 mm in size) into a dense $TiCl_4$ cloud, and up to 9% after each subsequent dropping of the same quantity of scavengers.

These promising facts justify the conclusion that this kind of research is useful and should be continued. The most promising areas stemming from this investigation should be explored. The more than 200 records on the falling of different types of models should be studied and we should concentrate on those showing high accelerations and low settling velocities (rectangles, ellipses, triangles). Special attention should be paid

to the fine, fiber mesh models. This investigation should be paralleled by experiments with smoke particle deposition on models performing a slight oscillatory motion in a wind tunnel. This study would furnish some idea of what the ultimate possibilities are for using inertial deposition techniques for particle scavenging. The final goal would be the study of the effect of a large quantity of dropped scavengers on the clearing of smoke clouds. At that stage, the nature of a specific smoke cloud should be explored by trying to combine inertial deposition with electrical charge effect, and other potentially effective mechanisms (microturbulence, phoretic forces).

LITERATURE CITED

1. Podzimek, J., 1970, Contribution to the problem of the collection efficiency of falling ice crystals, Proc. Conf. on Cloud Physics, Fort Collins, August; AMS, Boston, 13.

2. Magono, C., T. Endoh, F. Ueno, S. Kubota and M. Itasaka, 1979, Direct observations of aerosols attached to falling snow crystals, Tellus, 31, 102-114.

3. Sood, S.K., and M.R. Jackson, 1969, Scavenging of atmospheric particulate matter by falling hydrometeors, Proc. 7th Int. Conf. on Condens. and Ice Nuclei, Prague-Vienna, Academia, Prague, 299-302.

4. Starr, J.R., and B.J. Mason, 1966, The capture of airborne particles by water drops and simulated snow crystals, Quart. J. Roy. Met. Soc., 92, 490-499.

5. Sasyo, Y., 1971, Study of the formation of precipitation by the aggregation of snow particles and the accretion of cloud droplets on snowflakes, Papers in Met. and Geophys., 22, 69-142.

6. Yue, P.C., and J. Podzimek, 1976, A Laboratory Method for the Study of Droplet Deposition on Simple Ice Crystal Models, Tech. Rept. AG-6, GCCPR, Univ. Missouri-Rolla, Sept.

7. Pitter, R.L., H.R. Pruppacher, and A.E. Hamielec, 1973, A numerical study of viscous flow past thin oblate spheroid at low and intermediate Reynolds numbers, J. Atmos. Sci. 30, 125-134.

8. Yue, P.C., and J. Podzimek, 1980, Aerosol Scavenging by Free Falling Collectors, 1980 CSL Scientific Conference on Obscuration and Aerosol Research, 21-25 July, Aberdeen Proving Ground, MD.

9. Podzimek, J., 1965, Movement of ice particles in the atmosphere, Proc. Intl. Conf. Cloud Phys., Tokyo-Sapporo, May, p. 224.

10. Podzimek, J., 1968, Aerodynamic conditions of ice crystal aggregation, Proc. Intl. Conf. on Cloud Physics, Univ. Toronto, 295-299.

11. Podzimek, J., 1979, Survey of Techniques for Clearing Military Smoke Clouds, ARCSL-CR-79020, Chemical Systems Laboratory, May, ADA072166.

12. Stringham, G.E., D.B. Simons, and H.P. Guy, 1969, The Behavior of Large Particles Falling in Quiescent Liquids, Geolog. Survey Profess. Paper, 562-C, U.S. Gov. Print. Office, Washington, D.C.

13. Schemenauer, R.S., 1969, Measurements of the Drag Coefficients and Characteristic Motions of Snow Crystal, Graupel and Small Hail Models, M.S. Thesis, Univ. of Toronto, November.

14. Pruppacher, H.R., and J. D. Klett, 1978, Microphysics of Clouds and Precipitation. pp 328-337 D. Reidel, Publ. Co., Dordrecht.

15. Martin, J.J., P.W. Wang, and H.R. Pruppacher, 1980a, A theoretical determination of the efficiency with which aerosol particles are collected by simple ice crystal plates, J. Atmos. Sci., 37, 1628-1638.

16. Martin, J.J., P. W. Wang, and H.R. Pruppacher, 1980b, A theoretical study of the effect of electric charges on the efficiency with which aerosol particles are collected by ice crystal plates, J. Coll. Interf. Sci., 78, 44-56.

17. Martin, J.J., P.K. Wang, H.R. Pruppacher, and A.E. Hamielec, 1980c, On the efficiency with which aerosol particles of radius larger than 0.1 μm are collected by simple ice crystal plates, Pageoph., 118, 1109-1129.

18. Willmarth, W.W., N.E. Hawk, and R.L. Harvey, 1964, Steady and unsteady motions and wakes of freely falling disks, Physics Fluids, 7, 197-208.

19. Schenewerk, M.S., 1979, The solution of a two-dimensional viscous flow around a step, Presented at the Collegiate Academy of the Missouri Academy of Sci., 25 April.

20. Rimon, Y., 1969, Numerical solution of the incompressible time-dependent viscous flow past a thin oblate spheroid, Phys. Fluids, Supplement II, II-65 to 75.

21. Pitter, R.L., and H.R. Pruppacher, 1974, A numerical investigation of collision efficiencies of a simple ice plate colliding with supercooled water drops, J. Atmos. Sci., 31, 551-559.

22. Parker, L.W., 1973, Computer method for calculation of aerosol scavenging by snow, Proposal submitted to AEC, Div. Biomed. and Envir. Research, Washington, D.C., April.

23. Sood, S.K., and M.R. Jackson, 1970, Scavenging by Snow and Ice Crystals, Precipitation Scavenging, U.S. AEC Symp. Ser. 22, December, 121-136. Available from NTIS as Conf-700601.

24. Preining, O., J. Podzimek, and P.C. Yue, 1976, Magnification factor for sodium chloride Liesegang circles established with the aid of an aerosol centrifuge, Aerosol Sci., 7, 351-358.

25. Khorguani, V.G., 1966, O gidrodinamicheskom vzaimodeistvii dvukh osedaiuschikh sfericheskikh chastits v viazkoi srede, Trudy VGI, 5, 52.

26. Podzimek, J., 1969, The Growth of an Ice Crystal in a Mixed Cloud (in Czech), Part I, p. 183, Part II, p. 137, D.S. Thesis, Charles University, Prague.

27. Clark, T.L., and R. List, 1971, Dynamics of a falling particle zone, J. Atmos. Sci., 28, 718-727.

28. Girard, C., and R. List, 1975, Thermodynamics of falling precipitation zones, Pageoph, 113, 1035-1053.

29. Schiller, L., 1932, Hydro-und Aerodynamik, 2 Teil, Akad. Verlagsges., Leipzig, p. 374-378.

30. Lapple, C.E., and C. B. Shepherd, 1940, Calculation of particle trajectories, Ind. & Engin. Chemistry, 32, 605-617.

31. List, R., and R.S. Schemenauer, 1971, Free fall of planar snow crystals, conical graupel and small hail, J. Atmos. Sci., 28, 110-115.

32. Jayaweera, K.O.L., 1972: An equivalent disc for calculating the terminal velocities of plate-like crystals, J. Atmos. Sci., 29, 596-598.

33. Pedori, F., F. Prodi, and E. Wirth, 1973, Captures of droplets by simulated hexagonal plates: Preliminary results, Riv. Italiana de Geofisica, XXII, 160-164.

34. Prodi, F., 1976, Scavenging of aerosol particles by growing ice crystals, Preprints Int. Conf. on Cloud Physics, Boulder; AMS, Boston, 70-75.

35. Starr, J.R., 1967, Deposition of particulate matter by hydrometeors, Quart. J. Roy. Met. Soc., 93, 516-521.

36. Magono, C., T. Endoh, T. Harimaya, and S. Kubota, 1974, A measurement of scavenging effect of falling snow crystals on the aerosol concentration, J. Met. Soc., Japan, 52, 407-416.

37. Magono, C., F. Ueno, and S. Kubota, 1975a, Observations of aerosols attached to falling snow crystals. Part I, utilizing an optical microscope, J. Fac. Sci., Hokkaido Univ., S. VII., 4, 93-101.

38. Magono, C., T. Endoh, and M. Itasaka, 1975b, Observation of aerosol particles attached to falling snow crystals. Part II, utilizing an electron microscope, J. Fac. Sci., Hokkaido Univ., S. VII., 4, 103-119.

39. Greenfield, S.E., 1957, Rain scavenging of radioactive particulate matter from the atmosphere, J. Meteor., 14, 115-125.

40. Engelmann, R.J., 1965, Rain scavenging of zinc sulfide particles, J. Atmos. Sci., 22, 719-727.

41. Engelmann, R.J., and W.G.N. Slinn, 1970, Precipitation Scavenging, U.S. AEC, available from NTIS as Conf.-700601, December.

42. Kaplan, W., 1958, Ordinary Differential Equations, Addison-Wesley Publ. Comp., Reading, p. 344.

43. Katchurin, L.G., 1973, Fizicheskie osnovy vozdeistvia na atmosfernye protsessy, Gidrometeoizdat, Leningrad.

A P P E N D I X E S

APPENDIX A. Calculations

Note a.

The general system of equations of force couples N acting on a motion is

$$I_x \frac{d\omega_x}{dt} - (I_y - I_z)\ \omega_y\ \omega_z = N_x \qquad \text{(A-1)}$$

$$I_y \frac{d\omega_y}{dt} - (I_z - I_x)\ \omega_z\ \omega_x = N_y \qquad \text{(A-2)}$$

$$I_z \frac{d\omega_z}{dt} - (I_x - I_y)\ \omega_x\ \omega_y = N_z \qquad \text{(A-3)}$$

where ω_x, ω_y, ω_z, are the angular velocities around the principal axes and I_x, I_y, I_z are moments of inertia referred to the principal axes. The force couples have, in case of a falling thin plate with the surface (one side) area S (fig. 5), the form

$$N_x = C_{Dx} \frac{\rho_a}{2} u^2\ \ell_x S\ . \qquad \text{(A-4)}$$

The drag coefficient C_{Dx} is related to the x direction component of flow and ℓ_x is the x coordinate of the distance ℓ from the center of gravity of the plate to the point where the resultant of aerodynamic forces acts.

The angular velocities ω_x, ω_y, and ω_z can be deduced from the measurement of the three independent direction cosines n_x, n_y, n_z. However, for higher accuracy in the potential study of plate oscillation with rotation, all nine directional cosines referred to the three main axes should be measured (n_{xi}, n_{yi}, n_{zi} for i - 1,2,3,). Then the angular velocities resume the form

$$\omega_x = \sum_i n_{yi} \frac{dn_{zi}}{dt} = - \sum_i n_{zi} \frac{dn_{yi}}{dt} \qquad \text{(A-5)}$$

$$\omega_y = \sum_i n_{zi} \frac{dn_{xi}}{dt} = - \sum_i n_{yi} \frac{dn_{zi}}{dt} \qquad \text{(A-6)}$$

$$\omega_z = \sum_i n_{xi} \frac{dn_{yi}}{dt} = - \sum_i n_{yi} \frac{dn_{zi}}{dt} \ . \qquad \text{(A-7)}$$

In case of a two-dimensional motion, Eqs. (A-1, 2,3) will be simplified due to the fact that, e.g., $\omega_y = 0$

Several attempts were made to describe the plate trajectory[5] in the domain of validity of Stokes resistance law; however, an attempt to solve the unsimplified set of equations has not yet been made. For small amplitudes a better picture of a settling scavenger can be obtained by assuming a set of equations

$$m \frac{du}{dt} = - C_x^* \ u^2 + F_x \qquad \text{(A-8)}$$

$$m \frac{dv}{dt} = - C_y^* \ v^2 + F_y \qquad \text{(A-9)}$$

$$m \frac{dw}{dt} = - C_z^* \ w^2 + mg \ , \qquad \text{(A-10)}$$

where the inertial forces are compared to the particle drag (with a generalized drag coefficient $C_x^* = C_x \frac{\rho_a}{2} S$) and lift force component F_x. Further, one could assume under the assumption made before that $C_x^* = C_y^* = C_z^* = C$ and that $w = \bar{w}$ which implies $\frac{d\bar{w}}{dt} = 0$. Then $C = (mg)/w^2$, and a plausible assumption about the lift force can be made

$$F_x = \bar{F}_x + A \cos (\omega t + \lambda) \qquad \text{(A-11)}$$

$$F_y = \bar{F}_y + A \sin (\omega t + \lambda) \ . \qquad \text{(A-12)}$$

Even under these strong simplifying assumptions, the special types of Riccati equations cannot be solved analytically. Semi-analytical description (using data from the measured scavenger

position during its fall) will be attempted. Numerical solution is of course possible.

It is much easier to evaluate the motion of nonspherical scavengers in the domain of validity of Stokes resistance law. Their motion can be expressed by the equations[5]

$$m \frac{du}{dt} = - C_x u + F_x \tag{A-13}$$

$$m \frac{dv}{dt} = - C_y v + F_y \tag{A-14}$$

$$m \frac{dw}{dt} = C_z w - mg \ . \tag{A-15}$$

From the experiments (figs. 9 and 10), a relationship $C_x = C_y$ = const and $C_x = k\, C_x$ (k is a constant) can be assumed, and the components of a lift force are given by the equations (A-10) and (A-11). Finally for $\frac{dw}{dt} = 0 \Rightarrow w = \bar{w}$ the position of a falling disk is

$$x = \frac{\bar{F}_x}{C_x} t + \frac{A}{m\omega \sqrt{\gamma^2 + \omega^2}} \sin (\omega t + \lambda - y) \tag{A-16}$$

$$y = \frac{\bar{F}_y}{C_y} t + \frac{A}{m\omega \sqrt{\gamma^2 + \omega^2}} \cos (\omega t + \lambda - y) \tag{A-17}$$

with the initial position $x = 0$; $y = 0$ for $t = 0$ and

$$\gamma = \frac{C_x}{m} \ ; \ y = \tan^{-1} \frac{\omega}{\gamma} \ .$$

The equations (A-16) and (A-17) describe the trajectory of a disk in a horizontal plane with the components of uniform velocity $\bar{u}_x = \bar{F}_x/C_x$ and $\bar{u}_y = \bar{F}_y/C_y$ and a superimposed rotation with an amplitude (radius)

$$\bar{A} = \frac{A}{m\omega \sqrt{\gamma^2 + \omega^2}} \ . \tag{A-18}$$

Because the components of the lift force can be deduced from the time-lapsed camera pictures (assuming $mg = C_z w = C_z \frac{\Delta z}{\Delta t}$ for the time intervals Δt

$$F_x = \frac{C_x}{\Delta t} \left\{ \frac{\Delta x}{g} \frac{\Delta^2 x}{(\Delta t)^2} + \Delta x \right\} , \qquad \text{(A-19)}$$

$$F_y = \frac{C_y}{\Delta t} \left\{ \frac{\Delta z}{g} \frac{\Delta^2 y}{(\Delta t)^2} + \Delta y \right\} , \qquad \text{(A-20)}$$

one obtains from the plotting of $F_x = f(t)$ and $F_y = f(t)$ the amplitude A and angular velocity ω. The amplitude of scavenger motion $\bar{A}$ can be therefore determined for any plate-type scavenger with a mass m if a corresponding mean value of C_x is known.

Note b.

Equations (A-8) and (A-9) have the same form which can be written as

$$u' = - Au^2 + F(t) , \qquad \text{(A-21)}$$

where $A = C_D \frac{\rho_a S}{2m}$ has the form of a resistance force (or its x or y component) combined with the corresponding lift force, which can be expressed as a fluctuating function

$$F = F_o + \bar{f} \sin \omega t .$$

This indicates that the drag force is considered to be time independent and that the corresponding part of the lift $F_o = C_{LO} \frac{\rho_a}{2} u^2 S$ can be included in the expression of A. In fact, the restriction to a time-independent drag is not a "conditio sine qua non;" the Eq. (A-21) holds if one bears in mind that there is always a relationship between L and D for a given angle of attack β so that the terms of A and F(t) include both the steady and fluctuating

parts of both expressions for the drag and lift.

The Eq. (A-21), which is a special type of a Riccati equation, can be solved with the use of a Taylor series:

$$u' = - Au^2 + F(t)$$

$$u'' = - 2Auu' + F'(t)$$

$$u''' = - 2Au'^2 - 2Auu'' + F''(t)$$

$$u'''' = - 6Au'u'' - 2Auu''' + F'''(t) \quad \text{....etc.}$$

At $t = t_o = o$ we assume $u(o) = o$, therefore,

$$u(t_o) = o$$

$$u'(t_o) = F(t_o)$$

$$u''(t_o) = F'(t_o)$$

$$u'''(t_o) = - 2AF^2(t_o) + F''(t_o)$$

$$u''''(t_o) = - 6AF(t_o)F'(t_o) + F'''(t_o) \quad \text{....etc.}$$

Substituting the derivatives into a Taylor series

$$y(x) = y(x_o) + y'(x_o)\,\frac{x-x_o}{1!} + \ldots\ldots + y^{(n-1)}(x_o)\,\frac{(x-x_o)^{n-1}}{(n-1)!} +$$

$$+ \int_{x_o}^{x} \frac{(x-\xi)^{n-1}}{(n-1)!}\, y^{(n)}(\xi)\,d\xi$$

with $x_o = o$ and $t_o = o$, one obtains for the velocity u

$$u = F(t_o)\,t + 1/2\,F'(t_o)\,t^2 + 1/6\,[F''(t_o) - 2AF^2(t_o)]\,t^3 +$$
$$+ 1/24\,[F'''(t_o) - 6AF(t_o)\,F'(t_o)]\,t^4 \ldots. \qquad \text{(A-22)}$$

The two main questions are: For what values of t does the series (A-22) converge to a definite solution? What is the mean error after taking only a limited number of members?[42] A preliminary checking of the suitability of this approach for the case of a model falling in a liquid yielded an acceptable radius of convergence; however, an unacceptable mean error if three or four

members of a Taylor series were considered. More work on this line and the use of the parameters deduced from models falling in the air is anticipated.

Note c.

The simplest scavenging model can be based on the following assumptions:

1) Scavengers of a uniform size R are homogeneously dispersed in a sheet of the depth h' above the smoke layer of a depth h. They do not coagulate or aerodynamically interfere among themselves while settling through the smoke layer. Their mean settling velocity is constant (no considerable accretion of mass by scavenging is assumed) or characterized by a mean value $\bar{v}_R$, which signifies the mean velocity during an oscillatory motion. Their concentration is N_R.

2) Smoke consists of uniformly dispersed monodisperse spherical smoke particles with a radius r (an extension to, e.g., log-normal distribution can be easily done). The smoke particles do not coagulate among themselves and their concentration is n(r,t).

3) The collection efficiency of a single scavenger is E(R,r) and, if R >> r, a single scavenger sweeps out $\pi R^2 \bar{v}_R$ E(R,r) n (r,t) if $\bar{v}_R >> v_r$. For N_R scavengers in a unit of volume, the smoke particle concentration change $\Delta n(r,t)$ in a unit of time will be

$$\frac{\Delta n(r,t)}{\Delta t} = - \pi R^2 N_R \bar{v}_R \; n(r,t) \; E(R,r) \quad .$$

Using the infinitesimal quantities and integrating the last equation, one obtains the number of depleted smoke particles

$$n(r,t_1) = n(r,o)\ \exp(-\sigma t_1) \quad ,$$

where $\sigma = \pi R^2 N_R \bar{v}_R E(R,r)$ and t_1 corresponds to the fall of scavengers through the smoke layer of the depth h.

4) The other layer of scavengers (1 cm in depth) will also scavenge in the time t_1, but starting with the depleted concentration

$$n(r,t_2) = [1 - n(r,t_1)]\ \exp(-\sigma t_1) \quad .$$

After the ν-th layer of scavengers settle, the smoke layer will be depleted of

$$n(r,t_\nu) = [1 - n(r,t_{\nu-1})]\ \exp(-\sigma t_1) \quad . \qquad \text{(A-23)}$$

In total the amount of smoke particles depleted by a homogeneous layer of scavengers of the thickness h' and concentration N_R from the smoke of a vertical extension h will be

$$N_{dep}(r,\nu t_1) = \sum_{i=o}^{\nu} n(r,it_1)\exp(-\sigma t_1) \quad . \qquad \text{(A-24)}$$

There is a relationship between ν and t_1 and the scavenger fall velocity $\bar{v}_R$ and the thickness of the scavenger and smoke layer:

$$\nu t_1 = \bar{v}_R/h' \qquad \text{and} \qquad t_1 = \frac{\bar{v}_R}{h} \quad .$$

This implies the definition of $\nu = h/h'$. It should be stressed that $\bar{v}_R$ corresponds to the mean particle velocity along its path which, in case of a scavenger oscillatory motion or side wind conditions, is not exactly h or h'.

The knowledge of the number of depleted particles after a certain time (νt_1) also enables the calculation of the number of particles remaining in the fog layer after a time νt_1.

$$N_{rem}(r,\nu t_1) = n(r,o) - N_{dep}(r,\nu t_1) = n(r,o) - n(r,o) \cdot$$

$$\cdot \exp(-\sigma t_1) - [1 - n(r,t_1)] \exp(-\sigma t_1) -$$

$$- [1 - n(r,t_2)] \exp(-\sigma t_1) - \ldots - [1 - n(r,t_{\nu-1})] \exp(-\sigma t_1).$$

APPENDIX B. Scavenging Efficiency

The scavenging formula used in these calculations relates smoke concentration at a time t to that at a time 0:

$$n(t) = n_o \exp(-\Lambda t)$$

where $\Lambda = \Sigma \Lambda_j$ is a mean scavenging (collection) coefficient. Its magnitude can be defined for a disk of radius R_1

$$\Lambda_i = \Sigma P_j \int_{r_1}^{r_2} \pi (R_i + r)^2 E_i(R_i, r, \vec{U}, \vec{w}) [\vec{U}(R_i) - \vec{w}(r)] N(r) dr \quad \text{(A-25)}$$

where P_j means the number of positions of a disk (scavenger) in a specific fall regime, and $E_i(R_i, r, \vec{U}, \vec{w})$ is the coagulation kernel for a disk of radius R_i meeting aerosol particles characterized by their size distribution function N(r). The velocities of a scavenger and particle are $\vec{U}(R_i)$ and $\vec{w}(r)$, respectively.

The equation (A-25) can be modified for application to cylinders (fibers) if the disk scavenging cross section $(R_i + r)^2 = R_i^2$ is substituted by a thin fiber with a radius R_i and a total length L:

$$\Lambda_i = \Sigma P_j \int_{r_1}^{r_2} 2R \cdot L \, E_i (R_i, r, \vec{U}, \vec{w}) [\vec{U}(R_i) - \vec{w}(r)] N(r) dr.$$

If one assumes very fine, 1-mm distant fibers (scarf- or veil-type fabric) arranged in an area 1.0 cm x 1.0 cm, then the total 92-μm cross-sectional area (2RL) will be approximately 0.171 cm^2 for a fiber length of 18.6 cm. The settling velocity of this

type of scavenger was assumed to be $U(R_i) = 51.1$ cm s^{-1}, which is much larger than the settling rate of the smoke particles. The latter, therefore, will be neglected. The factor ΣP_j was estimated from different positions of a falling mesh-type scavenger which does not oscillate strongly. Therefore, plotting the changes of directional cosines of the mesh-type scavenger from a stroboscopic picture, we assumed the value of $\Sigma P_j = 0.901$. The coagulation kernel was taken from Starr's experimental work[35] after calculating the Stokes number for each aerosol size interval, considering the fiber diameter, the fall velocity of the scavenger, and two different smoke aerosol densities $\rho_s = 1.0$ g cm^{-3} and $\rho_s = 4.26$ g cm^{-3}. The air at standard pressure and temperature was assumed in table D-3.

The kernels from table D-3 were applied in the simplified formula for discrete particle sizes

$$\Lambda = N(R) \sum_i \frac{N(r)_i}{N(r)} E_i \cdot A \equiv N(R) \Lambda_i . \qquad \text{(A-26)}$$

N(R) is the number of scavengers per cubic centimeter and A signifies the scavenger's cross section multiplied by scavenger's settling velocity and the factor $P_j = 0.901$. In our specific case, A has a value of $A = 7.8776$ cm^3 s^{-1}. $N(r)_i/N(r)$ is the ratio of the particle concentration in a specific size class and the total concentration of smoke aerosol. Taking the values of E_i from table D-3, calculating the ratios $N(r)_i/N(r)$ from the aerosol laser cavity spectrometer data, and substituting $A = 7.8776$ cm^3 s^{-1} in Eq. (A-26), we finally obtained table D-4 which enables to estimate the scavenging efficiency of the described

mesh-type collector for a specific size of $TiCl_4$ smoke particles (Λ_i). For comparison, the scavenging coefficients of a disk having the same diameter as the fiber was attached. The case of Λ_i for $\rho(TiCl_4)$ = 4.26 g cm^{-3} will not be unlikely for the high hygroscopicity of the smoke particles.

Two tables similar to tables D-3 and D-4 were calculated for a mesh-type square 1.0 cm x 1.0 cm in area which consisted of very fine individual fibers (R = 23 μm) with a total length of 96.08 cm and total cross section of 0.44197 cm^2. Its mean fall velocity, evaluated from stroboscopic pictures, was 36.3 cm s^{-1}, and it fell quietly to the settling chamber's bottom ($\Sigma P_j = 1.0$). All the other parameters and smoke aerosol were the same as in the previous case. Then the coagulation kernels and Stokes numbers were calculated with the use of Starr's data[35] for E_i of a cylinder and were arranged in the table D-5 for the two extreme particle densities (ρ_p = 1.0 g cm^{-3}). A table similar to table A-4 was calculated for the scavenging efficiency of a collector with the total cross section of 0.44195 cm^2.

Glancing over the calculated scavenging efficiencies in tables D-4 and D-6, one concludes that a proper selection of mesh fiber and arrangement might result in scavenging efficiencies between several percent to tens of percent if the situation similar to that described in this experiment existed (with ρ_p around 2.0 g cm^{-3}).

APPENDIX C. Extinction Measurement

Extinction is defined in this study as the ratio of the difference of the measured light intensity I and the reference light intensity I_o divided by the reference light intensity I_o

$$E = \frac{I - I_o}{I_o} \quad \text{or} \quad E(\%) = 100 \frac{I - I_o}{I_o} \; . \tag{A-27}$$

There is a direct relationship of this formula to the extinction coefficient b because

$$b = - \frac{dI}{Idz} = \int_o^\infty \frac{\pi d_p^2}{4} K_{ext}(x,m) \, n_p(d_p) \, d(d_p) \tag{A-28}$$

which represents the fraction dI/I of the incident light scattered and absorbed by the particle cloud per unit length of the light path and per unit area normal to the beam. $s = \frac{\pi d_p}{\lambda}$, where λ, is the light wavelength, and d_p is smoke spherical particle diameter, K_{ext} is the extinction efficiency ($K_{ext} = K_{scat} + K_{abs}$). m is the index of refraction of the particle. D_{ext} has relatively simple form if $d_p << \lambda$. $n_p(d_p)$ is the particle size distribution function.

There is also a direct relationship of the formula (A-27) to the visual range L, or simply to the decrease in light intensity, if the light beam is passing through the aerosol from point x_1, to point x_2

$$I_2 = I_1 \, e^{-\tau(x_2 - x_1)} \tag{A-29}$$

where $\tau = \int_{L_1}^{L_2} b \, dz$ is the optical thickness of the medium.

The visual range

$$L = \frac{\ell n(1/\varepsilon)}{\pi n \int_0^\infty n_p(d_p) d_p^2 K_{ext}(x,m)\, d(d_p)} \qquad \text{(A-30)}$$

contains the factor characterizing the sensor (e.g. for human eye $\varepsilon = 0.02$). n is the total particle concentration in 1 cm^3. Expressing the term with Mie function in the integral in Eq. (A-30) as a mean value $\overline{r^2_p K_{ext}}$ and introducing the smoke particle mass content in 1 cm^3 of the cloud $q = (4/3)\, \pi \rho_p\, n\, \bar{r}^3_p$ (ρ_p is the particle density), one can rewrite Eq. (A-30) in the form, including particle radii instead of diameters,

$$L = \frac{4\rho_p\, \bar{r}^3_p\, \ell n\ 1/\varepsilon}{3q\, \overline{r^2_p K_{ext}}} . \qquad \text{(A-31)}$$

For our orientational study we would use the simplest form of Eq. (A-31) holding strictly for particles with $d_p << \lambda$, $m = 1.33$, $K_{ext} = 2.0$, $\varepsilon = 0.02$ and $\bar{r} = 0.35$ μm. Then for

$$\begin{aligned} \rho_p &= 1.0\ g\ cm^{-3} \qquad & L &= 3.4685\ n^{-1/3} q^{-2/3} \\ \rho_p &= 2.0\ g\ cm^{-3} \qquad & L &= 6.9370\ n^{-1/3} q^{-2/3} \end{aligned} \qquad \text{(A-32)}$$

if all quantities are expressed in cm gm sec units.[43] This is a direct relationship of a smoke aerosol to the visual range L if one measures the most common smoke particle parameters: number and mass concentration in 1 cm^3.

In this sense, visibility or the visual range improvement after dropping a certain number of scavengers into a smoke cloud

can be deduced directly or from the change of extinction or the light transmission (proportional to the change of light intensity I or detector voltage V). For this reason $\frac{V_2 - V_1}{V_1}$, $\frac{I_2 - I_1}{I_1}$ or $\frac{E_2 - E_1}{E_1}$, where index 1 means the value measured before the scavengers were dropped and 2 the values after they settled, is the measure of the scavenging effect directly related to the visual range L.

In fig. D-22 the effect of dropping of 60 plastic disks of 0.66 cm diameter on the light extinction is plotted as a function of time (Run 15). This curve is compared to the "natural" clearing of smoke in the chamber without the use of scavengers (Run 2). Comparing the mean slope of both curves ($\overline{\frac{dE}{dt}}$) one cannot observe any marked effect, except a certain disturbance in extinction after the models were dropped. This probably can be explained by the dynamic effect (air entrainment) in the particle falling zone.

Figure D-23 compares the dropping of 64 fine fiber mesh models (fiber diameter of 46 μm) in two different ways. All were released 22 minutes after smoke was introduced into the chamber, and the same number was dropped, in 4 groups of 16 scavengers each, at approximately 5-minute intervals. The effect of each dropping is not very significant; however, the effect of repeated dropping of scavengers in groups seems to be more effective than dropping all models at once. This is concluded from the comparison of the slopes of the extinction curves ($\overline{\frac{dE}{dt}}$) in fig. D-23.

In order to obtain some orientational numbers of the

potential scavenging effect of mesh-type models, which were considered to be more effective scavengers than the paper disks, we performed a calculation based on the following assumptions: 32 fine fiber scavengers (squares 1.5 x 1.5 cm with a total length of 96 cm, 46 μm in diameter) were dropped at the top of the chamber. During their fall, with mean velocity of 51.5 cm s^{-1}, they scavenged $TiCl_4$ smoke particles (of initial concentration of 10^5 cm^{-3} and a size distribution similar to fig. D-5) at a rate which corresponds to the collection efficiency of a cylinder 96 cm long and 46 μm in diameter. The calculated Stokes numbers for particle radii between 0.1 and 3.0 μm range from 1.356×10^{-3} to 1.221. Based on these assumptions, the change of attenuation after the evenly dispersed scavengers passed through the sensitive volume of the light intensity detector in the chamber (D = 1.6 cm, ΔL = 78 cm) was calculated. This rough calculation yielded the change in light extinction of 0.812%, which is a little smaller than the experimental value if one compares $\frac{\Delta E}{E}$ or $\frac{\Delta V}{V}$ on the "bumps" of the curves after the scavengers passed through the sensor's light beam. However, one has to bear in mind that relatively few scavengers settling in the chamber will manage to pass through the narrow light beam of the sensor.

The results of more than 50 evaluated experiments with the direct light-extinction measurement in the falling scavenger zone led to the conclusion that a significant scavenging effect can be expected when using a large quantity of scavengers with a high scavenging efficiency and dropping them successively in batches. Some preliminary results are described in the main text of this report.

Figure D-1 Plate type ice crystal with protrusions and deposited small droplets. The mean diameter of circumscribed circle is 1200 μm.

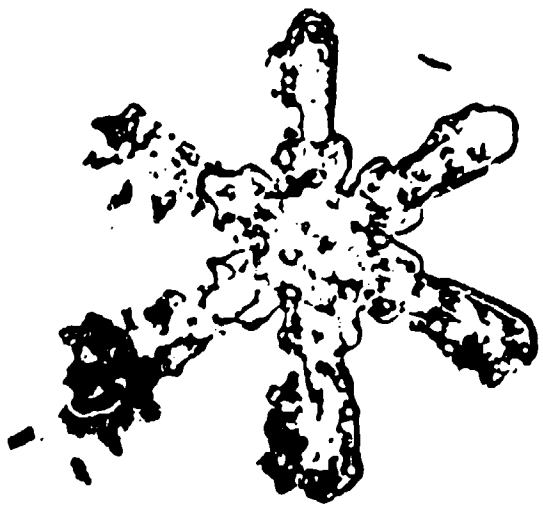

Figure D-2 Star type ice crystal with deposited frozen drops and aerosol particles. Mean size is 1000 μm.

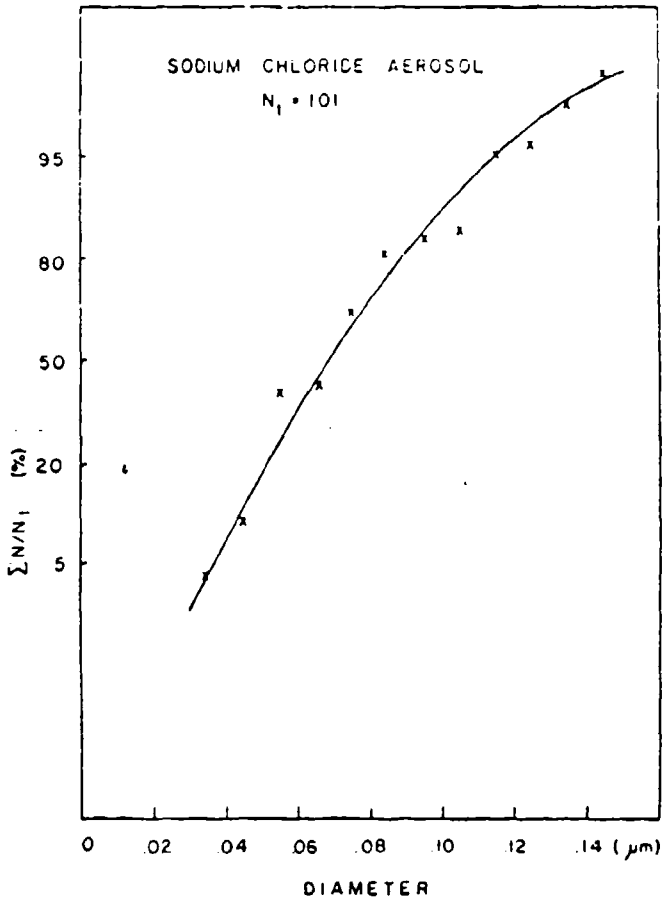

Figure D-3 Cumulative size spectrum of sodium chloride aerosol generated by fluid atomization aerosol generator. Particles, evaluated from SEM electronmicrographs, are plotted as a total number of particles smaller than a specific size.

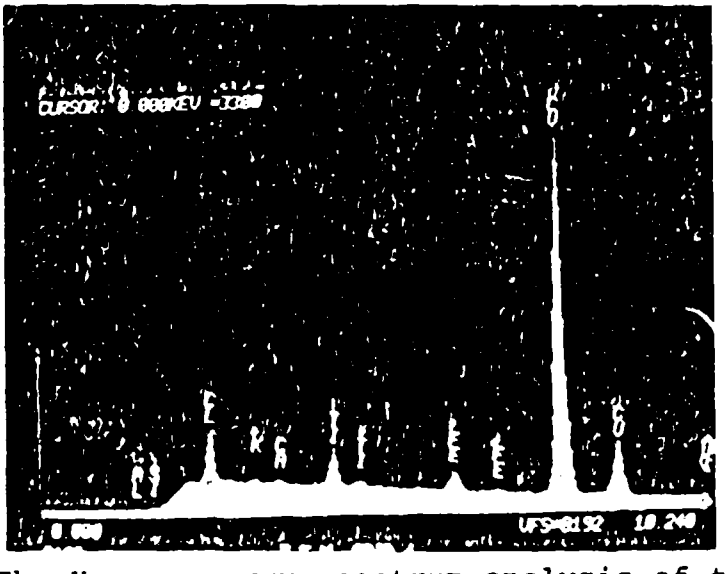

Figure D-4 The X-ray energy spectrum analysis of the $TiCl_4$ aerosol deposited on the electron microscopical grid.

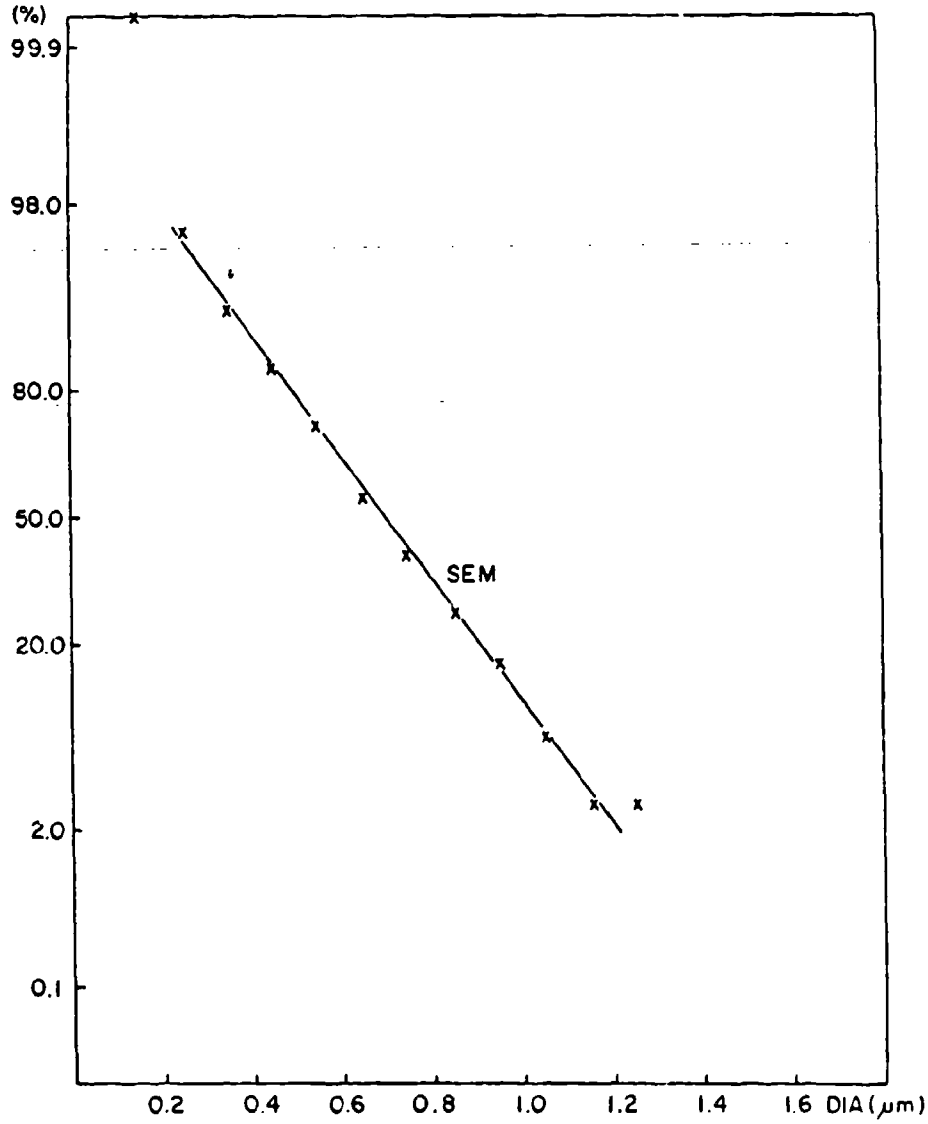

Figure D-5 Size distribution of $TiCl_4$ particles evaluated from SEM pictures. Particle frequency is plotted as a total number of particles larger than a specific size.

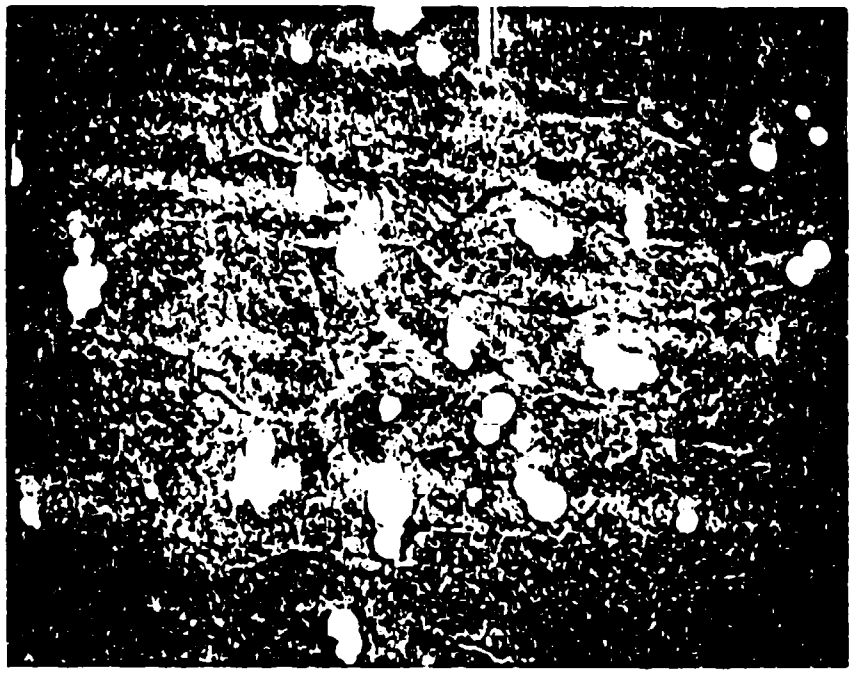

(a)

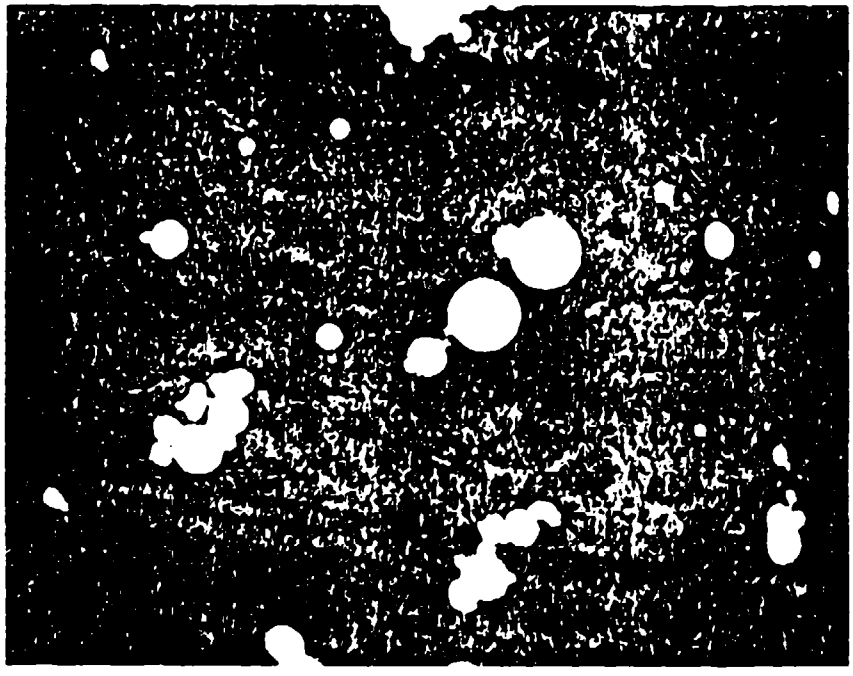

(b)

Figure D-6 $TiCl_4$ smoke particles deposited on a metallic substrate in an electrostatic precipitator. SEM picture at a 5000 x magnification.

Figure D-7 Red phosphorus smoke particles deposited on an electron microscopical grid. SEM magnification 2500 x.

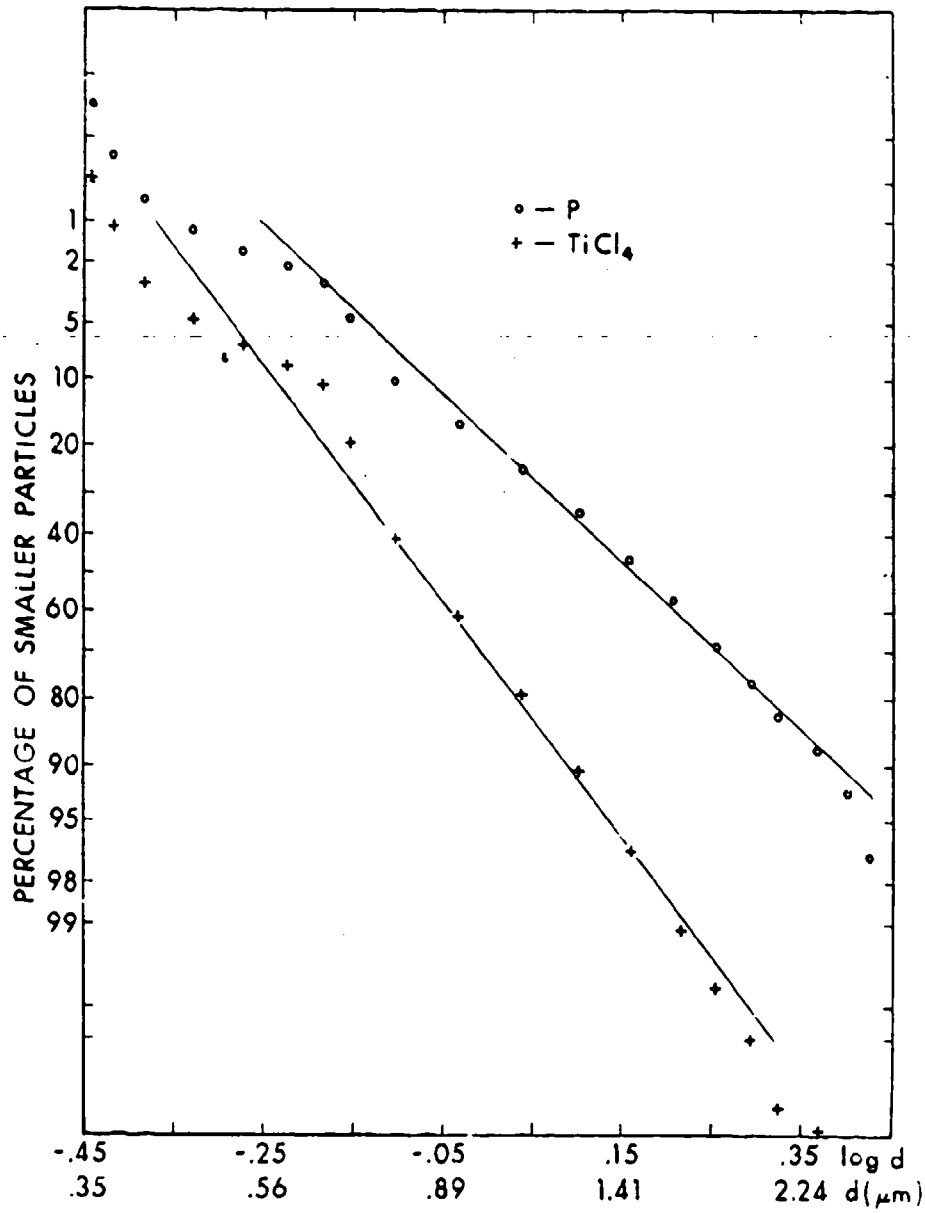

Figure D-8 Red phosphorus and titanium chloride particle size distribution evaluated from electronmicrographs. Plotted are cumulative particle size spectra (concentration of particles larger than a certain size--expressed in percent of the total number).

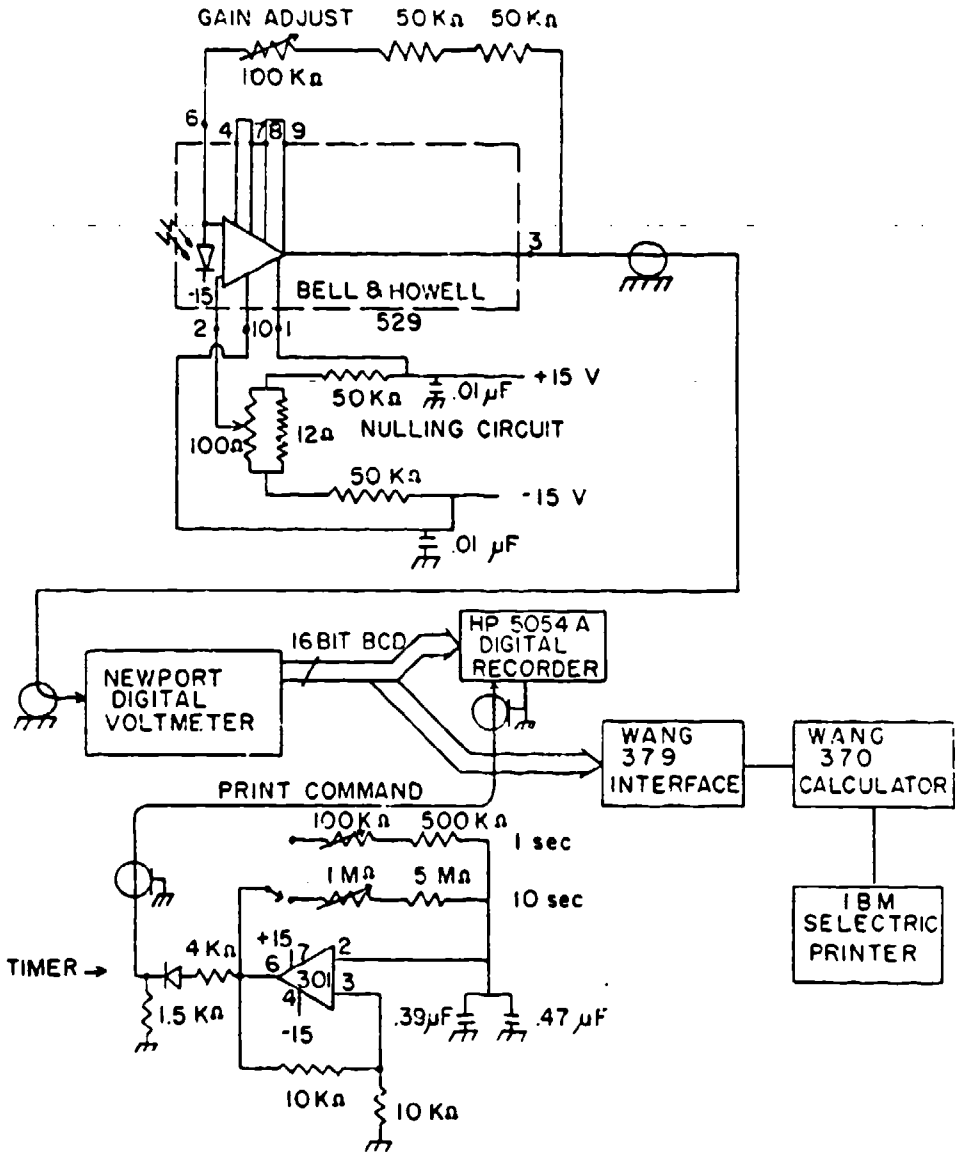

Figure D-9 Main parts and wiring diagram of the light extinction measurement.

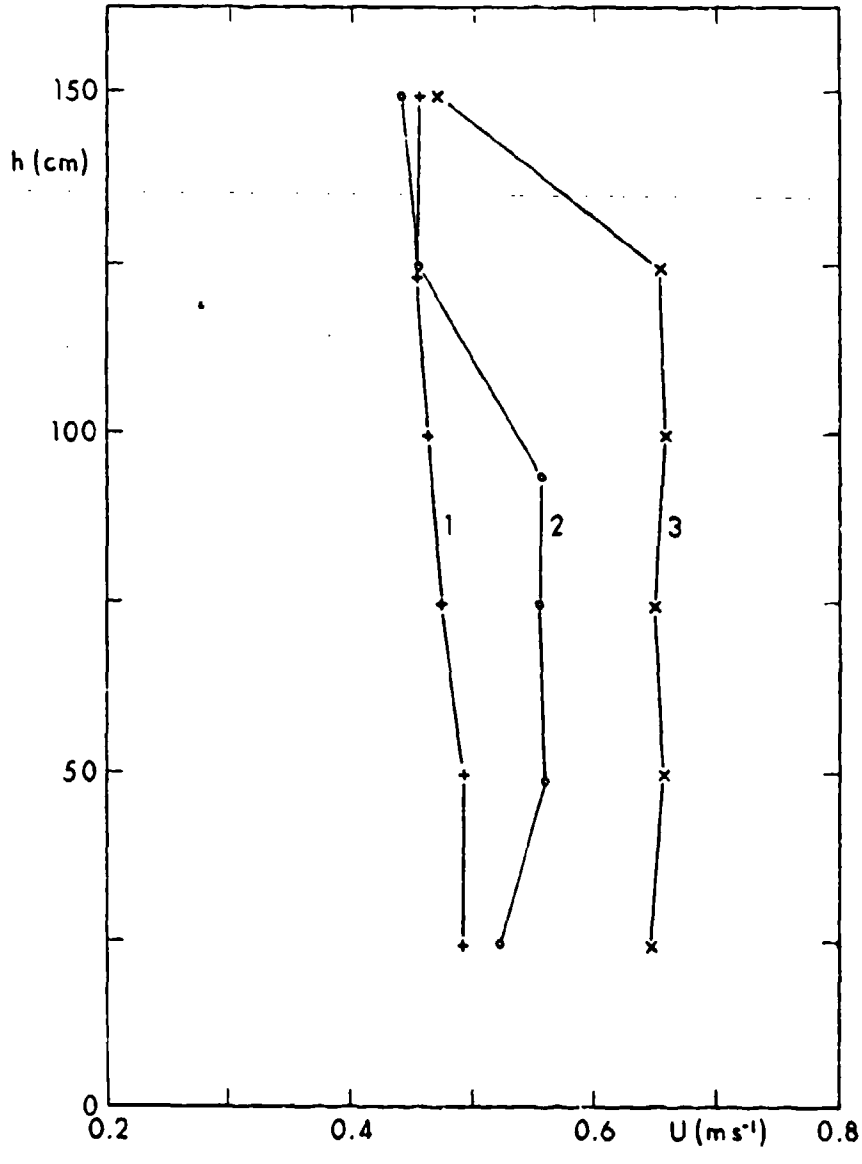

Figure D-10 Air velocity vertical profiles in the Large Environmental Chamber. Using different screens and flow straighteners three velocity profiles were finally reached. Arrangement 3 was used for most experiments. Later several experiments were also performed with arrangement 1.

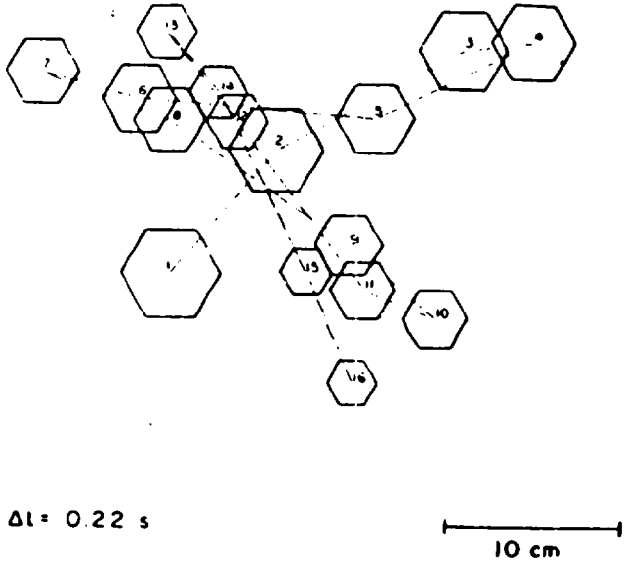

Figure D-11 Vertical camera record of a settling disk at a Re_z = 6120 (Podzimek, 1970)

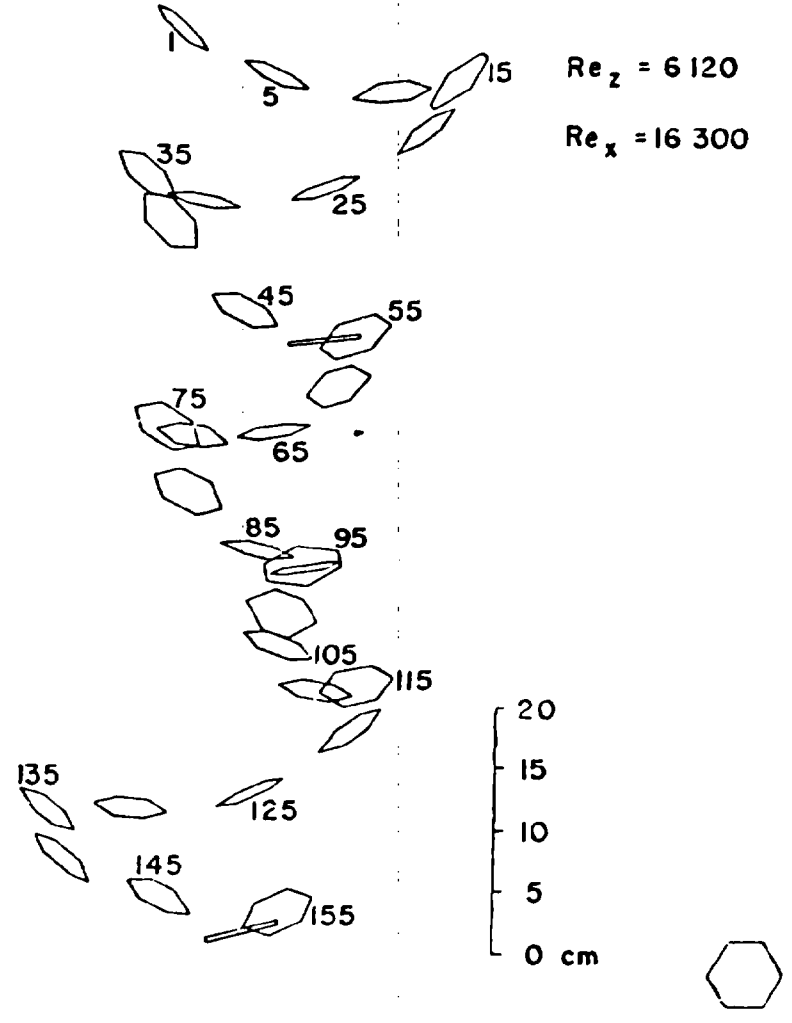

Figure D-12 Side view on a settling and oscillating disk at a Re_z = 6120 (Podzimek, 1970).

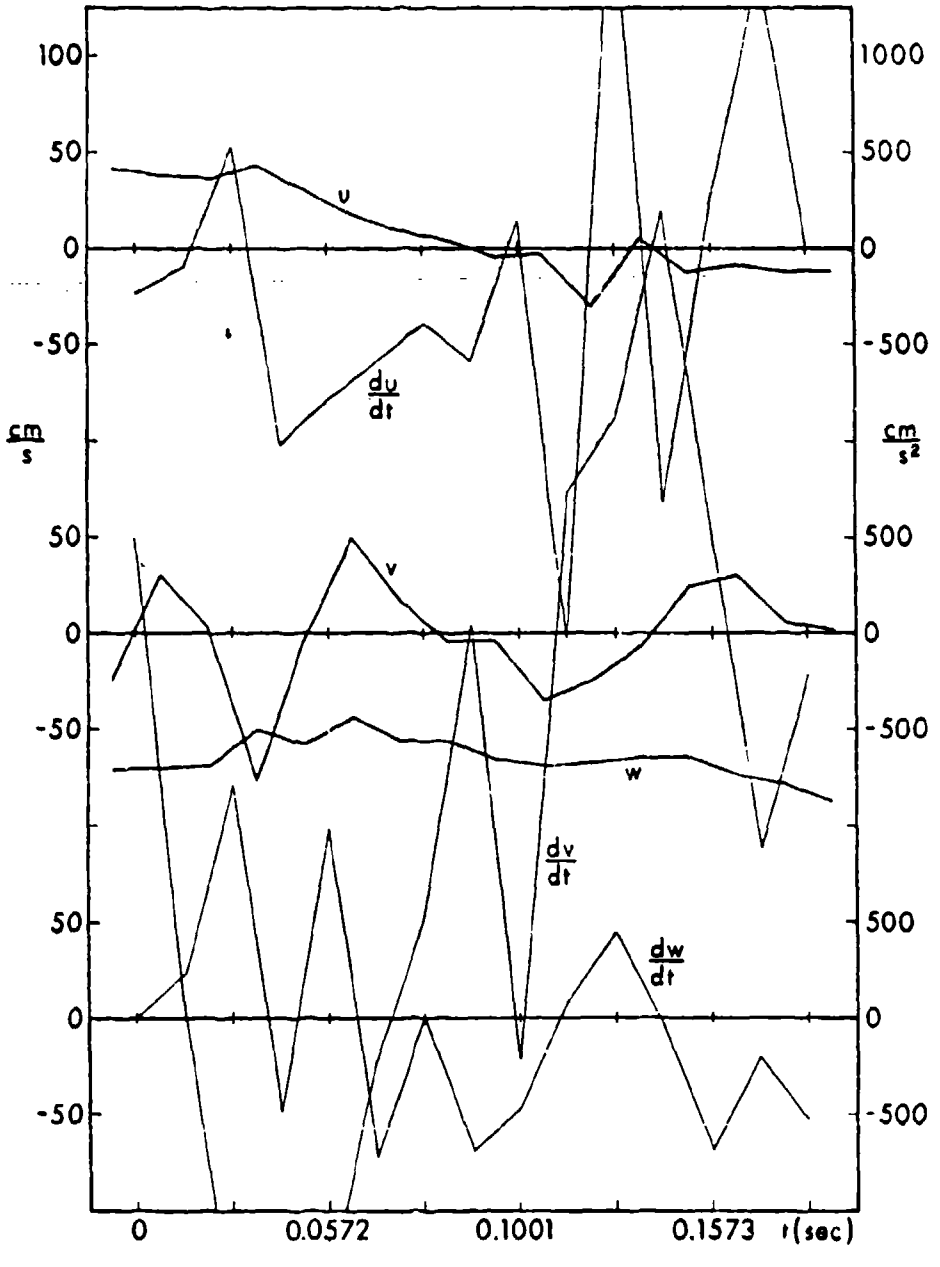

Figure D-13 Variation of the components of velocity and acceleration of a paper disk (d = 1.9 cm) falling in the air.

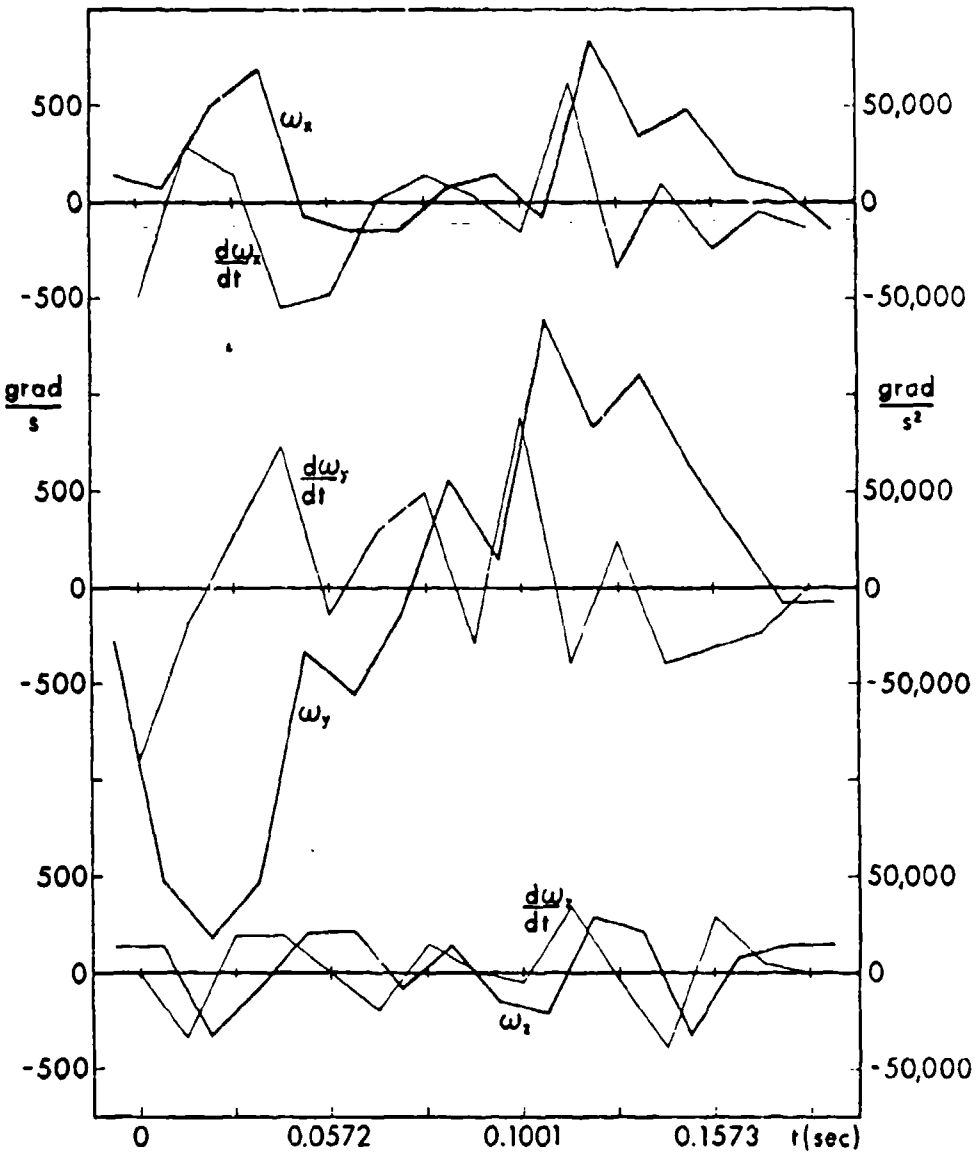

Figure D-14 Variation of the components of angular velocity and its time derivation of a paper disk (d = 1.9 cm) falling in the air.

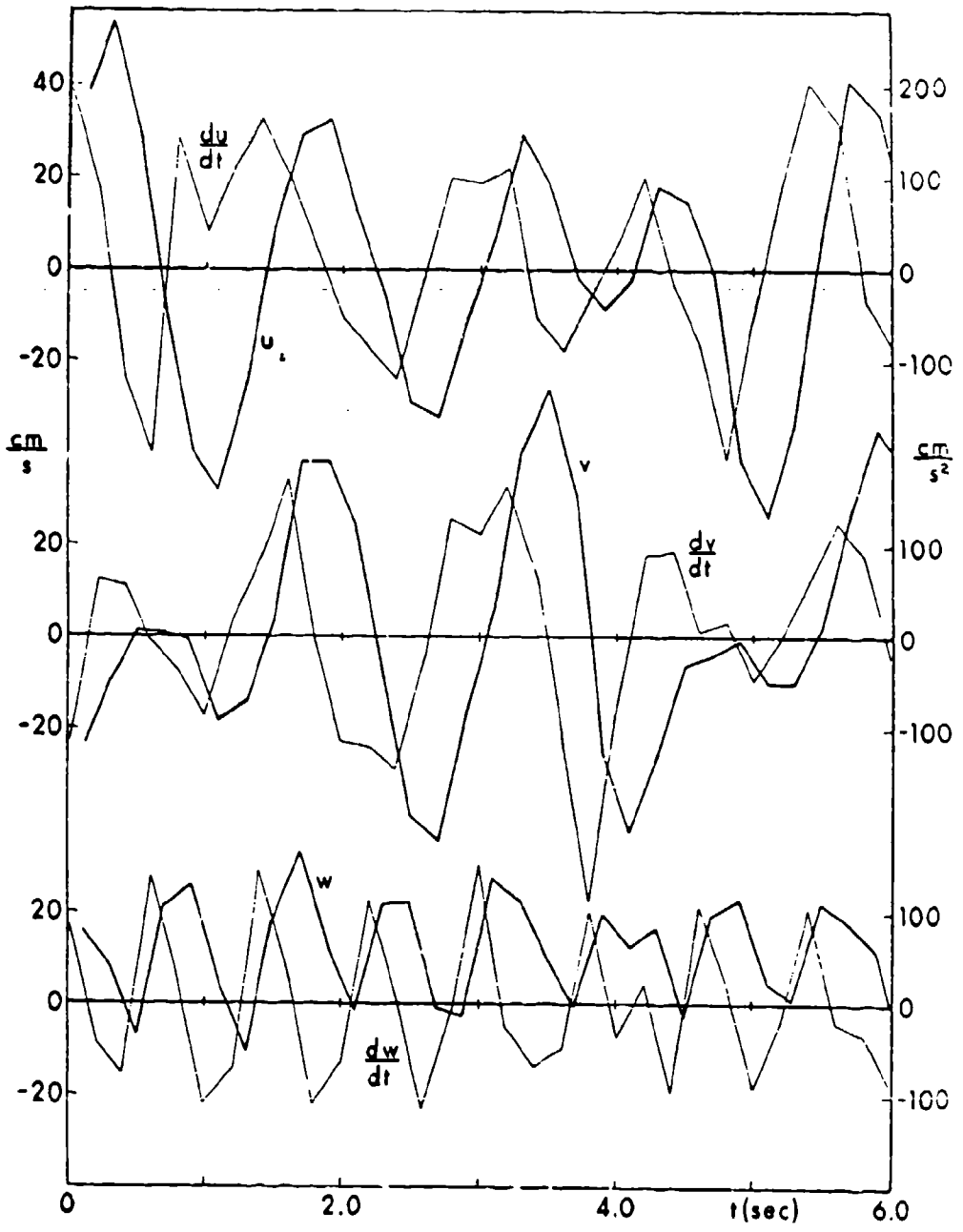

Figure D-13 Variation of the components of velocity and acceleration of an aluminum disk (d = 5.0 cm) falling in the water.

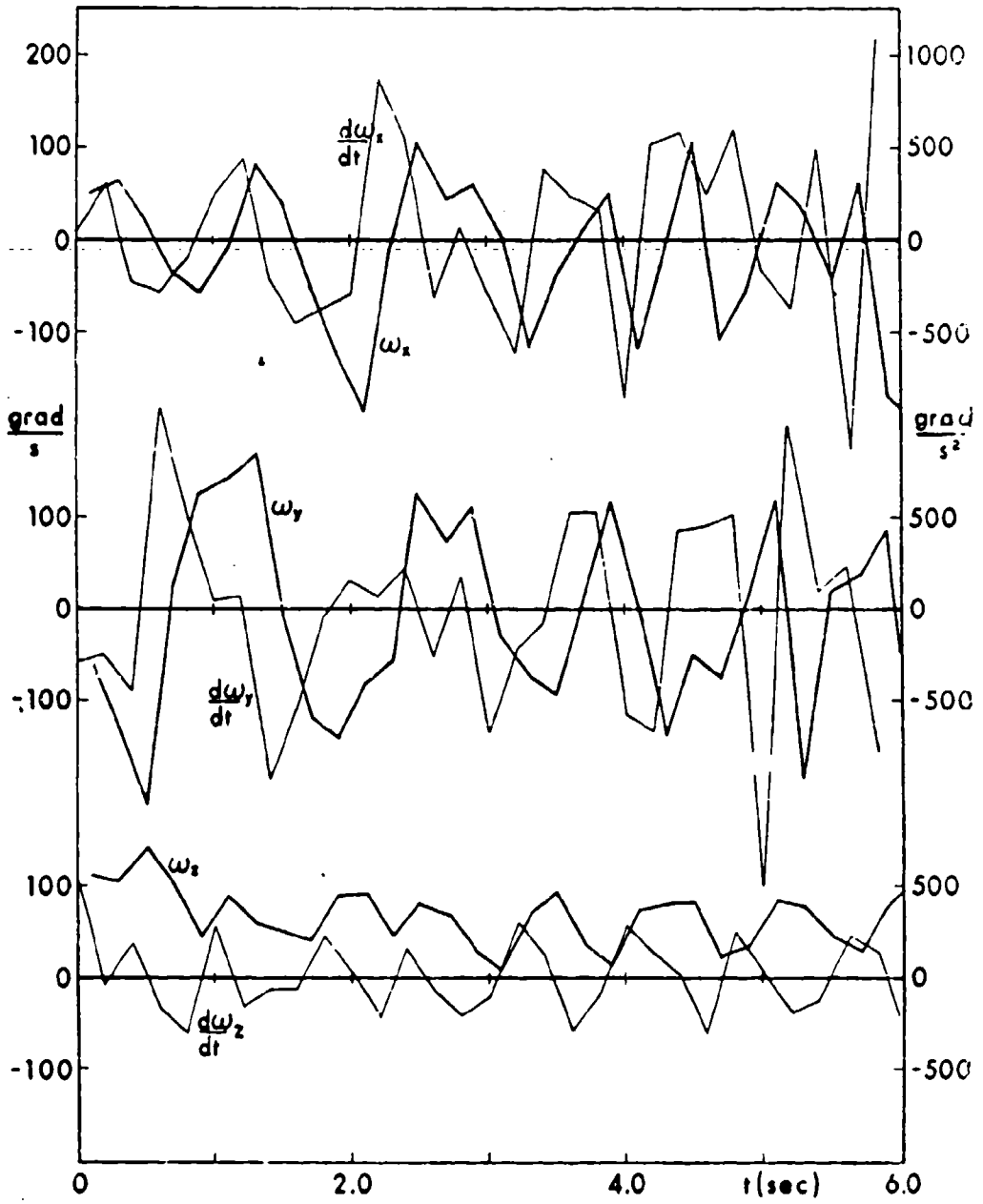

Figure D-16 Variation of the components of angular velocity and its time derivation of an aluminum disk (d = 5.0 cm) falling in the water.

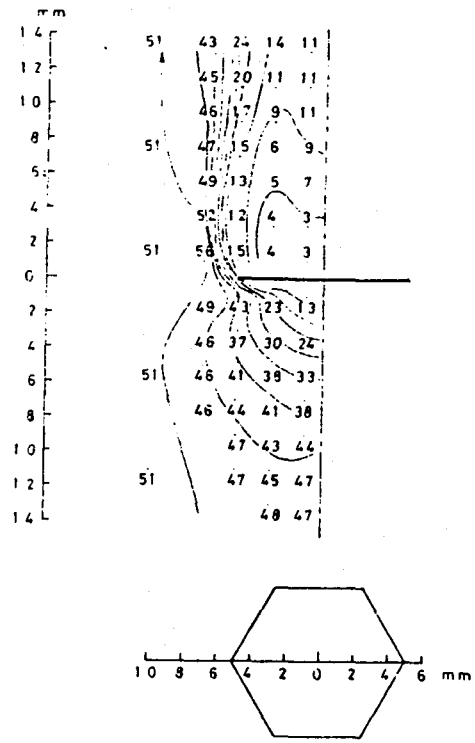

Figure D-17 Calculated velocity distribution around a hexagonal model (d = 1.0 cm) placed in the air flow of 0.5 m s^{-1} (Sasyo, 1971).

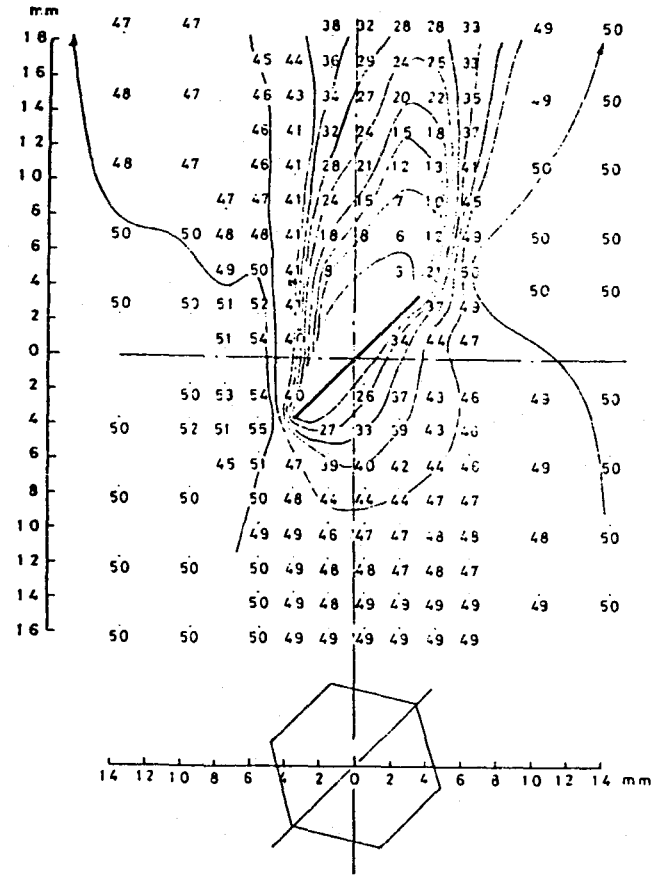

Figure D-18 Calculated velocity distribution around a hexagonal model (d = 1.0 cm) placed at 45° angle to the air flow of 0.5 m s^{-1} (Sasyo, 1971).

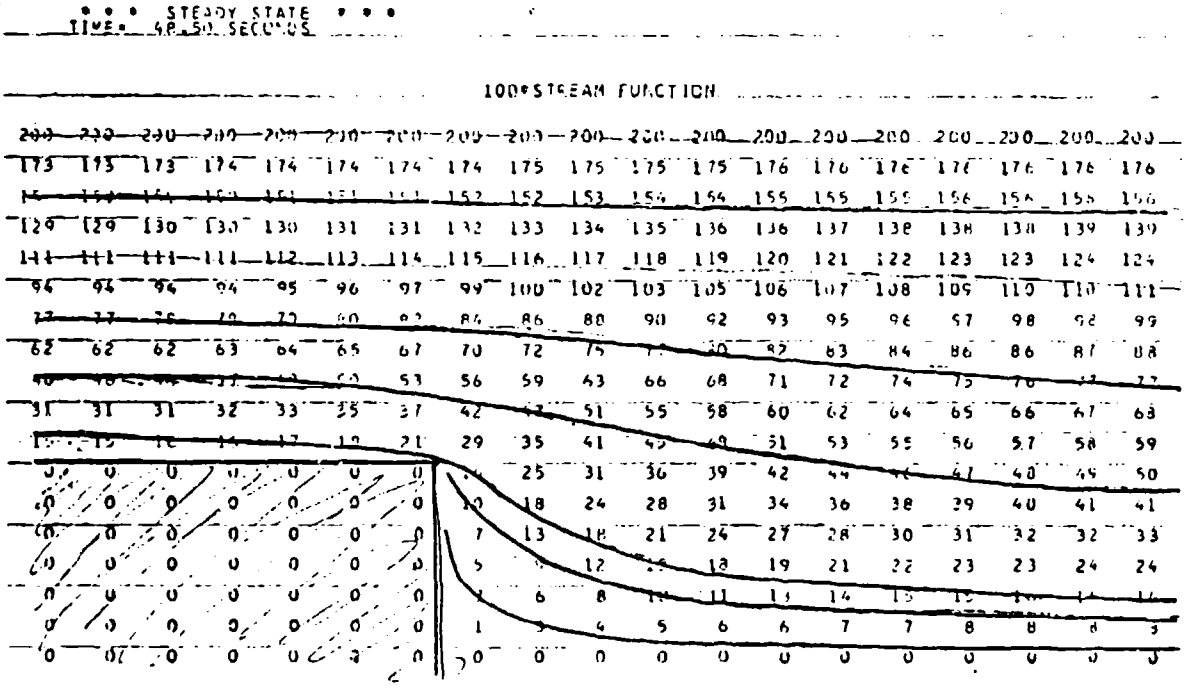

Figure D-19 Calculated streamlines of a viscous fluid around a two-dimensional obstacle at Re = 1000 (Schenewerk, 1979).

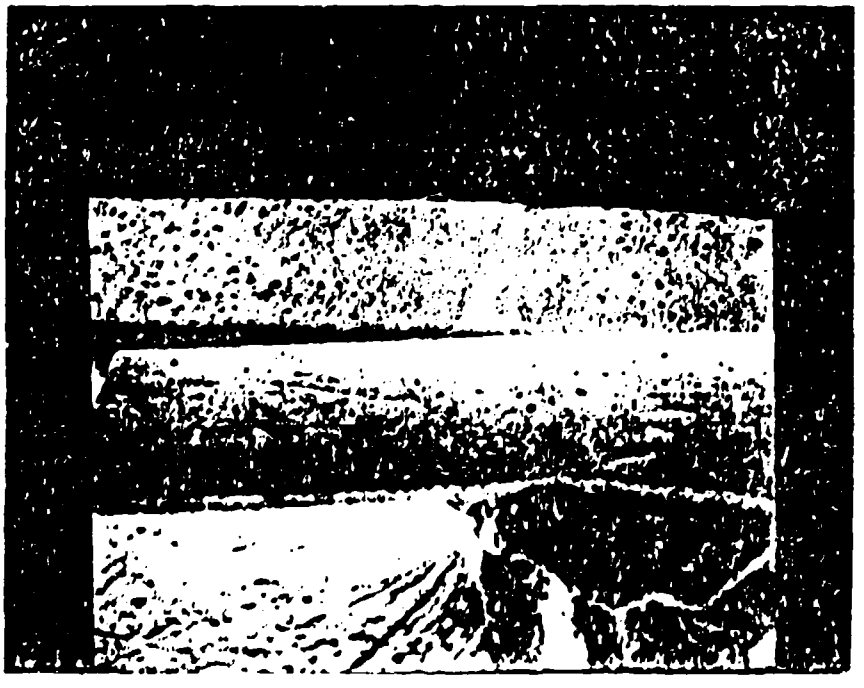

Figure D-20 Deposited $TiCl_4$ particles on two scavengers of 1 x 3 mm in size placed in a crossed position 1.2 mm one behind the other. In the lower part of the figure is the front plate (both plates were photographed in parellel positions unlike during the exposure).

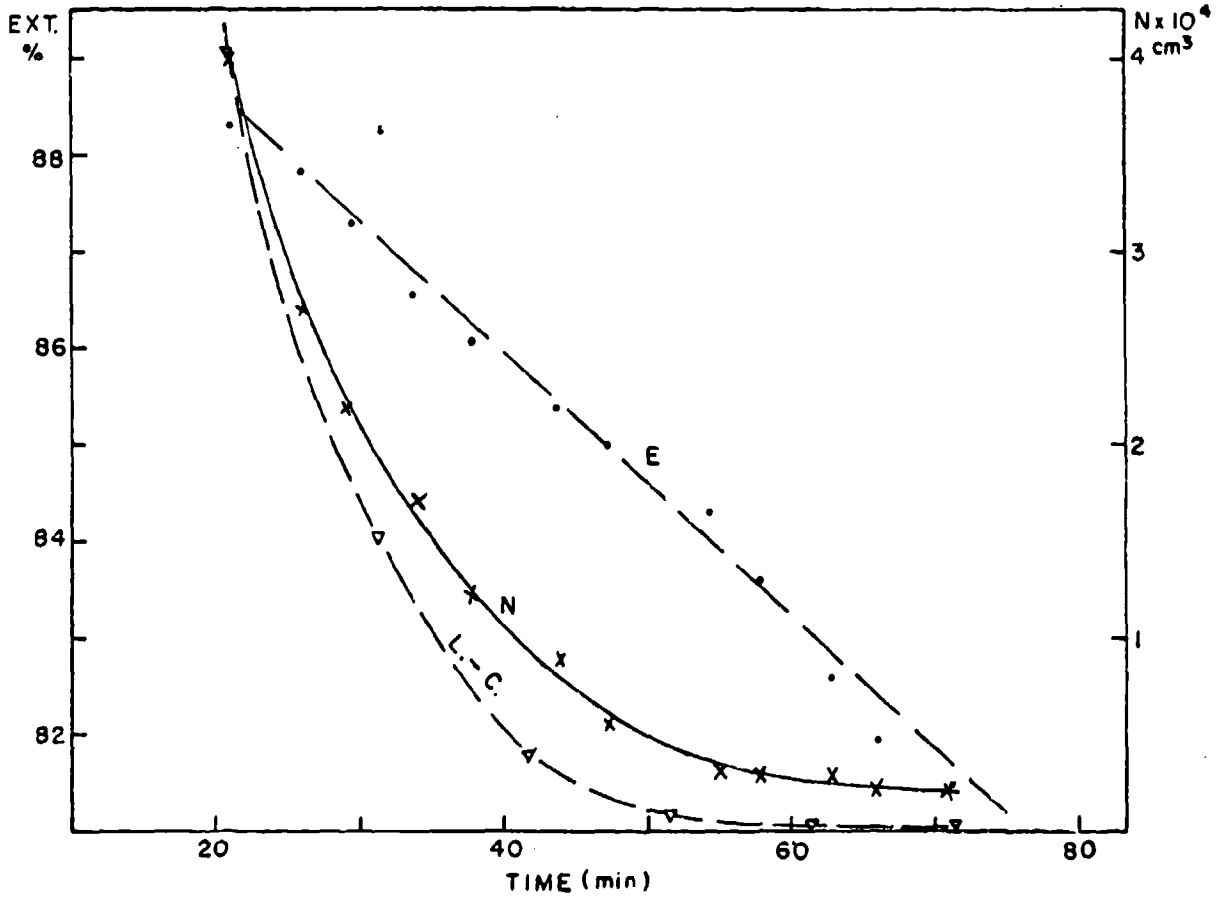

Figure D-21 Aitken nuclei counts (N) and smoke particle concentration calculated according to Lindauer-Castleman (1971) model plotted together with measured light extinction as a function of time in a clearing smoke cloud.

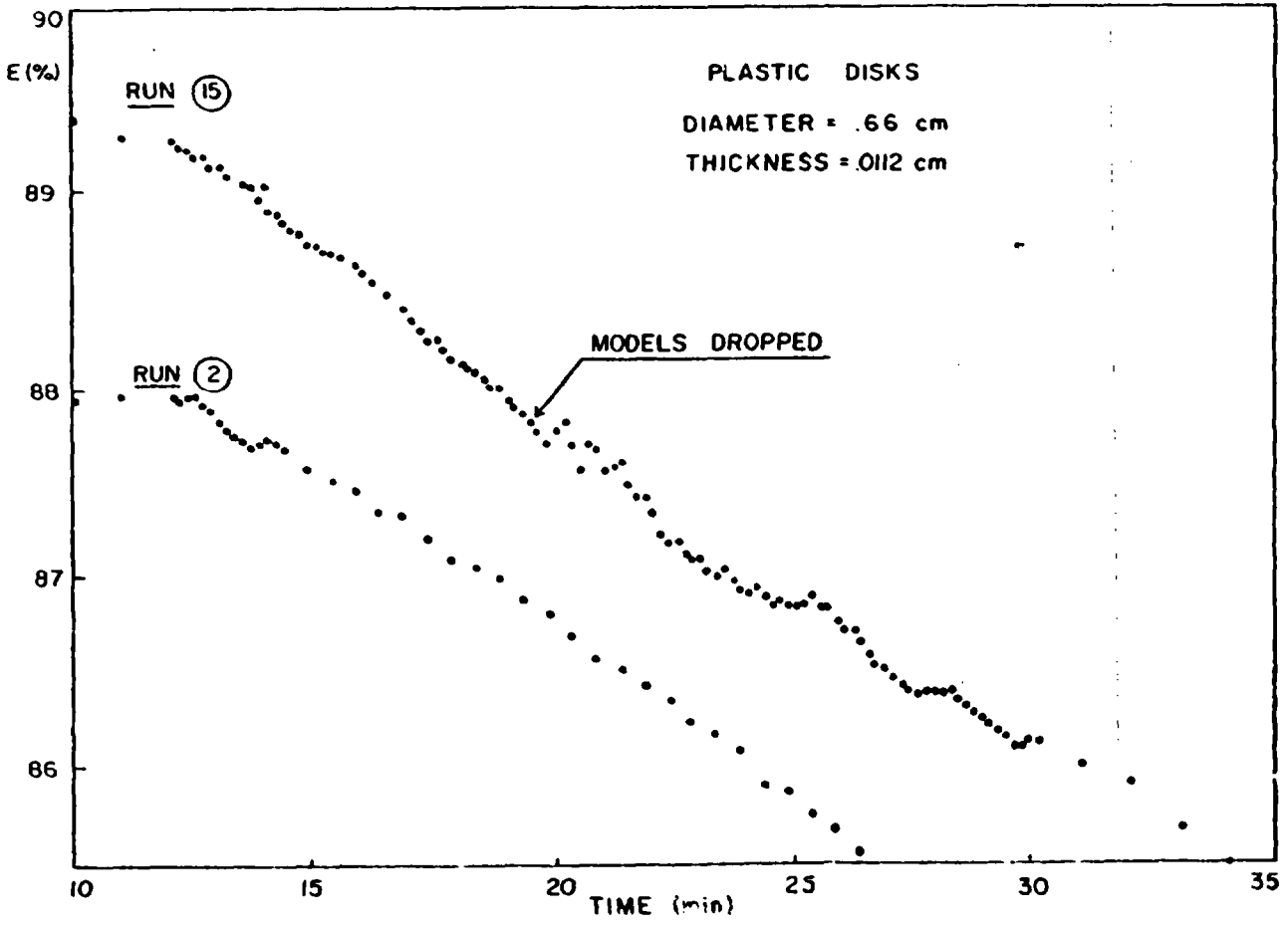

Figure D-22 Light extinction measurement in a $TiCl_4$ smoke cloud in which 60 plastic disks (d = 0.66 cm) were dropped.

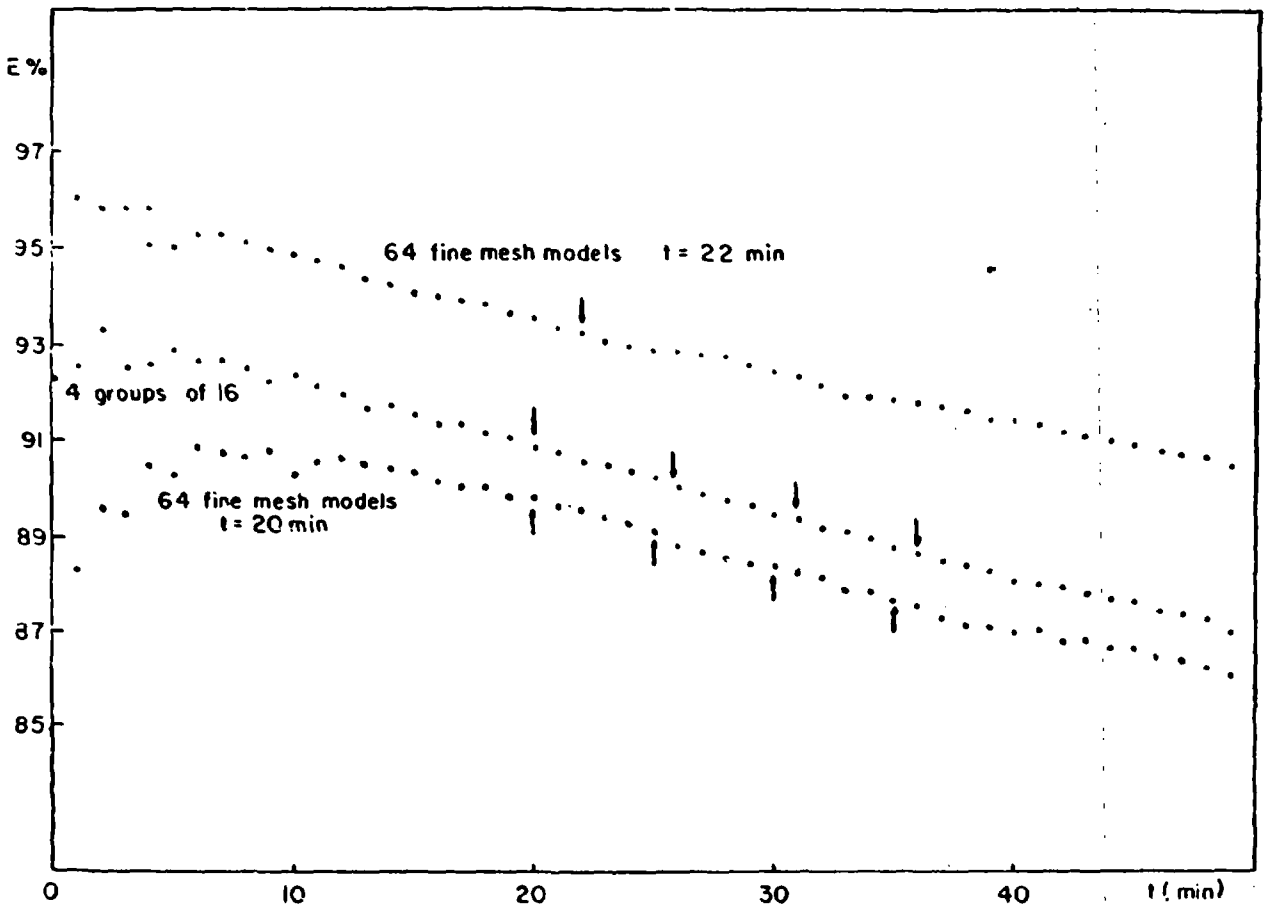

Figure D-23 Light extinction measurements in $TiCl_4$ smoke clouds in which 64 fine fiber mesh models (1.5 x 1.5 cm^2) were dropped at once or in several batches.

Table D-1. Settling of Scavengers in Quiescent Air

Model (material)	Dimension [cm]	Thick-ness [cm]	Cross section [cm^2]	Mass [g]	V_z [$cm\ s^{-1}$]	C_D	Re	Mode of fall	A [cm]	λ [cm]	I
Disk (paper)	0.66	0.017	0.342	0.0056	159.6	0.447	689.				
Disk (Plexiglas)	0.66	0.018	0.342	0.0073	274.0	0.152	1183.				
					291.0	0.134	1256.				
Disk (foam)	0.66	0.200	0.342	0.00197	124.7	0.670	538.				
					119.9	0.670	517.				
Disk (foam)	1.75	0.200	2.410	0.0104	92.5	0.790	1020.	slide-tumble	1.3	12.0	0.0985
					89.5	0.846	990.	slide-tumble	0.8	14.0	0.0985
					109.0	0.569	1210.	slide-tumble	3.6	20.0	0.0985
					101.0	0.664	1120.	slide-tumble	0.7	18.0	0.0985
Disk (paper)	1.83	0.018	2.630	0.0259	125.0	0.990	1450.	oscil.	0.8	28.0	0.2151
					123.0	1.020	1430.	oscil.	0.7	25.0	0.2151
					120.0	1.070	1440.	oscil.	0.7	24.0	0.2151
Disk (paper)	1.90	0.018	2.840	0.0286	144.0	0.760	1732.	oscil.	2.8	25.0	0.2114
					130.0	0.900	1567.	oscil.	3.6	28.0	0.2114
					129.0	0.950	1548.	oscil.	0.7	27.0	0.2114
					130.0	0.930	1565.	oscil.	1.2	30.0	0.2114
					137.0	0.840	1649.	oscil.	0.6	20.0	0.2114
Disk (foam)	2.54	0.620	4.910	0.2460	126.0	2.950	2030.	sliding	2.5	32.0	
					169.0	2.750	2720.	sliding			
					177.0	2.510	2850.	sliding			
					173.0	2.620	2780.	sliding			
Disk (paper)	2.80	0.018	6.160	0.0623	136.0	0.850	2415.	oscil.-slides	?	23.0	0.1487
					141.0	0.990	2245.	oscil.-slides	3.4	36.0	0.1487
					126.0	0.790	2502.	oscil.-slides	2.2	28.0	0.1487

Table D-1. Settling of Scavengers in Quiescent Air (cont'd)

Model (material)	Dimension [cm]	Thick-ness [cm]	Cross section [cm^2]	Mass [g]	$V_{z^{-1}}$ [cm s^{-1}]	C_D	Re	Mode of fall	A [cm]	λ [cm]	I
Square (paper)	0.90	0.018	0.810	0.0082	130.0	0.750	822.	oscil.			
					132.5	0.890	964.	oscil.			
					129.5	0.940	943.	oscil.			
Square (foam)	1.30	0.200	1.690	0.0075	76.1	1.200	800.	oscil.			
					90.5	0.851	951.	oscil.			
					95.4	0.766	1000.	oscil.			
Square (paper)	1.40	0.018	1.960	0.0193	132.0	0.886	1475.	oscil.			
					134.0	0.859	1510.	oscil.			
					128.0	0.943	1440.	oscil.			
Square (paper)	1.60	0.018	2.560	0.0258	122.5	1.100	1574.	oscil.			
					114.7	1.200	1484.	oscil.			
					121.7	1.100	1571.	oscil.			
Square (paper)	2.22	0.018	4.909	0.0628	123.2	1.050	2286.	oscil.			
					115.0	1.190	2113.	oscil.	0.7	20.0	
Rectangle (paper)	3.0x0.5	0.018	1.500	0.0159	153.0	0.300	482.	oscil.-slides	2.0	20.0	
					121.0	0.411	380.	oscil.-slides	2.5	20.0	
					130.0	0.475	408.	oscil.-slides	3.0	21.0	
Hexagon (paper)	0.87	0.018	0.584	0.0056	121.0	1.030	670.				
					136.0	0.813	776.				
Hexagon (paper)	1.23	0.018	1.190	0.0138	117.0	1.206	938.	oscil.			
					139.0	0.885	1098.	oscil.-slides	0.6	26.0	
Hexagon (paper)	1.72	0.018	2.220	0.0219	130.5	0.911	1420.	oscil.			
					129.0	0.933	1400.	oscil.			
Hexagon (foam)	1.72	0.200	2.220	0.0121	89.9	1.000	975.	oscil			

Table D-1. Settling of Scavengers in Quiescent Air (cont'd)

Model (material)	Dimension [cm]	Thick-ness [cm]	Cross section [cm^2]	Mass [g]	V_z [$cm\ s^{-1}$]	C_D	Re	Model of fall	A [cm]	λ [cm]	I
Hexagon (foam)	1.81	0.200	2.30	0.0124	96.5	0.872	1110.	oscil.			
Hexagon (paper)	1.87	0.018	2.750	0.0308	120.0	1.110	1565.	oscil.			
					121.0	1.100	1578.	oscil.			
					134.0	0.890	1738.	oscil.-slides	1.3	32.0	
Triangle (paper)	0.70	0.018	0.210	0.0039	142.0	0.917	604.	oscil.			
					115.5	1.360	490.	oscil.			
					132.0	0.812	560.	oscil.			
					143.0	0.774	1040.	oscil.			
Triangle (paper)	1.20	0.018	0.640	0.0063	124.0	1.080	1394	oscil.			
					131.0	0.970	1481	oscil.			
Ellipse (paper)	a=1.55;b=0.9	0.018	1.100	0.0104	121.0	1.010	954.	oscil.	0.2	29.0	
					125.0	0.950	998.	oscil.	0.3	34.4	
Ellipse (paper)	a=1.55;b=1.28	0.018	1.550	0.0151	127.0	0.947	1127.	oscil.	0.3	31.0	
					124.0	0.992	1098	oscil.	1.3	28.0	
Ellipse (paper)	a=2.20;b=1.26	0.018	2.190	0.0211	124.0	0.988	1398.	oscil.	0.5	35.0	
					128.0	0.921	1441.	oscil.	0.4	26.0	
Ellipse (paper)	a=2.20;b=1.90	0.018	3.110	0.0300	119.0	2.020	1592.	oscil.	0.7	31.0	
					102.0	1.470	1283.	oscil.	0.7	31.0	
Ellipse (paper)	a=2.85;b=1.64	0.018	3.630	0.0350	140.0	0.770	2054.	oscil.-slides	1.9	38.0	
Ellipse (paper)	a=2.85;b=2.33	0.018	5.215	0.0504	105.5	1.360	1558.	slides	0.7	34.5	
					124.0	0.980	2054.	slides	0.7	44.1	
					106.8	1.330	1667.	slides	1.2	35.0	

Table D-2. Settling of Scavengers at a Side Wind of 0.7 m s^{-1}

Model (material)	Dimension (dia. side) [cm]	Thickness [cm]	Cross section [cm^2]	Mass [g]	V_z [$cm\ s^{-1}$]	V_x [$cm\ s^{-1}$]	V [$cm\ s^{-1}$]	C_D	Re	Mode of fall	A [cm]	λ [cm]
Disk (paper)	0.728	0.017	0.416	0.0064	154.1	83.0	175.0	0.380	461.4	oscil.		
Disk (paper)	1.042	0.017	0.853	0.0146	132.6	69.6	149.7	0.587	987.5	oscil.-slides		
					105.8	52.9	118.3	0.940	780.4			
Disk (paper)	1.43	0.017	1.60	0.0286	208.0	90.0	226.6	0.27	2050.7	oscil.-slides		
					385.8	51.4	389.2	0.091	3522.5			
					245.8	40.0	249.0	0.220	2253.6			
					471.5	128.6	488.7	0.057	4423.3			
					137.2	40.0	142.9	0.670	1295.2		0.5	16.0
					445.8	117.2	460.9	0.060	4171.8			
					171.5	25.7	173.4	0.460	1569.2			
					154.3	17.2	155.3	0.570	1405.3			
					139.3	103.6	173.6	0.460	1571.3			
Disk (paper)	2.54	0.017	5.07	0.0828	137.9	79.6	159.2	0.500	2560.3	oscil.-slides		
					144.3	69.4	160.1	0.500	2574.0	tumbles		13.0
					181.0	27.5	183.1	0.380	3943.8			
					126.3	5.0	126.4	0.800	2032.5			
Disk (paper)	2.54	0.017	5.07	0.0829	162.0	24.8	163.9	0.470	2635.3	oscil.-slides	0.5	17.5
					139.9	52.0	149.3	0.570	2399.9	tumbles		
					172.9	12.5	173.4	0.420	2787.5			
					148.6	48.6	156.3	0.520	2513.7			
					185.3	103.8	212.4	0.280	3415.3			
					141.2	67.1	156.3	0.520	2513.8			
					169.6	128.5	212.8	0.280	3421.4			
					76.2	220.2	232.9	0.230	3746.2			
					205.3	11.6	205.6	0.300	3306.5			
					183.8	83.8	202.0	0.310	3248.2			
					163.3	75.5	179.9	0.390	2892.8			
					137.6	10.6	138.0	0.670	2219.2			
					172.5	52.7	180.4	0.390	2900.4			
					180.8	116.3	215.0	0.280	3456.8			

Table D-2. Settling of Scavengers at a Side Wind of 0.7 m s^{-1} (cont'd)

Model (material)	Dimension (dia. side) [cm]	Thick-ness [cm]	Cross section [cm^2]	Mass [g]	V_z [cm s^{-1}]	V_x [cm s^{-1}]	V [cm s^{-1}]	C_D	Re	Mode of fall	A [cm]	λ [cm]
Disk (foam)	2.54	0.6	5.07	0.0782	158.5	97.9	186.3	0.340	2995.3	oscil.-slides	0.6	18.0
					173.1	88.2	194.2	0.320	3123.4			
					135.3	77.2	155.7	0.490	2504.1			
					114.3	71.1	134.6	0.660	2164.7			
					115.5	67.4	133.7	0.670	2150.5			
					129.5	114.3	172.7	0.400	2777.3			
Disk (heavier scarf)	2.54		5.07	0.0249	99.2	58.1	114.9	0.290	1848.6	quiet settling		
					91.1	56.0	106.9	0.330	1719.5			
Disk (hair scarf)	2.54	fiber 0.0046	5.07	0.0054	44.4	59.3	74.1	0.150	1190.9	quiet settling		
					33.9	56.4	65.8	0.190	1058.4	in horizontal		
					42.3	61.4	74.6	0.150	1199.1	position		
					40.6	55.9	69.1	0.170	1111.2			
Disk (hair scarf)	2.532	0.0046 fiber	5.00	0.0054	31.0	48.9	57.9	0.240	931.0	quiet settling		
					28.8	41.5	50.5	0.320	812.3			
					35.2	49.5	60.7	0.220	976.7			
					41.7	63.1	75.6	0.140	1216.2			
					33.9	50.8	61.1	0.22	982.1			
Square (paper)	2.249	0.017	5.06	0.0794	191.9	54.3	199.4	0.300	2839.9	oscil.-slides		
					178.2	86.6	198.1	0.310	2821.4			
					158.2	23.0	152.9	0.470	2176.7			
					220.9	87.6	237.7	0.210	3384.9			
					174.1	61.6	184.7	0.350	2629.8			
					174.9	41.3	179.7	0.370	2559.1			
					173.4	54.1	181.6	0.370	2586.6			
					161.7	71.1	176.6	0.390	2515.4			
					185.8	13.4	186.3	0.350	2652.6			
					159.1	41.1	164.3	0.450	2339.9			
					162.4	114.7	194.8	0.310	2774.2			
					192.2	32.3	194.9	0.320	2775.4			

Table D-2. Settling of Scavengers at a Side Wind of 0.7 m s^{-1} (cont'd)

Model (material)	Dimension (dia. side) [cm]	Thick-ness [cm]	Cross section [cm^2]	Mass [g]	V_z [cm s^{-1}]	V_x [cm s^{-1}]	V [cm s^{-1}]	C_D	Re	Mode of fall	A [cm]	λ [cm]
Square (paper) (continued)					158.8	92.6	183.8	0.360	2617.7			
					187.5	55.1	195.4	0.320	2782.9			
					148.6	88.7	173.1	0.400	2464.4			
					147.8	47.6	155.3	0.500	2211.2			
Square (hair scarf)	2.236	fiber 0.0046	5.00	0.0054	47.2	63.5	79.1	0.127	1119.7	quiet settling		
					38.1	51.2	63.8	0.203	903.1			
					39.9	54.9	67.9	0.178	960.4			
Rectangle (paper)	1.0x5.0	0.017	5.00	0.0839	206.8	68.0	217.7	0.270	1377.8	oscil.-slides		
					169.3	59.7	179.5	0.400	1136.2	oscil.		
					207.5	113.4	236.5	0.230	1496.7	slides		
					202.4	63.1	212.0	0.290	1341.8	oscil.-slides		
					265.7	52.9	270.9	0.180	1714.6	slides		
Rectangle (paper)	1.0x5.0	0.017	5.00	0.0839	217.9	63.7	227.0	0.25	1436.9	slides-tumbles		
					215.8	46.4	220.7	0.27	1397.0			
					187.2	84.5	205.4	0.31	1300.2			
					129.5	203.1	240.9	0.22	1524.9			
					272.0	102.2	290.6	0.15	1839.5			
					186.2	76.6	201.3	0.32	1274.2			
					115.4	21.4	117.4	0.94	743.1			
					185.7	144.1	235.1	0.23	1488.2			
					95.1	117.7	151.3	0.57	957.7			
L-type (paper)	0.635x2.54x2.54	0.017	2.823	0.0357	110.8	55.4	123.9	1.270	498.0	oscil.		
L-type (paper)	1.0x3.0x3.0	0.017	5.00	0.0799	165.6	63.6	177.4	0.39	1122.7	oscil.-rotates		
					157.6	59.3	168.4	0.43	1065.8	many tumble		
					171.5	45.6	177.5	0.39	1126.2			
					198.7	23.5	200.1	0.31	1266.3			
					182.1	70.8	195.4	0.32	1236.6			
					214.6	60.7	223.0	0.25	1411.5			
					222.6	142.2	264.1	0.18	1671.8			

Table D-2. Settling of Scavengers at a Side Wind of 0.7 m s^{-1} (cont'd)

Model (material)	Dimension (dia. side) [cm]	Thick-ness [cm]	Cross section [cm^2]	Mass [g]	V_z [cm s^{-1}]	V_x [cm s^{-1}]	V [cm s^{-1}]	C_D	Re	Mode of fall	A [cm]	λ [cm]
L-type (paper)	0.635x5.08x1.27	0.017	3.629	0.0577	112.8	55.4	125.7	0.960	505.2	tumbles		
L-type (paper)	1.0x4.0x2.0	0.017	5.00	0.0803	168.5	123.5	208.9	0.28	1322.2	oscil.-slightly		
					177.0	111.3	209.1	0.28	1323.4	rotates		
					149.9	107.8	184.6	0.36	1168.4	several tumbles		
					174.9	92.4	197.8	0.32	1251.9			
					216.2	3.5	216.2	0.27	1368.4			
					146.9	112.6	185.1	0.36	1171.5			
					164.3	201.4	259.9	0.18	1644.9			
					198.5	98.3	221.5	0.25	1401.9			
					224.9	94.8	244.1	0.21	1544.9			
					226.3	45.5	230.8	0.23	1460.8			
Hexagon (paper)	d=2.70 outer	0.017	5.00	0.0809	156.1	21.2	157.5	0.50	937.3	slides		
					247.6	73.2	238.2	0.19	1536.3	several tumbles		
					192.5	114.0	223.7	0.25	1331.2	tumble		13.0
					164.1	23.0	165.7	0.45	985.9			
					241.5	123.9	271.4	0.17	1615.0			
Triangle (paper)	3.16;3.16;4.47	0.017	4.99	0.0799	232.5	229.5	326.7	0.12	4619.5	oscil.-slides		
					328.5	1.5	328.6	0.11	4646.4	rotates		
					244.5	185.4	306.8	0.13	4338.2			
					241.6	11.6	241.9	0.21	3420.5			
					246.5	180.5	305.5	0.13	4319.8			22.0
					210.0	36.6	213.2	0.27	3014.7			
					219.3	111.6	246.1	0.20	3479.9			
					147.7	81.6	168.7	0.43	2385.4			
					265.3	56.2	271.2	0.17	3834.8			
Star (paper)	d=4.000	0.017	9.47	0.1129	146.4	71.6	163.0	0.350	4244.5	oscil.-slides		
					258.6	98.5	276.7	0.120	7205.3			
					159.6	74.3	176.1	0.300	4585.6			
					204.8	135.7	245.7	0.150	6398.0			

Table D-2. Settling of Scavengers at a Side Wind of 0.7 m s^{-1} (cont'd)

Model (material)	Dimension (dia. side) [cm]	Thick-ness [cm]	Cross section [cm]	Mass [g]	V_z [cm s^{-1}]	V_x [cm s^{-1}]	V [cm s^{-1}]	C_D	Re	Mode of fail	A [cm]	λ [cm]
Cross (paper)	(1.0x3cm)x2	0.017	5.00	0.0850	262.6	92.3	278.4	0.17	5286.1	oscil.-rotates		
					167.5	3[illegible].9	171.3	0.45	3252.5	around the z-		
					176.1	1[illegible]6.5	216.8	0.28	4117.0	axis		
					167.1	91.5	190.5	0.36	3617.3			

Table D-3. Calculated Stokes numbers and collection efficiency E (taken from Starr, 1967) for different smoke particle sizes, two different particle densities and fiber diameter of 46 μm. Scavenger's settling velocity was $V = 51.1 \text{ cm s}^{-1}$.

Particle radius r [μm]	$\rho = 1.0 \text{ g cm}^{-3}$		$\rho = 4.26 \text{ g cm}^{-3}$	
	St. no.	E_i	St. no.	E_i
0.05	3.3909×10^{-4}	0.000	1.4445×10^{-3}	0.000
0.1	1.3564×10^{-3}	0.000	5.2780×10^{-3}	0.001
0.3	1.2207×10^{-2}	0.000	5.2003×10^{-2}	0.005
0.5	3.3909×10^{-2}	0.001	1.4445×10^{-1}	0.015
0.7	6.6462×10^{-2}	0.005	2.8313×10^{-1}	0.060
1.0	1.3564×10^{-1}	0.010	5.7782×10^{-1}	0.170
1.5	3.0518×10^{-1}	0.065	1.3001	0.370
2.0	5.4255×10^{-1}	0.130	2.3113	0.560
3.0	1.2207	0.360	5.2003	0.725
5.0	3.3909	0.630	14.4450	0.850

Table D-4. Scavenger efficiencies of a fine fiber mesh scavenger (d = 46 μm) for a population of smoke particles with a specific size distribution (V = 51.1 cm s^{-1}).

Particle radius r [μm]	$N(r)_i / N(r)$	E_i ρ_p=1.0 g cm^{-3}	E_i ρ_p=4.26 g cm^{-3}	Λ_i ρ=1.0 g cm^{-3}		Λ_i ρ=4.26 g cm^{-3}	
				disk x 10^{6}	cyl. x 10^{3}	disk x 10^{5}	cyl.x 10^{1}
0.1-0.2	0.03	0.000	0.002		0.0000	0.01834	0.00473
0.2-0.3	0.06	0.000	0.005		0.0000	0.09182	0.02363
0.3-0.4	0.07	0.000	0.010		0.0000	0.21424	0.05146
0.4-0.5	0.12	0.001	0.015	0.36727	0.9453	0.55000	0.14157
0.5-0.6	0.18	0.003	0.032	1.65272	4.2530	1.76000	0.45302
0.6-0.7	0.15	0.005	0.060	2.29545	5.9080	2.75000	0.70785
0.7-0.8	0.13	0.007	0.092	2.78515	7.1690	3.66000	0.94208
0.8-0.9	0.10	0.009	0.130	2.75454	7.0902	3.98000	1.02440
0.9-1.0	0.09	0.012	0.170	3.30545	8.5082	4.68000	1.20460
1.0-1.1	0.04	0.016	0.210	1.95878	5.0419	2.57000	0.66152
1.1-1.2	0.03	0.024	0.252	2.20363	5.6721	2.31000	0.59459
1.2-1.3	0.01	0.034	0.295	1.04060	2.6785	0.00000	0.23166
1.3-1.4	0.00	0.048	0.335	0.00000	0.0000	0.00000	0.00000
1.4-1.5	0.00	0.065	0.375	0.00000	0.0000	0.00000	0.00000
1.5-1.6	0.00	0.085	0.420	0.00000	0.0000	0.00000	0.00000

Table D-5. Calculated Stokes numbers and collection efficiency (taken from Starr, 1967) for different smoke particle sizes, two different particle densities and fiber diameter of 92 μm. Scavenger's settling rate was V = 36.3 cm s^{-1}.

Particle radius r [μm]	ρ_p = 1.0 g cm^{-3}		ρ_p = 4.26 g cm^{-3}	
	St. no.	E_i	St. no.	E_i
0.05	4.8177×10^{-4}	0.000	$2.0523.10^{-3}$	0.000
0.1	1.9271×10^{-3}	0.000	8.2093×10^{-3}	0.001
0.3	1.7344×10^{-2}	0.000	7.3883×10^{-2}	0.005
0.5	4.8177×10^{-2}	0.001	2.0523×10^{-1}	0.030
0.7	9.4426×10^{-2}	0.005	4.0225×10^{-1}	0.120
1.0	1.2971×10^{-1}	0.010	8.2093×10^{-1}	0.290
1.5	4.3359×10^{-1}	0.125	1.8471	0.480
2.0	7.7082×10^{-1}	0.270	3.2837	0.625
3.0	1.7344	0.420	7.3883	0.790
5.0	4.8177	0.685	20.5232	0.830

Table D-6. Scavenging efficiencies of a very fine fiber mesh scavenger (d = 92 μm) for a population of smoke particles with a specific size distribution (V = 36.3 cm s^{-1}).

Particle radius r [μm]	$N(r)_i$ / $N(r)$	E_i ρ_p=1.0	E_i ρ_p=4.26	Λ_i ρ=1.0		Λ_i ρ=4.26	
				disk x 10^7	cyl.x10^3	disk x 10^5	cyl. x 10^2
0.1-0.2	0.03	0.000	0.000	0.00000	0.0000	0.00000	0.00000
0.2-0.3	0.06	0.000	0.005	0.00000	0.0000	0.01600	0.0602
0.3-0.4	0.07	0.000	0.015	0.00000	0.0000	0.05700	0.21433
0.4-0.5	0.12	0.000	0.030	0.00000	0.0000	0.19500	0.7332
0.5-0.6	0.18	0.000	0.065	0.00000	0.0000	0.63600	2.3915
0.6-0.7	0.15	0.005	0.110	4.07663	1.5329	0.89700	3.3729
0.7-0.8	0.13	0.006	0.150	4.23965	1.5942	1.06700	3.9859
0.8-0.9	0.10	0.008	0.200	4.34837	1.6351	1.08700	4.0870
0.9-1.0	0.09	0.012	0.250	5.90000	2.2185	1.22300	4.5998
1.0-1.1	0.04	0.020	0.300	4.30000	1.6169	0.65200	2.4516
1.1-1.2	0.03	0.040	0.350	6.50000	2.4442	0.57100	2.1471
1.2-1.3	0.01	0.070	0.395	3.80000	1.4289	0.21500	0.8085
1.3-1.4	0.00	0.113	0.440	0.00000	0.0000	0.00000	0.00000

Table D-7. Evaluation of Two Crossed Punch Card Models

($TiCl_4$ particles at 1.8 m s^{-1}; plates 1x3 mm, crossed; Re = 114)

Particle d(μm)	Zone 1	2	3	4	5	6	7	8	9	10	Σ
	0.3	0.6	0.9	1.2	1.5	1.8	2.1	2.4	2.7	3.0	
Front Plate											
<1.5	15	16	10	9	14	13	9	12	7	9	114
1.5-3.0	8	7	4	3	7	11	6	7	6	5	64
3.0-6.0	7	6	3	4	3	6	4	6	5	3	47
6.0-9.1	4	4	3	3	3	4	3	3	4	4	35
9.1-12.1	3	3	2	2	2	2	2	3	3	4	26
12.1-15.2	3	2	2	1	3	2	2	2	2	2	21
15.2-18.2	2	2	2	1	2	1	3	3	1	1	18
18.2-21.2	1	1	1	1	1	1	1	1	0	0	13
21.2-24.2	1	0	0	1	1	2	2	1	1	0	9
24.2-27.3	1	0	1	1	1	1	1	1	0	0	7
27.3-30.0	0	1	1	0	0	2	1	0	0	0	5
	46	42	30	26	37	46	35	40	29	28	359
Rear Plate											
<1.5	25	27	24	19	7	8	6	10	25	26	177
1.5-3.0	22	14	8	7	4	5	4	8	18	19	109
3.0-6.0	16	8	12	6	2	2	2	9	14	12	83
6.0-9.1	14	5	5	7	2	2	1	8	11	8	63
9.1-12.1	10	4	6	5	1	1	1	7	6	7	48
12.1-15.2	8	3	5	2	1	1	1	4	3	4	32
15.2-18.2	4	3	4	1	0	0	0	3	3	3	21
18.2-21.2	1	2	4	1	0	0	0	1	2	1	12
21.2-24.2	1	1	3	0	1	0	1	0	2	1	10
24.2-27.3	0	1	2	0	0	0	0	0	1	1	5
27.3-30.0	1	0	2	0	0	0	0	0	2	0	5
30.0-33.0	1	1	0	0	0	0	0	0	0	1	3
	103	69	77	48	18	18	15	50	87	83	568

DISTRIBUTION LIST FOR ARCSL-CR-82003

Names	Copies
CHEMICAL SYSTEMS LABORATORY	
ATTN: DRDAR-CLB	1
ATTN: DRDAR-CLB-C	1
ATTN: DRDAR-CLB-P	1
ATTN: DRDAR-CLB-PS	4
ATTN: DRDAR-CLB-R	1
ATTN: DRDAR-CLB-T	1
ATTN: DRDAR-CLB-TE	1
ATTN: DRDAR-CLC-B	1
ATTN: DRDAR-CLC-C	1
ATTN: DRDAR-CLF	1
ATTN: DRDAR-CLJ-R	2
ATTN: DRDAR-CLJ-L	2
ATTN: DRDAR-CLJ-M	1
ATTN: DRDAR-CLN	1
ATTN: DRDAR-CLN-S	1
ATTN: DRDAR-CLN-ST	1
ATTN: DRDAR-CLT	1
ATTN: DRDAR-CLY-A (Pennsyle, Hundley)	2
ATTN: DRDAR-CLY-R	1
COPIES FOR AUTHOR(S)	
Research Division (CPO)	10
RECORD COPY: DRDAR-CLB-A	1
DEPARTMENT OF DEFENSE	
Defense Technical Information Center	
ATTN: DTIC-DDA-2	12
Cameron Station, Building 5	
Alexandria, VA 22314	
Director	
Defense Intelligence Agency	
ATTN: DB-4G1	1
Washington, DC 20301	
Deputy Under Secretary of Defense for	
Research and Engineering (R&AT)	
ATTN: Dr. Musa	1
ATTN: COL Friday	1
ATTN: COL Winter	1
Washington, DC 20301	
Defense Advanced Research Projects Agency	
ATTN: Dr. Tegnelia	1
Washington, DC 20301	

Names	Copies
Advanced Research Projects Agency	1
1400 Wilson Boulevard	
Arlington, VA 22209	
DEPARTMENT OF THE ARMY	
HQDA	
ATTN: DAMO-NCC	1
ATTN: DAMO-NC/COL Robinson (P)	1
WASH DC 20310	
HQDA	
Office of the Deputy Chief of Staff for	
Research, Development & Acquisition	
ATTN: DAMA-CSS-C	1
Washington, DC 20310	
HQ Sixth US Army	
ATTN: AFKC-OP-NBC	1
Presidio of San Francisco, CA 94129	
Commander	
DARCOM, STITEUR	
ATTN: DRXST-STI	1
Box 48, APO New York 09710	
Commander	
USASTCFEO	
ATTN: MAJ Mikeworth	1
APO San Francisco 96328	
Army Research Office	
ATTN: DRXRO-CB (Dr. R. Ghirardelli)	1
ATTN: DRXRO-GS	1
ATTN: Dr. W. A. Flood	1
P.O. Box 12211	
Research Triangle Park, NC 27709	
HQDA ODUSA (OR)	
ATTN: Dr. H. Fallin	1
Washington, DC 20310	
HQDA (DAMO-RQD)	
ATTN: MAJ C. Collat	1
Washington, DC 20310	

PRECEDING PAGE BLANK

HQDA, OCE
ATTN: DAEN-RDM (Dr. Gomez) 1
Massachusetts Ave, NW
Washington, DC 20314

OFFICE OF THE SURGEON GENERAL

Commander
US Army Medical Research and
Development Command
ATTN: SGRD-UBG (Mr. Eaton) 1
ATTN: SGRD-UBG-OT (CPT Johnson) 1
ATTN: LTC Don Gensler 1
Fort Detrick, MD 21701

Commander
US Army Medical Bioengineering Research
and Development Laboratory
ATTN: SGRD-UBD-AL, Bldg 568 1
Fort Detrick, Frederick, MD 21701

Commander
USA Medical Research Institute of
Chemical Defense
ATTN: SGRD-UV-L 1
Aberdeen Proving Ground, MD 21010

US ARMY MATERIEL DEVELOPMENT AND
READINESS COMMAND

Commander
US Army Materiel Development and
Readiness Command
ATTN: DRCDE-DM 1
ATTN: DRCLDC 1
ATTN: DRCMT 1
ATTN: DRCSF-P 1
ATTN: DRCSF-S
ATTN: DRCDL (Mr. N. Klein) 1
ATTN: DRCBI (COL Gearin) 1
ATTN: DRCBSI-EE (Mr. Giambalvo) 1
ATTN: DRCDMD-ST (Mr. T. Shirata) 1
5001 Eisenhower Ave
Alexandria, VA 22333

Commander
US Army Foreign Science & Technology
Center
ATTN: DRXST-MT3 1
ATTN: DRXST-M73 (Poleski) 1
220 Seventh St., NE
Charlottesville, VA 22901

Director
DARCOM Field Safety Activity
ATTN: DRXOS-SE (Mr. Yutmeyer) 1
Charlestown, IN 47111

PM Smoke/Obscurants
ATTN: DRCPM-SMK-E (A. Van de Wal) 1
ATTN: DRCPM-SMK-M 1
ATTN: DRCPM-SMK-T 1
Aberdeen Proving Ground, MD 21005

Director
US Army Materiel Systems Analysis Activity
ATTN: DRXSY-MP 1
ATTN: DRXSY-CA (Mr. Metz) 1
ATTN: DRXSY-FJ (J. O'Bryon) 1
ATTN: DRXSY-GP (Mr. Fred Campbell) 1
Aberdeen Proving Ground, MD 21005

USA AVIATION RESEARCH AND
DEVELOPMENT COMMAND

Director
Applied Technology Lab
USARTL (AVRADCOM)
ATTN: DAVDL-ATL-ASV 1
ATTN: DAVDL-ATL-ASW 1
ATTN: DAVDL-EV-MOS (Mr. Gilbert) 1
Ft. Eustis, VA 23604

Commander
USA Avionics R&D Activity
ATTN: DAVAA-E (M. E. Sonatag) 1
Ft. Monmouth, NJ 07703

USA MISSILE COMMAND

Commander
US Army Missile Command
Director, Energy Directorate
ATTN: DRSMI-RHFT 1
ATTN: DRSMI-RMST 1
ATTN: DRSMI-YLA (N. C. Katos) 1
Redstone Arsenal, AL 35809

Commander
US Army Missile Command
Redstone Scientific Information Center
ATTN: DRSMI-REO (Mr. Widenhofer) 1
ATTN: DRSMI-RGT (Mr. Matt Maddix) 1
ATTN: DRDMI-CGA (Dr. B. Fowler) 1
ATTN: DRDMI-KL (Dr. W. Wharton) 1
ATTN: DRDMI-TE (Mr. H. Anderson) 1
Redstone Arsenal, AL 35809

Commander
US Army Missile Command
Redstone Scientific Information Center
ATTN: DRSMI-RPR (Documents) 1
Redstone Arsenal, AL 35809

USA COMMUNICATIONS-ELECTRONICS COMMAND

Commander
USA Communications-Electronics Command
ATTN: DRSEL-WL-S (Mr. J. Charlton) 1
Ft. Monmouth, NJ 07703

USA ELECTRONICS RESEARCH AND DEVELOPMENT COMMAND

Commander
USA Electronics Research and Development Command
ATTN: DRDEL-CCM (Dr. J. Scales) 1
ATTN: DELHD-RT-CB (Dr. Sztankay) 1
2800 Powder Mill Road
Adelphi, MD 20783

Commander
Harry Diamond Laboratories
ATTN: DRXDO-RCB (Dr. Donald Wortman) 1
ATTN: DRXDO-RCB (Dr. Clyde Morrison) 1
ATTN: DRXDO-RDC (Mr. D. Giglio) 1
2800 Powder Mill Road
Adelphi, MD 20783

Commander
USA Materials & Mechanics Research Center
ATTN: DRXMR-MDE (Dr. Saul Isserow) 1
Watertown, MA 02172

Commander
USA Cold Region Research Engineering Laboratory
ATTN: George Aitken 1
Hanover, NH 03755

Commander/Director
Combat Surveillance and Target Acquisition Laboratory
ERADCOM
ATTN: DELCS-R (E. Frost) 1
Ft. Monmouth, NJ 07703

Director
US Army Atmospheric Sciences Laboratory
ATTN: DELAS-AS (Dr. Charles Bruce) 1
ATTN: DELAS-AS-P (Mr. Tom Pries) 1
ATTN: DELAS-EO-EN (Dr. Donald Snider) 1
ATTN: DELAS-EO-EN (Mr. James Gillespie) 1
ATTN: DELAS-EO-ME (Dr. Frank Niles) 1
ATTN: DELAS-EO-ME (Dr. Ronald Pinnick) 1
ATTN: DELAS-EO-MO (Dr. Melvin Heaps) 1
ATTN: DELAS-EO-MO (Dr. R. Sutherland) 1
ATTN: DELAS-EO-S (Dr. Louis Duncan) 1
White Sands Missile Range, NM 88002

US ARMY ARMAMENT RESEARCH AND DEVELOPMENT COMMAND

Commander
US Army Armament Research and Development Command
ATTN: DRDAR-LCA-L 1
ATTN: DRDAR-LCE-C 1
ATTN: DRDAR-LCU-CE 1
ATTN: DRDAR-NC (COL Fields) 3
ATTN: DRDAR-SCA-T 1
ATTN: DRDAR-SCF 1
ATTN: DRDAR-SCP 1
ATTN: DRDAR-SCS 1
ATTN: DRDAR-TDC (Dr. D. Gyorog) 1
ATTN: DRDAR-TSS 2
ATTN: DRCPM-CAWS-AM 1
Dover, NJ 07801

US Army Armament Research and Development Command
ATTN: DRDAR-TSE-OA (Robert Thresher) 1
National Space Technology Laboratories
NSTL Station, MS 39529

Requirements and Analysis Office
Foreign Intelligence and Threat Projection Division
ATTN: DRDAR-RAI-C 1
Aberdeen Proving Ground, MD 21010

Commander
ARRADCOM
ATTN: DRDAR-QAC-E 1
Aberdeen Proving Ground, MD 21010

Director
USA Ballistic Research Laboratory
ARRADCOM
ATTN: DRDAR-BLB 1
ATTN: DRDAR-TSB-S 1
Aberdeen Proving Ground, MD 21005

US ARMY ARMAMENT MATERIEL READINESS COMMAND

Commander
US Army Armament Materiel Readiness Command
ATTN: DRSAR-ASN 1
ATTN: DRSAR-IRI-A 1
ATTN: DRSAR-LEP-L 1
ATTN: DRSAR-SF 1
Rock Island, IL 61299

Commander
US Army Dugway Proving Ground
ATTN: Technical Library (Docu Sect) 1
Dugway, UT 84022

US ARMY TRAINING & DOCTRINE COMMAND

Commandant
US Army Infantry School
ATTN: CTDD, CSD, NBC Branch 1
Fort Benning, GA 31905

Commandant
US Army Missile & Munitions Center and School
ATTN: ATSK-CM 1
Redstone Arsenal, AL 35809

Commander
US Army Logistics Center
ATTN: ATCL-MG 1
Fort Lee, VA 23801

Commandant
US Army Chemical School
ATTN: ATZN-CM-C 1
ATTN: ATZN-CM-AD 2
ATTN: ATZN-CN-CDM (Dr. J. Scully) 1
Fort McClellan, AL 36205

Commander
USAAVNC
ATTN: ATZQ-D-MS 1
Fort Rucker, AL 36362

Commander
USA Combined Arms Center and Fort Leavenworth
ATTN: ATZL-CAM-IM 1
ATTN: ATZL-CA-SAN 1
ATTN: ATZL-CA-TM-K 1
Fort Leavenworth, KS 66027

Commander
US Army Infantry Center
ATTN: ATSH-CD-MS-C 1
ATTN: ATSH-CD-MS-F 1
ATTN: ATZB-DPT-PO-NBC 1
Fort Benning, GA 31905

Commander
USA Training and Doctrine Command
ATTN: ATCD-N 1
ATTN: ATCD-TEC (Dr. M. Pastel) 1
ATTN: ATCD-Z 1
Fort Monroe, VA 23651

Commander
US Army Armor Center
ATTN: ATZK-CD-MS 1
ATTN: ATZK-PPT-PO-C 1
Fort Knox, KY 40121

Commander
USA TRADOC Systems Analysis Activity
ATTN: ATAA-SL 1
ATTN: ATAA-TDB (L. Dominguez) 1
White Sands Missile Range, NM 88002

Commander
USA Field Artillery School
ATTN: ATSF-GD-RA 1
Ft. Sill, OK 73503

Director
USA Concepts Analysis Agency
ATTN: MOCA-SMC (Hal Hock) 1
8120 Woodmont Avenue
Bethesda, MD 20014

Los Alamos National Laboratory
ATTN: T-DOT, MS B279 (S. Gerstl) 1
Los Alamos, NM 87545

US ARMY TEST & EVALUATION COMMAND

Commander
US Army Test & Evaluation Command
ATTN: DRSTE-CM-F 1
ATTN: DRSTE-CT-T 1
ATTN: DRSTE-AD-M (Warren Baity) 1
Aberdeen Proving Ground, MD 21005

Commander
USA EPG
ATTN: STEEP-MM-IS 1
ATTN: STEEP-MT-DS (CPT Decker) 1
Ft. Huachuca, AZ 85613

Commander
Dugway Proving Ground
ATTN: STEDP-MT (Dr. L. Solomon) 1
Dugway, UT 84022

DEPARTMENT OF THE NAVY

Commander
Naval Research Laboratory
ATTN: Code 5709 (Mr. W. E. Howell) 1
ATTN: Code 6532 (Mr. Curcio) 1
ATTN: Code 6532 (Dr. Trusty) 1
ATTN: Code 6530-2 (Mr. Gordon Stamm) 1
ATTN: Code 8320 (Dr. Lothar Ruhnke) 1
ATTN: Code 8326 (Dr. James Fitzgerald) 1
ATTN: Code 43202 (Dr. Hermann Gerber) 1
4555 Overlook Avenue, SW
Washington, DC 20375

Chief, Bureau of Medicine & Surgery
Department of the Navy
ATTN: MED 3C33 1
Washington, DC 20372

Commander
Naval Air Systems Command
ATTN: Code AIR-301C (Dr. H. Rosenwasser) 1
Washington, DC 20361

Commander
Naval Sea Systems Command
ATTN: SEA-62Y13 (LCDR Richard Gilbert) 1
ATTN: SEA-62Y21 (A. Kanterman) 1
ATTN: SEA-62Y21 (LCDR W. Major) 1
Washington, DC 20362

Project Manager
Theatre Nuclear Warfare Project Office
ATTN: TN-09C 1
Navy Department
Washington, DC 20360

Institute for Defense Analysis
400 Army-Navy Drive
ATTN: L. Biberman 1
ATTN: R. E. Roberts 1
Arlington, VA 22202

Commander
Naval Surface Weapons Center
Dahlgren Laboratory
ATTN: DX-21 1
ATTN: Mr. R. L. Hudson 1
ATTN: F-56 (Mr. Douglas Marker) 1
Dahlgren, VA 22448

Commander
Naval Intelligence Support Center
ATTN: Code 434 (H. P. St.Aubin) 1
4301 Suitland Road
Suitland, MD 20390

Commander
Naval Explosive Ordnance Disposal
Technology Center
ATTN: AC-3 1
Indian Head, MD 20640

Officer-in-Charge
Marine Corps Detachment 1
Naval Explosive Ordnance Disposal
Technology Center
Indian Head, MD 20640

Commander
Naval Air Development Center
ATTN: Code 2012 (Dr. Robert Helmbold) 1
Warminster, PA 18974

Commander
Naval Weapons Center
ATTN: Code 382 (L. A. Mathews) 1
ATTN: Code 3882 (Dr. C. E. Dinerman) 1
ATTN: Code 3918 (Dr. Alex Shlanta) 1
China Lake, CA 93555

Commanding Officer
Naval Weapons Support Center
Applied Sciences Department
ATTN: Code 50C, Bldg 190 1
ATTN: Code 502 (Carl Lohkamp) 1
Crane, IN 47522

US MARINE CORPS

Commanding General
Marine Corps Development and
Education Command
ATTN: Fire Power Division, D091 1
Quantico, VA 22134

DEPARTMENT OF THE AIR FORCE

HQ AFLC/LOWMM 1
Wright-Patterson AFB, OH 45433

HQ AFSC/SDZ 1
ATTN: CPT D. Riediger
Andrews AFB, MD 20334

USAF TAWC/THL 1
Eglin AFB, FL 32542

USAF SC
ATTN: AD/YQ (Dr. A. Vasiloff) 1
ATTN: AD/YQO (MAJ Owens) 1
Eglin AFB, FL 32542

AFAMRL/TS
ATTN: COL Johnson 1
Wright-Patterson AFB, OH 45433

Commander
Hanscom Air Force Base
ATTN: AFGL-POA (Dr. Frederick Volz) 1
Bedford, MA 01731

Headquarters
Tactical Air Command
ATTN: DRP 1
Langley AFB, VA 23665

AFOSR/NE
ATTN: MAJ H. Winsor 1
Bolling AFB, DC 20332

AD/XRO 1
Eglin AFB, FL 32542

Dr. Charles Arpke 1
OSV Field Office
P.O. Box 1925
Eglin AFB, FL 32542

OUTSIDE AGENCIES

Battelle, Columbus Laboratories
ATTN: TACTEC 1
505 King Avenue
Columbus, OH 43201

Toxicology Information Center, JH 652
National Research Council 1
2101 Constitution Ave., NW
Washington, DC 20418

Dr. W. Michael Farmer, Assoc.Prof., Physics
University of Tennessee Space Institute 1
Tullahoma, TN 37388

ADDITIONAL ADDRESSEES

Office of Missile Electronic Warfare
ATTN: DELEW-M-T-AC (Ms Arthur) 1
White Sands Missile Range, NM 88002

US Army Mobility Equipment Research and
Development Center
ATTN: DROME-RT (Mr. O. F. Kezer) 1
Fort Belvoir, VA 22060

Director
US Night Vision and EO Laboratories
ATTN: DRSEL-NV-VI (Dr. R. G. Buser) 1
ATTN: DRSEL-NV-VI (Mr. R. Bergemann) 1
ATTN: DELNV-VI (Luanne Obert) 1
ATTN: DELNV-L (D. N. Spector) 1
Fort Belvoir, VA 22060

Commandant
Academy of Health Sciences, US Army
ATTN: HSHA-CDH 1
ATTN: HSHA-IPM 2
Fort Sam Houston, TX 78234

Commander
217th Chemical Detachment
ATTN: AFVL-CD 1
Fort Knox, KY 40121

Headquarters
US Army Medical Research and
Development Command
ATTN: SGRD-RMS 1
Fort Detrick, MD 21701

Commander
US Army Environmental Hygiene Agency
ATTN: Librarian, Bldg 2100 1
Aberdeen Proving Ground, MD 21010